CHEMICAL REVIEWS

REVIEW

pubs.acs.org/CR

# Commensurate Adsorption of Hydrocarbons and Alcohols in Microporous Metal Organic Frameworks

Haohan Wu, Qihan Gong, David H. Olson, and Jing Li*

Department of Chemistry and Chemical Biology, Rutgers University, Piscataway, New Jersey 08854, United States

## CONTENTS



## 1. INTRODUCTION

### 1.1. Background and History

Commensurate adsorption is an interesting and important phenomenon occurring during adsorption processes, where the molecular size and shape of the adsorbate (guest molecule) lead to an orientation and adsorbed amount (at equilibrium) that is compatible and self-consistent with the crystal symmetry and pore structure of the adsorbent.[1−4] Some early examples referred to adsorption of noble gas and small molecules on two-dimensional (2D) surfaces of organic substrates, such as $CH_4$,[5,6] Kr,[7,8] $N_2$,[9] benzene,[10] and Xe[11] on graphite at low temperatures. Later studies included both organic and inorganic surfaces, for example, $CH_4$,[12] Kr,[13] Xe,[14] $H_2$,[15−17] $D_2$,[16−18] HD,[16,17] $CF_3Cl$,[19] $^4He$,[20,21] CO,[22,23] and $N_2$[24,25] on graphite substrate, Xe,[26−28] Kr,[29] Ar[30] on Pt(111), Xe on Cu(110),[31,32] $H_2$ on Fe(211),[33] $H_2$ on Rh(311),[34] Ar on Ag(111),[35] CO on Pd-(100),[36] and Ar on several surfaces of ZnO.[37] The surface structures were characterized and confirmed both experimentally and theoretically, for example, by neutron diffraction, high resolution X-ray scattering, density functional theory (DFT), and molecular simulations. In the late 1980s, the concept was introduced to crystalline porous materials of three-dimensional (3D) network structures such as zeolites,[3,4,38−68] where more complex interactions exist between adsorbate molecules and adsorbent systems. Commensurate adsorption (in some cases referred to as freezing/locking) of hydrocarbons (e.g., *p*-xylene, *n*-hexane, *n*-heptane, benzene, etc.) was found in several different types of zeolites, for instance, MFI, ITW, ERI, CHA, LTA, AFX, and silicalites (Table 1).[4,40,42,45,46,51−55,61−66,69,70] The observed adsorption of an integral number of adsorbate molecules that correlates with adsorbent structure was attributed to the close match of the size and/or shape of the hydrocarbon molecules to the zeolite pore features such as channel/cage size, shape, and segment length, crystal symmetry and multiplicity of special and general crystallographic positions, which determine the location and orientation of the adsorbate molecules, their packing order, and level of adsorption. Accordingly, when the geometry of an adsorbate is commensurate with the pore structure or topology of a zeolite/silica adsorbent, highly ordered packing of the adsorbed molecules will result.

### 1.2. Examples of Commensurate Adsorption of Hydrocarbons

A well-known case is the adsorption of *p*-xylene in ZSM-5 (a zeolite material crystallized in orthorhombic system with cell parameters $a = 20.07$, $b = 19.92$, $c = 13.42$ Å, and Si/Al = 86). The framework has a 2D pore structure containing two intersecting 1D channels (Figure 1). The straight channels running parallel to [010] and zigzag (sinusoidal) channels running parallel to [100] have a window size of ~5.4 × 5.6 Å and 5.1 × 5.5 Å, respectively (both defined by 10-membered rings).[3] Three distinct adsorption sites (straight and zigzag channels, and their intersections)

**Special Issue:** 2012 Metal-Organic Frameworks

**Received:** June 11, 2011
**Published:** January 18, 2012

  

**Table 1. Summary of Commensurate Adsorption of Hydrocarbons in Selected Zeolites[a]**

| Zeolite | Crystal & Pore Features | Adsorbate | Adsorbed Amount (molec/UC, molec/cage) @ T, P* | | Note | Refs. |
|---|---|---|---|---|---|---|
| | | | Experimental | Simulation/ Structure Refinement | | |
| ZSM5/ Silicalite -1, MFI type zeolite | 3D framework with 2 intersecting 1D channels (window sizes: 5.4×5.6 Å (straight) and 5.1×5.5 Å (sinusoidal)). There are 4 of each intersections, straight channel segments and sinusoidal channel segments per unit cell. | *p*-Xylene | ~4 molec/UC @ 343 K, P/Po=0.03<br>7.63 molec/UC @ 313.2 K, P/Po=0.048, | 8 molec/UC @ 180K | Adsorption hierarchy: intersections > sinusoidal | 3-4,38-42,45-47,49-60,64,67,70 |
| | | *n*-Hexane | 7.1 molec/UC @ 363 K<br>7.85 molec/UC @ 308.1 K, P/Po=0.138,<br>~8 molec/UC @ 298 K | 8 molec/UC @ 180K | Adsorption hierarchy: sinusoidal > straight | |
| | | *n*-Heptane | 7.3 molec/UC @ 298 K | 8 molec/UC @ 180K | Adsorption hierarchy: straight > sinusoidal | |
| | | Benzene | ~8 mo/UC @ 273 K, 10 torr or 303 K, 80 torr | 8 molec/UC @ 303K | Adsorption hierarchy: intersections > sinusoidal | |
| | | Propane | 11.7 molec/UC @ 303 K, 4 atm | 12 molec/UC @ 303K | Adsorption hierarchy: sinusoidal > straight > intersections | |
| | | 2,2-Dimethyl-butane | ~4 molec/UC @ 298 K | 4 molec/UC @ 362K, 1atm | Only adsorbed in intersection | |
| ITQ-12, ITW type zeolite | 3D frameworks with 2 of 1D channels (narrow window along (100), 2.4 ×5.3 Å, and wide window along (001), 3.8 × 4.1 Å). | Propene | ~2 molec/UC @ 303 K, 640 torr | 2 molec/UC @ 303K, 640 torr | Only wide window channels are accessible to propene | 43-44,48 |
| ERI type zeolite | 3D frameworks with elongated cylindrical cages of 13Å in length and 6.3 Å in diameter connected by 3.6 × 5.1 Å windows. | *n*-C7,*n*-C8, *n*-C9 | | 1 molec/cage @ 300K | | 61-65,69 |
| CHA type zeolite | 3D frameworks with ellipsoidal cage of about 10 × 6.7 Å across connected by 3.8 × 3.8 Å windows | *n*-C6-, *n*-C7, *n*-C8, *n*-pentanol, *n*-hexanol | <1 molec/cage | 1 molec/cage @ 300K | | 61-66,68-69 |

[a] * molec/UC = number of molecules per unit cell, molec/cage = number of molecules per cage, T = temperature, P = pressure.

were identified. Every unit cell contains four of each straight, zigzag channel, and channel intersection sites. The adsorption isotherms showed two distinct steps at loadings of four and eight *p*-xylene molecules.[3] The first four *p*-xylene molecules are located in the channel intersection sites with their methyl groups along the straight channels and the next four *p*-xylene molecules occupy the four zigzag channel positions (giving a total number of 8 *p*-xylene molecules per unit cell). Both the crystal structure determination and simulation studies showed such arrangement is energetically most favorable.[38,57]


dx.doi.org/10.1021/cr200216x |*Chem. Rev.* 2012, 112, 836–868

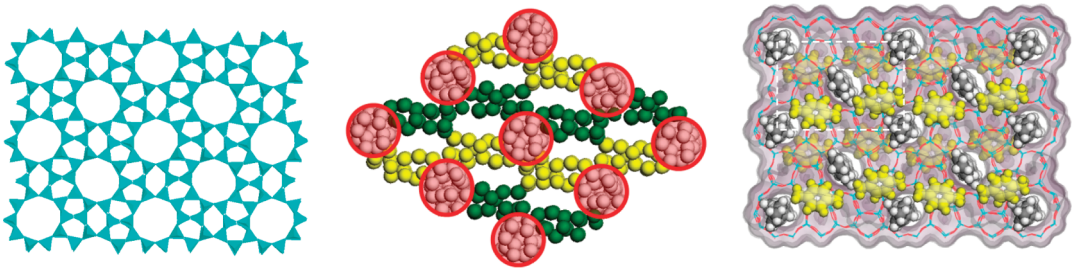


**Figure 1.** (a) The framework of ZSM-5 projected along the [010] direction. (b) Simulated helium adsorption in ZSM-5 at 1 K, 1 atm, viewed along the [010] direction. Helium atoms are modeled as spheres and give an outline of the channel and cross-section shapes. The red circles outline the cross section of straight channels. The two sets of the zigzag channels running along the [100] direction are outlined by He atoms in green and yellow at different heights. (c) Simulated *p*-xylene adsorption viewed along the [010] direction. Within a unit cell, the first four molecules loaded occupy the intersection sites of the straight and zigzag channels (gray), and the second four molecules take the positions within the zigzag channels (yellow). Color scheme: Si and Al (blue), O (red), *p*-xylene (gray and yellow), and the Connolly surface[71] (purple). The unit cell is outlined by white dotted line.

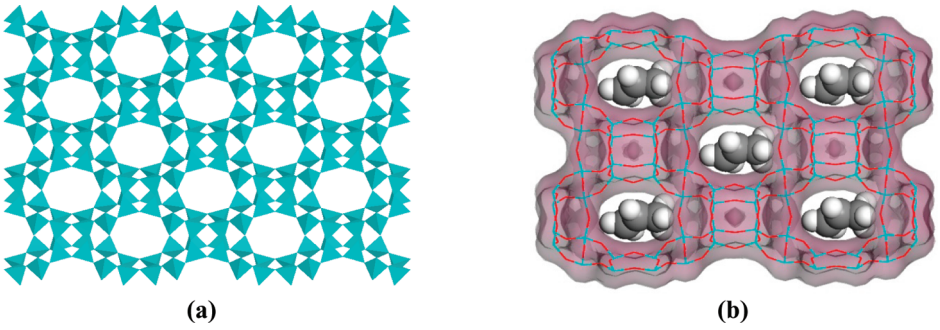


**Figure 2.** (a) The framework of ITQ-12 projected along the [001] direction. (b) Simulated structure showing adsorbed propene molecules in the cages with a window size of ~3.8 × 4.1 Å. Color scheme: Si and Al (blue), O (red), C (gray sphere), H (white sphere), and the Connolly surface[71] (purple).

A second example concerns adsorption of benzene molecules in silicalite, an aluminum-free form of ZSM-5.[42,72,73] The sorption kinetics study suggested that the initial stage of benzene adsorption took place preferentially at the channel intersections until a critical concentration of 4 molecules per unit cell was reached. This absorbed amount corresponds to one molecule occupying each available channel intersection site (4 per unit cell).

Propene adsorption in ITQ-12 represents another typical example of commensurate adsorption in zeolites.[43,44] ITQ-12 is a 3D framework having 2D pore structure (Figure 2a). The channel running along the [100] has a narrow window made of eight-membered ring with a size ~2.4 × 5.3 Å. The channel along [001] has a more circular window aperture, ~3.8 × 4.1 Å. The cage between the windows has a flat shape and size that gives a good match with the molecular geometry of propene, allowing it to diffuse in and be adsorbed much more rapidly than propane. At both 30 and 80 °C, the adsorbed amount of propene corresponds to 1 molecule per cage. Illustrated in Figure 2b is a simulated structure showing adsorbed propene molecules.

## 2. HYDROCARBON ADSORPTION IN MMOFs

### 2.1. Gas Adsorption and Adsorptive Separation

The past three decades have witnessed an exponential growth in research and development of crystalline microporous materials. The discovery of a new family of such materials, microporous metal organic frameworks (MMOFs), has offered emerging opportunities for revolutionizing industrial applications, in particular, separation and purification of hydrocarbons.[74−82]

MMOFs are crystalline solids with extended network structures. They are comprised of single metal cations (primary building unit or PBU) or metal clusters (secondary building unit or SBU) and organic ligands with multiple binding sites linked via coordinative bonds. As a subset of the general family of metal organic framework (MOFs, also known as coordination polymers or CPs), they possess perfectly ordered and well-defined pore structures and their pore dimensions are in the range of micropore (less than 2 nm) according to the IUPAC definition. Being a new type of adsorbent material, MMOFs possess numerous interesting and appealing features, including but not limited to, a large internal surface area and pore volume;[74−77,83−100] high gas adsorption enthalpies, often significantly higher than those found in other adsorbates characteristic of physisorption;[101−105] great structural flexibility;[74,99,103−105] remarkable adsorption selectivity;[78,79,106,107] and interesting sorption kinetics.[107,108] Their crystal structures (e.g., framework dimensionality, connectivity, and topology), chemical composition (e.g., the type and form of metals and ligands), and pore characteristics (e.g., pore size and shape, pore volume and the chemical functionality of the pore walls) can be systematically and deliberately tuned to enhance targeted properties and to achieve improved performance.

The initial interests in gas adsorption on MMOF materials were largely driven by the search for appropriate structures


dx.doi.org/10.1021/cr200216x |*Chem. Rev.* 2012, 112, 836–868

**Table 2. Summary of Experimental Hydrocarbon and Alcohol Adsorption in Selected MMOFs[a]**

| MMOF[&] | Crystal & Pore Structure | Adsorbate | T(K) | Phase[#] | P or R.C.[%] | Experimental Adsorbed Amount | Note | Refs. |
|---|---|---|---|---|---|---|---|---|
| [$V^{IV}O$(bdc)] (MIL-47) | 3D framework with 1D diamond shaped channels along *a* axis (window size ~7.0×5.7 Å) | *p*-Xylene (*p*X) | 298 | L | 0.8 M | 37 wt%, | | 171,175,177,180 |
| | | | 343 | V | 0.04 bar | 40 wt%, | | |
| | | *o*-Xylene (oX) | 298 | L | 0.8 M | 35 wt% | | |
| | | | 343 | V | 0.04 bar | 37 wt% | | |
| | | *m*-Xylene (*m*X) | 298 | L | 0.8 M | 30 wt% | NRS^ | |
| | | | 343 | V | 0.04 bar | 37 wt% | | |
| | | Ethyl-benzene (EB) | 298 | L | 0.8 M | 17 wt% | NRS | |
| | | | 343 | V | 0.04 bar | 33 wt% | | |
| | | Styrene | 298 | L | 0.45 M | 21 wt% | | |
| | | Ethane | 303 | V | 25 bar | 6.0 mo/UC | | |
| | | Propane | 303 | V | 10 bar | 4.5 mo/UC | | |
| | | Butane | 303 | V | 10 bar | 4.2 mo/UC | | |
| | | *n*-Octane | 343 | V | 0.05 bar | 23 wt% | | |
| [$Al^{III}$(OH)(bdc)] (MIL-53-Al) | 3D framework with 1D diamond shaped channels along the *a* axes (window size ~7.2×5.3 Å) | *p*-Xylene | 298 | L | 0.55 M | 43 wt% | | 171,173,176,183 |
| | | | 343 | V | 0.035 bar | 36 wt% | | |
| | | *o*-Xylene | 298 | L | 0.55 M | 46 wt% | | |
| | | | 343 | V | 0.035 bar | 42 wt% | | |
| | | *m*-Xylene | 298 | L | 0.55 M | 25 wt% | NRS | |
| | | | 343 | V | 0.035 bar | 37 wt% | | |
| | | Ethyl-benzene | 298 | L | 0.55 M | 16 wt% | NRS | |
| | | | 343 | V | 0.035 bar | 28 wt% | | |
| | | Styrene | 298 | L | 0.45 M | 24 wt% | | |
| | | Ethyl-toluene isotherms | 298 | L | 0.55 M | Competitive adsorption | Ortho- is preferable | |
| | | Cymene isotherms | 298 | L | 0.55M | Competitive adsorption | | |
| | | Hexane | 313 | V | 0.95 P/Po | 2.4 molec/UC | Inflection at different pressure and different uptake | |
| | | Heptane | 313 | V | 0.95 P/Po | 2.2 molec/UC | | |
| | | Octane | 313 | V | 0.95 P/Po | 1.5 molec/UC | | |
| | | Nonane | 313 | V | 0.95 P/Po | 1.3 molec/UC | | |
| [$Cr^{III}$(OH)(bdc)] (MIL-53-Cr) | Same as MIL-53-Al | Ethane | 303 | V | 30 bar | ~0.33 cc(liquid)/g | | 179-180,183,201 |
| | | Propane | 303 | V | 10 bar | ~0.35 cc(liquid)/g | | |
| | | Butane | 303 | V | 1.8 bar | ~0.39 cc(liquid)/g | | |
| | | Hexane | 313 | V | 0.95 P/Po | 3.0 molec/UC | | |
| | | Heptane | 313 | V | 0.95 P/Po | 2.5 molec/UC | | |
| | | Octane | 313 | V | 0.95 P/Po | 1.8 molec/UC | | |
| | | Nonane | 313 | V | 0.95 P/Po | 1.4 molec/UC | | |
| [$Fe^{III}$(OH)(bdc)] (MIL-53-Fe) | Same as MIL-53-Al | Ethane | 303 | V | 30 bar | 6.6 mmol/g | Inflection at 1.2 mmol/g | 202 |
| | | Propane | 303 | V | 10 bar | 4.0 mmol/g | Inflection at 2.8 mmol/g | |
| | | Butane | 303 | V | 1.8 bar | 3.9 mmol/g | Inflection at 2.8 mmol/g | |
| [$Cu_2$(pzdc)$_2$(dpyg)] | 3D framework with 1D channel along the *a* axis (window size ~4×6 Å) | Methanol | 298 | V | 1.0 P/Po | 6.2 mmol/g | hysteresis | 203 |
| [$Cu_2$(pzdc)(bpee)] | 3D framework with 1D channel along the *c* axis (window size ~3.5×4.5 Å) | Methanol | 298 | V | 1.0 P/Po | 35 cc(STP)/g | hysteresis | 187 |
| | | Ethanol | 298 | V | 1.0 P/Po | Negligible | | |


dx.doi.org/10.1021/cr200216x |*Chem. Rev.* 2012, 112, 836–868

Table 2. Continued

| MMOF[&] | Crystal & Pore Structure | Adsorbate | T(K) | Phase[#] | P or R.C.[%] | Experimental Adsorbed Amount | Note | Refs. |
|---|---|---|---|---|---|---|---|---|
| [Cd(4-btapa)$_2$(NO$_3$)$_2$] | Two-fold Interpenetrating 3D framework with 3D zig-zag channels (window size 4.7×7.3 Å) | Methanol | 298 | V | 0.9 P/Po | 130 cc(STP)/g | hysteresis | 204 |
| [Ni(bpe)$_2$(N(CN)$_2$)](N(CN)$_2$) | Two-fold Interpenetrating 3D framework with 1D hexagonal channel along the *c* axis (window size 6.5×4.7 Å | Methanol | 298 | V | 0.9 P/Po | 85 cc(STP)/g | hysteresis | 163 |
| | | Ethanol | 298 | V | 0.9 P/Po | 32 cc(STP)/g | | |
| [Cu(etz)] | 3D framework containing large cages ($d$ = 9 Å) connected by small flexible hydrophobic apertures (window size, $d$ = 1.5 Å) | Methanol | 298 | V | 1.0 P/Po | 175 mg/g | | 186 |
| | | Ethanol | 298 | V | 1.0 P/Po | 245 mg/g | | |
| | | Benzene | 298 | V | 1.0 P/Po | 200 mg/g | | |
| | | *cyclo*-Hexane | 298 | V | 1.0 P/Po | negligible | | |
| [Ce(tci)(H$_2$O)] | 3D framework with 1D channel along *a* axis (window size 2.8×2.7 Å) | Methanol | 298 | V | 0.9 P/Po | 2 molec/UC | | 185 |
| | | Ethanol | 298 | V | 0.9 P/Po | negligible | | |
| Ag$_2$[Cr$_3$O(OOCC$_2$H$_5$)$_6$(H$_2$O)$_3$]$_2$[α-SiW$_{12}$O$_{40}$] | Nonporous flexible ionic 2D layers of polyoxometalates ([α-SiW$_{12}$O$_{40}$]$^{4-}$) and macrocations ([Cr$_3$O(OOCC$_2$H$_5$)$_6$(H$_2$O)$_3$]$^+$) stacking along the *b* axis | Ethane | 298 | V | 0.7 P/Po | ~0.2 mol/mol | | 184 |
| | | Propane | 298 | V | 0.7 P/Po | ~0.2 mol/mol | | |
| | | *n*-Butane | 298 | V | 0.7 P/Po | ~0.2 mol/mol | | |
| | | Ethylene | 298 | V | 0.3 P/Po | ~2.0 mol/mol | | |
| | | Propylene | 298 | V | 0.4 P/Po | ~2.0 mol/mol | | |
| | | *n*-Butene | 298 | V | 0.6 P/Po | ~1.0 mol/mol | | |
| | | *n*-Penetene | 298 | V | 0.8 P/Po | ~0.2 mol/mol | | |
| | | Isobutene | 298 | V | 0.8 P/Po | ~0.4 mol/mol | | |
| | | Acetylene | 298 | V | ~0.03 P/Po | ~1.2 mol/mol | | |
| | | Methyl Acetylene | 298 | V | 0.18 P/Po | ~1.7 mol/mol | | |
| [Zn$_2$(bpdc)$_2$(bpee)]·2DMF (RPM3-Zn) | 3D Framework with 1D channels along the *b*-axis (window size: ~5.1×8.8 Å) | Methanol | 303 | V | 85 torr | 126 mg/g | | 1,181,205 |
| | | Ethanol | 303 | V | 41 torr | 115 mg/g | | |
| | | *n*-Propanol | 303 | V | 12 torr | 143 mg/g | | |
| | | *n*-Butanol | 303 | V | 3.5 torr | 152 mg/g | | |
| | | *n*-Pentanol | 303 | V | 1.2 torr | 155 mg/g | | |
| | | Benzene | 303 | V | 74 torr | 192 mg/g | | |
| | | *p*-Xylene | 303 | V | 6.0 torr | 124 mg/g | | |
| | | *o*-Xylene | 303 | V | 3.9 torr | 130 mg/g | | |
| [Zn$_2$(bpdc)$_2$(bpe)]·2DMF (RPM4-Zn) | 3D frameworks with 1D channel along the *b*-axis (window size: ~4.5×8.0 Å) | Ethanol | 303 | V | 41 torr | 82 mg/g | | 206-207 and this work |
| | | *n*-Propanol | 303 | V | 12 torr | 126 mg/g | | |
| | | *n*-Butanol | 303 | V | 3.5 torr | 128 mg/g | | |
| | | *n*-pentanol | 303 | V | 1.2 torr | 106 mg/g | | |
| | | Benzene | 303 | V | 74 torr | 139 mg/g | | |
| | | *p*-Xylene | 303 | V | 6.0 torr | 125 mg/g | | |
| | | *o*-Xylene | 303 | V | 3.9 torr | 80 mg/g | | |
| Cu$_4$O(OH)$_2$(Me$_2$trzpba)$_4$ | 3D framework with 3D channel system (window size: 4.5×5.5 Å along the *a*- and *b*- axes, 3.5×8.5 Å along the *c*-axis) | Methanol | 298 | V | 0.9 P/Po | 14 mmol/g | | 191 |


dx.doi.org/10.1021/cr200216x |*Chem. Rev.* 2012, 112, 836–868

Table 2. Continued

| MMOF[&] | Crystal & Pore Structure | Adsorbate | T(K) | Phase[#] | P or R.C.[%] | Experimental Adsorbed Amount | Note | Refs. |
|---|---|---|---|---|---|---|---|---|
| [Cu(dhbc)$_2$(4,4'-bpy)]·$H_2O$ | 2D framework with 1D channels along the *a*-axis (pore size: 2.9×4.8 Å and 4.7×2.5 Å) | Benzene | 313 | V | 61 torr | 202 mg/g | | This work |
| | | Toluene | 313 | V | 17.6 torr | 153 mg/g | | |
| | | *p*-Xylene | 313 | V | 5.1 torr | 55 mg/g | | |
| | | Propane | 303 | V | 664 torr | 39 mg/g | | |
| | | *n*-butane | 303 | V | 640 torr | 43 mg/g | | |
| | | *n*-Pentane | 303 | V | 352 torr | 49 mg/g | | |
| | | *n*-Hexane | 303 | V | 100 torr | 54 mg/g | | |
| [$Mn_3$(fa)$_6$] | 3D framework with 1D zig-zag channels | Acetylene | 196 | V | 1 bar | 68.2 cc(STP)/g | | 208 |
| | | | 275 | V | 1 bar | 57.7 cc(STP)/g | | |
| | | | 298 | V | 1 bar | 51.2 cc(STP)/g | | |
| [$Mg_3$(fa)$_6$] | 3D framework with 1D zig-zag channels | Acetylene | 196 | V | 1 bar | 72.5 cc(STP)/g | | 208 |
| | | | 275 | V | 1 bar | 69.4 cc(STP)/g | | |
| | | | 298 | V | 1 bar | 65.7 cc(STP)/g | | |
| [$Zn_2$(bptc)] | Two types of interconnecting pores with openings of 3.9 × 5.1 Å and 3.9 × 5.2 Å | Ether | 298 | V | 1 P/Po | 13 wt% | | 188 |
| | | Methanol | 298 | V | 1 P/Po | 10 wt% | | |
| | | Benzene | 298 | V | 1 P/Po | 9 wt% | | |
| | | Toluene | 298 | V | 1 P/Po | 13 wt% | | |
| | | *n*-Pentane | 298 | V | 1 P/Po | 7 wt% | | |
| | | *n*-Hexane | 298 | V | 1 P/Po | 8.5 wt% | | |
| [Cu(gla)(4,4'-bipy)$_{0.5}$] | 1D hydrophobic elliptical channels of window size 3.3×5.1 A | Methanol | 298 | V | 0.96 P/Po | 2.1 mmol/g | | 140 |
| [$Al_{12}O(OH)_{18}(H_2O)_3(Al_2(OH)_4)(btc)_6$]·$24H_2O$ (MIL-96) | Three types of cages, of which two are accessible with small window opening of ~5 Å after removal of water molecules | *trans*-Piperylene | 298 | L | 0.65 M | 12 wt% | | 136,172 and this work |
| | | *trans*-1,3-Hexadiene | 298 | L | | <1 wt% | Length exclusion | |
| | | *cis*-Piperylene | 298 | L | 0.35 M | 0.6 molec/Cage (A/B) | Steric constraint | |
| | | Isoprene | 298 | L | 0.35 M | 0.5 molec/Cage (A/B) | Steric constraint | |
| [$Cu_2$(pzdc)$_2$(pyz)]·$2H_2O$ | 3D framework consisting of 1D channels with window size of 4×6Å | Acetylene | 270 | V | 1 bar | 42 cc(STP)/g | | 111 |
| | | | 300 | | | | | |
| | | | 310 | | | | | |
| [$Zn_2$(bdc)$_2$-(dabco)]·4DMF·$0.5H_2O$ | Tetragonal 3D framework having two 1D interconnected channels (pore apertures ~7.5×7.5 Å and 3.2×4.8 Å) | Methanol | 298 | V | 0.42 P/Po | 5.02 mg/g | | 131,209 |
| | | Ethanol | 298 | V | 0.42 P/Po | 418 mg/g | | |
| | | Isopropanol | 308 | V | 0.9 P/Po | 160 cc(STP)/g | Inflection at 3mo/UC | |
| [Zn(bim)$_2$] (ZIF-7) | Sodalite topology with a window opening of ~3 Å | Propane, propene, ethane, ethene | 298 | V | 1 bar | 4 mo/cage | Quick loading of 3mo/UC | 210 |
| [Zn(tbip)] | 3D frameworks with 1D channel along the *c*-axis (window size: 4.5 Å) | Methanol | 298 | V | 90 torr | 110 mg/g | | 106 |
| | | Dimethyl-ether (DME) | 303 | V | 650 torr | 30 mg/g | | |


dx.doi.org/10.1021/cr200216x |*Chem. Rev.* 2012, 112, 836–868

Table 2. Continued

| MMOF[&] | Crystal & Pore Structure | Adsorbate | T(K) | Phase[#] | P or R.C.[%] | Experimental Adsorbed Amount | Note | Refs. |
|---|---|---|---|---|---|---|---|---|
| [Cu(hfipbb)($H_2$hfipbb)$_{0.5}$] | 3D frameworks with 1D straight channel along the *b*-axis (window size: 3.2Å) | Methane | 298 | V | 760 torr | 0.39 wt% | | 1,107 and this work |
| | | Ethane | 298 | V | 760 torr | 1.2 wt% | | |
| | | Propane | 298 | V | 0.063 P/Po | 2.6 wt% | | |
| | | Propene | 298 | V | 0.019 P/Po | 2.0 Wt% | | |
| | | *n*-Butane | 298 | V | 0.33 P/Po | 4.0 wt% | | |
| | | Methanol | 298 | V | 0.6 P/Po | 2.0 wt% | | |
| [$Co_3$(fa)$_6$] | 1D zig-zag channel along the *b*-axis (window size: 4.5Å) | Methane | 303 | V | 684 torr | 14 mg/g | | 130,133,208,211-212 and this work |
| | | Ethane | 303 | V | 684 torr | 64 mg/g | | |
| | | Propane | 303 | V | 684 torr | 91 mg/g | | |
| | | Propene | 303 | V | 684 torr | 87 mg/g | | |
| | | *n*-Butane | 303 | V | 684 torr | 124 mg/g | | |
| | | *n*-Pentane | 303 | V | 353 torr | 94 mg/g | | |
| | | *n*-Hexane | 303 | V | 100 torr | 102 mg/g | | |
| | | *n*-Heptane | 303 | V | 28 torr | 110 mg/g | | |
| | | Methanol | 303 | V | 85 torr | 99 mg/g | | |
| | | Ethanol | 303 | V | 41 torr | 106 mg/g | | |
| | | *n*-Propanol | 303 | V | 12 torr | 143 mg/g | | |
| | | *n*-Butanol | 303 | V | 3.5 torr | 168 mg/g | | |
| | | *n*-Pentanol | 303 | V | 1.2 torr | 108 mg/g | | |
| | | Benzene | 303 | V | 74 torr | 174 mg/g | | |
| | | Toluene | 303 | V | 18 torr | 148 mg/g | | |
| | | *p*-Xylene | 303 | V | 6.0 torr | 48 mg/g | | |
| | | Ethylbenzene | 303 | V | 5.8 torr | 130 mg/g | | |

[a] [&] bdc = 1,4-benzenedicarboxylate, pzdc = pyrazine-2,3-dicarboxylate, dpyg = 1,2-di(4-pyridyl)glycol, 4-btapa = 1,3,5-benzene tricarboxylic acid tris-[N-(4-pyridyl)amide], bpee = 1,2-bis(4-pyridyl)ethane, bpe = 1,2-bis(4-pyridyl)ethane, dhbc = 2,5-dihydroxybenzoic acid, $Me_2$trzpba = 4-(3,5-dimenthyl-4H-1,2,4-triazol-4-yl)benzoate, etz = 3,5-diethyl-1,2,4-triazolate, tci = 3,3′,3″-(2,4,6-trioxo-1,3,5-triazinane-1,3,5-triyl)tripropionate, fa = formate, bptc = 4,4′-bipyridine-2,6,2′,6′-tetracarboxylate, gla = glutarate, 4,4′-bipy = 4,4′-bipyridine, btc = 1,3,5-benzenetricarboxylate, pyz = pyrazine, dabco = 1,4-diazabicyclo[2.2.2]-octane, bim = benzimidazole , $H_2$hfipbb = 4,4′-(hexafluoroisopropylidene)bis(benzoic acid), tbip = 5-*tert*-butylisophthalicate, bpdc = 4,4′-biphenyldicarboxylate. [#] L = Liquid phase adsorption, V = vapor phase adsorption. [%] For vapor phase adsorption, the pressure (P) is used. For liquid phase adsorption, R. C. = relative concentration of adsorbate in a non-interacting solvent, in unit of mol/L (M). [Λ] NRS = not reaching saturation.

to store small gas molecules (i.e., hydrogen, methane, and carbon dioxide).[87−90,95,96,101,103,105,109−126] More recent efforts are geared toward selective adsorption and adsorptive separation of small gases (e.g., $N_2$, $O_2$, $CH_4$, $H_2$, CO, $CO_2$, $NO_x$, NCCl, $NH_3$, $SO_2$, and $H_2S$)[86,116,117,121,127−169] and various hydrocarbons.[1,43,44,104,106,107,130,131,146,163,170−193] Selected examples of hydrocarbon adsorption in MMOFs are given in Table 2. Adsorption based separation is one of the most important separation technologies utilized in petroleum refining industries and has been extensively developed for zeolites and related materials since the 1960s.[194−198] Adsorptive separation of a hydrocarbon mixture may be achieved via equilibrium, steric or kinetic mechanisms, or combinations of these in more complex systems.[195,199] In an equilibrium process, separation is based on differences in the relative amounts of various hydrocarbon species adsorbed in the adsorbent once equilibrium is established. The process is dictated by the difference in the binding energies (i.e., isosteric heat of adsorption, $Q_{st}$). It should be pointed out that the differences in the thermodynamic state of the adsorbates can also contribute to the amount adsorbed.[200] Separation based on steric mechanism is a consequence of shape/size exclusion or molecular sieving effect, when some adsorbate species cannot get through the pore openings while others can. The kinetic mechanism is based on the differences of the rates of adsorption and transport for different adsorbates. Hydrocarbons with substantially faster adsorption kinetics will adsorb on an adsorbent well before those with slower kinetics.

## 2.2. Selective Adsorption of Hydrocarbons in MMOFs

Recent reports focusing on the adsorption behavior of hydrocarbons in MMOF structures have provided numerous examples where selective adsorption and sorptive separation may be achieved via one or a combination of the aforementioned mechanisms.

Among possible olefin/paraffin separation via equilibrium-based adsorption processes,[171,172,174,194,213,214] preferential adsorption of styrene (also known as vinyl benzene, VB) over ethylbenzene (EB) in MIL-53-Al serves as a good example.[171] The crystal structure of MIL-53-Al[215] is very similar to that of MIL-47.[216] Both are built on octahedral metal vertices of $V^{IV}$ (MIL-47) and $Al^{III}$ (MIL-53-Al) interconnected by bdc linkers. Both contain 1D channels of diamond-shaped cross-section, but they are more rigid in MIL-47 than in MIL-53-Al.[183] Liquid-phase competitive adsorption experiments using heptane as a noninteracting solvent were carried out at room temperature (298 K).[171] Both compounds displayed preferred adsorption of VB over EB. A comparison of apparent adsorption enthalpies of the two showed that they are comparable in MIL-47, but significantly different in MIL-53-Al. The values are −9.0 kJ/mol (VB) and −10.1 kJ/mol (EB) for MIL-47, and −24.2 kJ/mol (VB) and −13.1 kJ/mol (EB) for MIL-53-Al, respectively. The enthalpy loss of EB in MIL-53-Al was attributed to the structure distortion induced by EB which took place only in the more flexible framework of MIL-53-Al. The same trend was found from vapor-phase adsorption experiments where adsorption


dx.doi.org/10.1021/cr200216x |*Chem. Rev.* 2012, 112, 836–868

enthalpies obtained at low-loading were consistent with the liquid-phase data (−59.1 and −48.9 kJ/mol for VB and EB, respectively). The selective adsorption of dimethylether (DME) over methanol in Zn(tbip) represents another interesting example of sorptive separation based on equilibrium mechanism. [Zn(tbip)] is a guest-free MMOF featuring 1D microchannels.[106] Tetrahedral zinc metal centers (as PBU) are linked by tbip ligands to yield a 3D framework containing hexagonal close-packed 1D open channels of a small window diameter (∼4.5 Å, excluding the van der Waals radius of hydrogen). The phenyl rings of the tbip ligands that form the channel walls are oriented in such a way that all *tert*-butyl groups protrude into the channels, making the material highly hydrophobic and essentially absorb no water (<∼1 mg/g at room temperature and $P/P_o$ = 0.65). The DME adsorption shows a typical Type-I profile, while no MeOH adsorption occurs until a pressure threshold is reached, at which point, capillary condensation takes place. The pressure threshold increases as a function of temperature. Thus, Zn(tbip) exhibits the potential for the separation of DME from MeOH. For example, facile separation of DME can be performed by selective adsorption at a given $T$ and $P$ that is below the MeOH capillary condensation point. Clearly, such a process is based on the difference in the adsorbate−adsorbent interactions. The isosteric heat of DME adsorption computed from adsorption isotherms at $Q$ = 10 mg/g loading is 51 kJ/mol, which is much higher than that of MeOH when the adsorbate−adsorbate contribution is excluded.

Industrial separation of C2−C4 olefins from paraffins is one of the most energy- and cost-intensive distillation-based technologies.[217,218] Our recent studies reveal that kinetic separation of propane ($C_3^\circ$) and propene ($C_3^=$) by metal-imidazolate zeolitic framework (ZIF) materials is highly feasible as a result of the remarkable differences in their diffusion rates through the pores.[189] Under equilibrium conditions, [Zn(2-mim)$_2$] (ZIF-8, 2-mim = methylimidazole)[219,220] adsorbs essentially the same amount of $C_3^\circ$ and $C_3^=$, 155 and 160 mg/g at 30 °C and 600 Torr, respectively. Additionally, their isosteric heats at low loading are 34 and 30 kJ/mol, respectively, indicative of similar adsorbate−adsorbent interactions for the two systems. While thermodynamic separation is impractical for this particular case, a striking difference in the adsorption rates was noticed. At 30 °C, the ratio of their diffusion rate coefficients, $D(C_3^\circ)/D(C_3^=)$, is 125, suggesting a high possibility in kinetic separation of these two very similar molecules. Of course, for a more rigorous treatment of diffusion control in a separation process the measurement of counter-diffusivities is required.[131,221] It should be mentioned that in this case, although the size difference is minimal (0.2−0.3 Å) for the two molecules,[222] the energy barriers can be very different. The activation energies of propene and propane to pass through the pore openings are calculated to be 9.7 and 74.1 kJ/mol, respectively, for [Zn(2-cim)$_2$] (2-cim = 2-chloroimidazole). The very large variation in their activation energies for diffusion is clearly the main reason for the remarkable difference in their diffusion rates. The effective size of the pore opening is believed to be the dominating factor for the separation capability in a number of previously reported systems, including several crystallographic eight-membered ring (8MR) zeolites, where separation was controlled critically by the window size of the cages,[43,44,223−228] although the window flexibility effects observed in zeolites may sometimes be quite different from those found in MMOFs.[221,229] In addition, [Cu$_3$(btc)$_2$][230] and MIL-100 (Fe)[231] also show capability for separation of propane and propene via preferential adsorption of propene. Separation of ethane and ethene may be achieved using ZIF-8 membrane.[232]

Multiple effects on the sorptive separation of three hexane isomers, *n*-hexane (nHEX), 3-methylpentane (3MP) and 2,2-dimethylbutane (22DMB), in Zn(bdc)(ted)$_{0.5}$ have been discussed in several recent experimental and simulation studies.[170,212,233] Zn(bdc)(ted)$_{0.5}$ is a 3D framework structure composed of three intersecting channels.[85,131] Two types of intersecting 1D channels exist in this tetragonal crystal system. The large channel runs along the *a*-axis with a cross section of ∼7.5 × 7.5 Å. The two smaller and identical channels are parallel to the *b*- and *c*-axis (cross section: ∼3.8 × 4.7 Å). While all three hexane isomers can be adsorbed in the larger channel, the smaller channels can only take up linear nHEX (having smaller kinetic diameter) and exclude branched 3MP and 22DMB, due to size exclusion (steric effect). The nHEX also interact more strongly with the framework than the other two isomers (equilibrium effect). As a result, Zn(bdc)(ted)$_{0.5}$ adsorbs a significantly larger amount of nHEX than those of 3MP and 22DMB. Separation of nHEX from 3MP and 22DMB could be achieved by fixed-bed adsorption via binary breakthrough experiments.[170]

Numerous MMOFs are found to be capable for separating hydrocarbons based on a steric effect. MIL-96, with a formula of $Al_{12}O(OH)_{18}(H_2O)_3(Al_2(OH)_4)[btc]_6\cdot 24H_2O$ (btc = 1,3,5-benzenetricarboxylate), was first reported in 2006.[136] It has three types of cages, among which only two (A- and B-type) are accessible after removal of water molecules by thermal activation. Both have a small window size of ∼5 Å. The compound adsorbs a large amount of *trans*-piperylene (or *trans*-1,3-pentadiene, ∼12 wt %), but significantly less of both *cis*-piperylene and isoprene (3−4 wt %).[172] While all three hydrocarbons are C5 diolefins with similar zero-coverage adsorption enthalpies (−52.1, −53.0, and −54.6 kJ/mol for isoprene, *cis*- and *trans*-piperylene, respectively), the geometry of *trans*-piperylene allows a much better fit of this C5 isomer to the shape and size of the pores, resulting in packing of multiple molecules within a single cage. This is not possible for the other two C5 species. Similarly, C6 diolefin such as *trans*-1,3-hexadiene is only one $-CH_3$ longer than *trans*-piperylene, but its uptake is negligibly small (<1 wt %), as a result of length exclusion. The separation between the C5 isomers (e.g., *trans*- and *cis*-piperylene) or between C5 and C6 diolefins (e.g., *trans*-1,3-pentene and *trans*-1,3-hexadiene) can thus be regarded as a steric-based mechanism. [Cu(hfipbb)(H$_2$hfipbb)$_{0.5}$], a 3D structure containing segmented channels of small pore diameter, has demonstrated strong capability of separating short-chain normal hydrocarbons (C4 or less) from all branched and all long-chain normal hydrocarbons (>C4) via a size exclusion effect.[107] This unusual behavior is due to the shape of the MOF pore structure: the straight 1D channel is composed of a periodic array of cages (∼5.1 × 5.1 Å) with a small neck (∼3.2 × 3.2 Å) at a length of ∼7.3 Å. This length is just greater than that of *n*-C4 (∼6.4 Å) and just smaller than that of *n*-$C_5$ (∼7.7 Å). Thus, normal paraffins and olefins of C4 and shorter chains can fit in the cage, while those of normal C5 or longer chains cannot. Although the neck is large enough to allow passage of the latter group, it is too small for this region to be an equilibrium position for them. On the other hand, all branched paraffins and olefins are excluded from entering the channels. To the best of our knowledge, all zeolites that adsorb *n*-C4 also take up normal hydrocarbons of longer chains and do not show such adsorption selectivity with a cutoff in carbon numbers.


dx.doi.org/10.1021/cr200216x |*Chem. Rev.* 2012, 112, 836–868

## 2.3. Adsorption: Methods and Characterization

**2.3.1. Experimental Methods.** One of the most important and commonly adopted experimental methods for characterization of an adsorption process is the measurement of gas adsorption isotherms at a fixed temperature.[234−238] Gas adsorption isotherms, namely, the adsorbed amount as a function of pressure can be obtained by volumetric or gravimetric method, carrier gas and calorimetric techniques, nuclear resonance as well as by a combination of calorimetric and impedance spectroscopic measurements.[234−237] Among these, the most frequently used are the volumetric (manometric) and gravimetric methods. The gravimetric method is based on a sensitive microbalance and a pressure gauge. The adsorbed amount can be measured directly, but a pressure dependent buoyancy correction is necessary. The gravimetric method is very accurate and convenient to use for the adsorption measurements not too far from room temperature. The adsorbent is not in direct contact with the thermostat, and it is thus more difficult to control and measure the exact temperature of the adsorbent at both high and cryogenic temperatures. Therefore, the volumetric method is recommended to measure the adsorption of nitrogen, argon, and krypton at the temperatures of liquid nitrogen (77.35 K) and argon (87.27 K).[238] The volumetric method is based on calibrated volumes and pressure measurements by applying the general gas equation. The adsorbed amount is calculated by determining the difference of the total amount of gas admitted to the sample cell with the adsorbent and the amount of gas in the free space. Hence, the void volume needs to be known very accurately. One way to determine this is to introduce a nonadsorbing gas such as helium prior to (or after) every analysis in order to measure the void (free space) volumes at room temperature and at the temperature at which the adsorption experiment is performed. The helium void volume measurement procedure is based on various assumptions: (i) Helium *is not adsorbed* on the adsorbent; (ii) helium does not penetrate into regions which are inaccessible for the adsorptive (e.g., nitrogen). However, these prerequisites are not always fulfilled, in particular, in the cases of microporous adsorbents. The use of helium can be avoided if the measurement of the void volume can be separated from the adsorption measurement by applying the so-called NOVA (NO void analysis) concept (see ref 234, Chapter 14). Further, the determination of the void volume can be completely avoided by using difference measurements, that is, an apparatus consisting of identical reference and sample cells, and the pressure difference being monitored by a differential pressure transducer. Correction for nonideality of the adsorptive in the cold zone also needs to be applied. Another complication is that for gas pressures below ca. 80−100 mTorr (i.e., $P/P_o < 10^{-4}$ for nitrogen and argon adsorption at 77 and 87 K, respectively) pressure differences along the capillary of the sample bulb on account of the Knudsen effect need to be taken into account (i.e., thermal transpiration correction).

Many hydrocarbons are in liquid phase at room temperature and ambient pressure. For adsorption isotherm measurements of these molecules under ambient conditions, a special design of vapor bubbler can be used to generate vapor of hydrocarbons from its liquid phase. In such cases, the temperature at which vapor is being generated is controlled to be below room temperature in order to avoid condensation in the pipeline during transportation of hydrocarbon vapors. The vapor pressure is controlled by a mass flow controller, ranging from 0−0.9 $P/P_o$ with the aid of nitrogen gas.[1,39,44,106,107,130,131,181,189,205,239]

Alternatively, adsorption of hydrocarbons in liquid phase can be measured using gas chromatography (GC).[171,172,174−177,240,241] A solvent that is incapable of being adsorbed and has no competitive effect with the adsorbate is selected as a carrier. The desired adsorbate concentration can be achieved by mixing the appropriate amount of the solvent and adsorbate, in the same manner as the pressure control in the vapor phase adsorption. It is interesting to compare isotherms obtained by vapor- and liquid-phase adsorption.[173,175−177] Comparable level of adsorption can be achieved in both cases for a given range of temperature, pressure, or relative concentration (R.C.), whereas the adsorption strength may vary. For example, the adsorption strength of C8 aromatics on MIL-47 is in the descending order of *p*-xylene, *o*-xylene, *m*-xylene, and ethylbenzene based on liquid-phase adsorption data at 298 K,[177] which is consistent with those of vapor-phase adsorption at 343 K.[175] However, such order changes at higher temperature. The adsorption strength of *p*-xylene in the vapor phase decreases much faster than other isomers and becomes weaker than *o*-xylene and even *m*-xylene as the temperature rises. As thermal energy increases along with increasing temperature, *p*-xylene as the longest isomer will have the most difficult time to achieve a dense and efficient packing at low pressure regime. Effectively packing and an ordered state may be reached only when the pressure is sufficiently high.

Another method, gas adsorption microcalorimetry, has recently been developed and reported for several zeolite and related microporous materials.[242] This technique can provide information on the surface state of an adsorbate, adsorption enthalpy, phase transition during an adsorption process, and adsorption mechanisms. Specifically, isotherms and adsorption enthalpy of various adsorbates can be obtained simultaneously at low temperature (77 K) and room temperature using a volumetric apparatus coupled with a Tian-Calvet type microcalorimeter. This method is currently being successfully applied to a number of MOF materials.[180,201,243,244] For example, hydrogen and alkane adsorption behavior in MIL-47(V) and MIL-53(Cr) as well as their interaction energies have been fully characterized.[180,201,243]

Diffusion studies of hydrocarbons in microporous MOF materials represent another new topic in adsorption related research. Transport properties of guest molecules are investigated by measuring their transport diffusivity and surface permeability employing state-of-the-art and high temporal and spatial resolution IR microimaging and interference (IF) microscopy.[245] For example, the diffusion behaviors of selected paraffins (e.g., ethane, propane, and *n*-butane) in Zn(tbip) have been analyzed in depth. Direct measurements of surface and transport resistances are made possible by these two techniques.[69,246−249]

**2.3.2. Modeling and Simulations.** Atomic and molecular level modeling and simulations provide essential tools to complement experimental methods to explain the adsorption associated phenomena, to help understand the principle of adsorption, and to provide insight and guidelines for future experiments.[105,250,251] Grand canonical Monte Carlo (GCMC) simulation is the most extensively used method for calculation of equilibrium adsorption isotherms and isosteric heats of adsorption. The conventional Monte Carlo method works very well for noble gases and small molecules but is insufficient for long chain hydrocarbons.[52,252−256] The configurational-bias Monte Carlo (CBMC) method has subsequently been developed to deal with long chain molecules.[257] The original CBMC technique was developed for lattice models[258,259] and later extended to continuous models.[260] The method has been successfully used in


dx.doi.org/10.1021/cr200216x |*Chem. Rev.* 2012, 112, 836–868

simulating long chain, branched, and cyclic hydrocarbon adsorption in zeolites.[48,52,70,261−291]

The many unique and useful gas adsorption properties of microporous MOFs have prompted intense investigations not only by the experimentalists but also by theorists. Molecular simulation studies have been performed on a large number of systems with a variety of different structures. The computational studies are powerful and often complementary to the experiments.[105,110,122,212,233,292−297] Methane adsorption in IR-MOF-1,[110] one of most extensively investigated MOFs, illustrates a good example. The simulated $CH_4$ adsorption isotherm at 298 K and up to 40 atm matches almost perfectly with the experimental data over the entire pressure range, revealing that simulation can be a powerful tool to assess and predict the adsorption behavior and capacity of MMOFs, and to quantify adsorption energy and guest−host interactions. More recent simulation work on the adsorption of *n*-alkanes in $Co_3(fa)_6$ serves as another excellent case.[212] Isotherms of C3 through C8 alkanes are simulated employing the CBMC method, and molecular self-diffusivities are computed via molecular dynamics (MD) simulation. The simulation study not only confirms the experimentally observed commensurate−incommensurate adsorption phenomena but also offers helpful explanations and insight to such observations. The calculations show that for these alkane species, the chain length, which correlates with the commensurate−incommensurate behavior of the molecules, plays a key role in their nonmonotonic behavior in Henry coefficients and self-diffusivities.

In this work, we have included numerous simulation results using Cerius2 Sorption software (Accelrys, Inc.). This program module employs the GCMC method and Burchard Universal Force Field.[298] In a typical calculation, a box of 35−40 Å in each dimension is selected, which usually consists of multiple unit cell length along each crystallographic axis. Periodic boundary conditions are applied in all three dimensions. Usually $n \times 10^7$ ($n$ = 1−3) configurations are selected for a single simulation, depending on the energy convergence. Helium adsorption is simulated at a temperature of 1 K and pressure of 1 kPa. Simulations on hydrocarbon gas adsorbates are generally carried out under the same conditions used in experiments to mimic real-world conditions.

**2.3.3. Physical Properties of Adsorbates.** Physical properties of adsorbates are an important aspect regarding commensurate adsorption. The adsorption behavior and mechanisms are largely affected by the type and degree of adsorbate−adsorbent interactions, for which the molecular composition, shape and size, polarity, polarizability, diffusivity, and other properties of the adsorbate all play a dominant role.

The molecular models of selected hydrocarbons are built and their energies are optimized by Visualizer module (Matarial Studio 4.4, Accelrys Software Inc.). The optimized molecular structures are exported to Crystal Maker program (Version 6.1 for Mac OS, Crystal Maker Software Ltd.) from which physical dimensions of the molecules are determined. The size of each molecule is measured by its molecular length and the cross section, defined in Figure 3. Covalent radii (from built-in database of Material Studio 4.4) of the outmost atoms are added to both the length and diameter values. The saturated vapor pressure of hydrocarbons is calculated from the Antoine equation if the data are not directly available from the NIST Chemistry Webbook on thermophysical properties of fluid systems:

$$\log_{10} P = A - B/(C + T)$$

where $P$ is the vapor pressure of a hydrocarbon at given temperature $T$, and $A$, $B$, and $C$ are component-specific constants.

Relevant physical properties of hydrocarbon adsorbates are tabulated in Table 3, including the physical dimensions (length and diameter), kinetic diameter, critical temperature, and vapor pressure. The length of an adsorbate, L1, is defined to be the longest dimension of the molecule and is the distance between the centers of the two outmost atoms projected onto the *z*-axis, taken as the molecular axis (Figure 3a,c). The diameter of the molecule, D1, is taken to be the distance between the centers of the two outmost atoms projected onto the *xy* plane (Figure 3b,d).

## 3. COMMENSURATE ADSORPTION OF HYDROCARBONS IN MMOFS

### 3.1. Crystal and Pore Structures

Commensurate adsorption of hydrocarbons has been reported only in a few zeolite structure types. Most adsorption occurs incommensurately, meaning adsorbate molecules are randomly distributed in the pores. This is most likely due to the following two reasons: (a) the dimensions of the cages or channels in zeolite frameworks are generally much larger than the adsorbate molecules, and (b) the topology and symmetry of the cavities/pores do not correlate well to the shape and geometry of the adsorbate molecules. Adsorption of benzene and toluene in zeolite-Y serves as a good example to illustrate these points.[310−317] A random packing of five benzene molecules and three toluene molecules in a single supercage is shown in Figure 4, panels a and b, respectively.[310,317]

Unlike zeolites, commensurate adsorption much more commonly occurs in metal organic frameworks in the vicinity of room temperature,[1,2] especially in ultramicroporous structures (a subfamily of MMOFs with pore diameters less than 7 Å) or in supermicroporous structures (a subfamily of MMOFs having pore diameters between 7 and 20 Å) with a small pore window size.[103,130] In addition to small pores or windows, their pore structures usually possess a rich hierarchy of complexity, as a result of a vast variety of framework types and broad range of surface functionalization. Among numerous MMOFs for which commensurate hydrocarbon adsorptions have been observed, a majority have 1D open channel structures built on cavities (segment) with distinct shapes. For example, $[M_3(fa)_6]\cdot$DMF (M = Mn, Co, Ni) crystallize in a monoclinic crystal system in which the metal network has a diamondoid connectivity. The overall framework gives rise to a 1D zigzag channel system proceeding along the *b* axis.[130] The diameters of the cage and window of the "zig" or "zag" segment are 5.5 and 4.5 Å, respectively with a repeating length of 7.1 Å. Both $[M_3(bpdc)_3(bpy)]\cdot 4DMF\cdot H_2O$ (M = Co, Zn)[103,239] and $[Cu(hfipbb)(H_2hfipbb)_{0.5}]$[107] are characterized as 1D pore systems having straight channels. In the former, these channels are composed of alternating large diameter cages (~10.6 × 10.6 × 5 Å, calculated based on van der Waals radius of carbon) and smaller windows (triangular in shape with an effective maximum dimension of ~8 Å), while in the latter, the 1D channels consist of oval-shaped cages (~5.1 Å in diameter) at ~7.3 Å interval connected by narrow windows of ~3.2 Å in diameter. A brief description of pore structures (e.g., type of channels and pores, shape and dimensions of channel/pore segments) for selected compounds are presented in Table 4.


dx.doi.org/10.1021/cr200216x |*Chem. Rev.* 2012, 112, 836–868

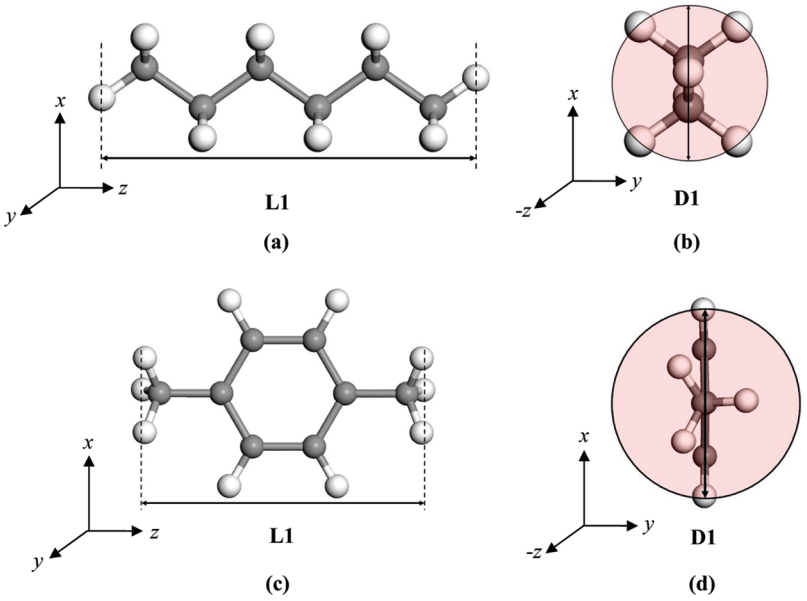


**Figure 3.** Illustration of molecular dimensions in the Cartesian coordinate system (*x*, *y*, z). L1 is along the *z*-axis and D1 is in the *xy* plane. (a, b) *n*-Hexane and (c, d) *p*-xylene. Color scheme: C (gray), H (white).

Hydrocarbon adsorptions that are commensurate with the MMOF structures have been found in both flexible and rigid frameworks. In this review, a rigid framework is referred to one that remains intact or is accompanied with only very minor changes in its crystal structure when guest or solvent molecules are removed. On the contrary, a flexible framework is associated with notable structure changes upon removal of guest/solvent molecules. In the following section, examples from both categories will be discussed and results from experimental adsorption measurements and simulation work will be analyzed and compared. The crystal structures of MMOFs selected from both groups are drawn in Figure 5. When crystal structures of guest-free compounds are not available simulations are generally performed using the as-synthesized (guest-containing) structures. In such cases, the results may deviate significantly from the real situation and should always be verified by experimental data.

## 3.2. Commensurate Adsorption in Selected MMOFs

**3.2.1. $[M_3(fa)_6]\cdot sol$ (M = Mg, Mn, Co, Ni).** The $[M_3(fa)_6]\cdot sol$ (M = Mg, Mn, Co, Ni; fa = HCOO or formate, sol = solvent molecule) series of compounds have very similar crystal structures (Figure 5a). Their frameworks are considered rigid since the crystal structures remain intact upon removal of the solvent molecules, evident from the powder X-ray diffraction (PXRD) patterns taken before and after guest removal. All $[M_3(fa)_6]$ frameworks embrace 1D zigzag channels.[130,133,208,211] Simulated helium filling in the channels outlines such features nicely, as shown in Figure 6a. The repeating unit of the channel comprises a "zig" and "zag" segment with a segment diameter of ~5.5 Å and window opening of ~4.5 Å. The length of a zig (or zag) segment is estimated to be ~7.1 Å (between the centers of the two outmost He atoms). Each unit cell (UC) contains two pairs of zigzag units or four distinct segments. Data from experimental adsorption isotherms (Table 5) indicate light alcohols such as ethanol, propanol, and butanol, and alkanes such as ethane, propane, and *n*-butane, all achieve an adsorption level of ~4 molecules/UC (or 1 molecule per channel segment).[130] The simulations reveal that the packing of these molecules is commensurate with the zigzag shaped pore structure of the channel, which also correlates very well with the shape outlined by He simulation (see Figure 6b,c). On the other hand, the uptake of methanol is 5.5 molecules/UC and those of pentanol and *n*-hexane are 2.2 and 2.1 molecules/UC, one-half loading with respect to short-chain alcohols and alkanes. For methanol, the strong intermolecular interactions coupled with the short length of the molecule (~4.1 Å) give rise to three molecules within a zigzag unit (see Figure S1, Supporting Information). Pentanol and *n*-hexane, with a molecular length of 8.8 and 8.9 Å, respectively, are too long to fit in a single segment.

The commensurate and incommensurate adsorption of linear alkanes (C1−C3 and *n*-C4−*n*-C7) in the $[Co_3(fa)_6]$ structure was also investigated by simulations employing the CBMC method.[212] For C1−C3 that are shorter than the segment length, the adsorption level was found to be 4 molecules/UC, while for *n*-C5−*n*-C7 that are longer than the length of a single segment, the loading is one-half of the C1−C3 group, with one molecule bestriding the two adjacent channel segments. This corresponds to 2 molecules/UC. With its molecular length slightly longer than the channel segment, *n*-C4 tends to extend slightly into the adjacent segment at lower pressure. At higher pressure, however, it adopts a more constrained conformation to fully fit within one segment. The simulation data are in excellent agreement with the experimental uptake values for C3 and *n*-C6, which yield 3.8 and 2.1 molecules per unit cell, respectively (Figure 7, Table 5). The simulation results also show that adsorption strength is in the order of C3 > C2 > C1, C3 > *n*-C4 > *n*-C5 and *n*-C7 > *n*-C6 > *n*-C5. In the case of short alkanes C1−C3, the channel segment is sufficiently large to house one molecule per segment, but C3 has a length that is more commensurate with the segment size, and therefore, interacts more effectively with the MMOF pore walls (higher adsorption strength). For longer alkane group *n*-C5−*n*-C7, the adsorption


dx.doi.org/10.1021/cr200216x |*Chem. Rev.* 2012, 112, 836–868

**Table 3. Physical Properties of Hydrocarbon Adsorbates**[299−309]

| | | size (Å)[a] | | | | | | | | |
|---|---|---|---|---|---|---|---|---|---|---|
| | | length | | diameter | | | | vapor pressure (Torr)[b] | | |
| | adsorbate | L1 | L2 | D1 | D2 | kinetic diameter (Å @298 K) | critical temp (K) | 291 K[c] | 298 K | 303 K |
| paraffins and olefins | methane | 1.9 | 2.6 | 2.1 | 2.8 | 3.8 | 190 | N/A | N/A | N/A |
| | ethane | 3.2 | 3.9 | 2.9 | 3.6 | 4.443 | 305 | 27049.0 | 31441.0 | 32369.9 |
| | acetylene | 3.5 | 4.2 | 0.0 | 0.7 | 3.3 | 308 | 31412.2 | 36864.2 | 41147.0 |
| | propane | 4.4 | 5.1 | 2.9 | 3.6 | 4.3−5.1 | 370 | 6115.4 | 7327.8 | 34904.0 |
| | 1-propene | 4.2 | 4.9 | 3.3 | 4.0 | 4.7 | 365 | 7263.9 | 8687.0 | 9813.7 |
| | *n*-butane | 5.6 | 6.4 | 2.9 | 3.6 | 4.7 | 425 | 1459.5 | 1821.2 | 2119.8 |
| | *n*-pentane | 6.9 | 7.7 | 2.9 | 3.6 | 4.5 | 470 | 392.4 | 512.5 | 614.9 |
| | *n*-hexane | 8.2 | 8.9 | 2.9 | 3.6 | 4.3 | 508 | 110.7 | 151.3 | 187.1 |
| | *n*-heptane | 9.5 | 10.2 | 2.9 | 3.6 | N/A | 540 | 31.2 | 45.1 | 58.0 |
| | *n*-octane | 10.8 | 11.5 | 2.9 | 3.6 | N/A | 569 | 8.5 | 12.9 | 17.2 |
| | *n*-nonane | 12.1 | 12.8 | 2.9 | 3.6 | N/A | 594 | 2.3 | 3.4 | 4.6 |
| | *trans*-butene | 5.3 | 6.0 | 3.3 | 4.0 | N/A | 429 | 1401.5 | 1759.3 | 2054.8 |
| | *cis*-butene | 4.7 | 5.5 | 3.2 | 3.9 | 4.2 | 436 | 1271.0 | 1602.1 | 1876.2 |
| | 2-methylpropane | 4.4 | 5.1 | 3.9 | 4.6 | 5.3 | 408 | 2133.3 | 2630.9 | 3035.8 |
| | 2-methylbutane | 5.6 | 6.4 | 3.9 | 4.6 | 5 | 460 | 534.2 | 688.0 | 823.1 |
| | 3-methylpentane | 6.9 | 7.7 | 3.9 | 4.6 | 5.5 | 504 | 140.6 | 189.8 | 232.9 |
| | 2,2′-dimethylpropane | 4.4 | 5.1 | 5.2 | 5.9 | 6.2−6.6 | 434 | 1022.1 | 1285.8 | 1503.8 |
| | *trans*-piperylene | 7.1 | 7.9 | 3.3 | 4.0 | N/A | ∼484 | 182.4 | 200.9 | 215.1 |
| | *cis*-piperylene | 6.1 | 6.9 | 3.2 | 3.9 | N/A | ∼484 | 166.1 | 183.2 | 196.4 |
| | isoprene | 6.0 | 6.7 | 4.5 | 5.2 | N/A | ∼484 | 253.1 | 277.6 | 296.3 |
| | *trans*-1,3-hexadiene hexadiene | 8.4 | 9.1 | 3.3 | 4.0 | N/A | 527 | N/A | N/A | N/A |
| | 2,2′-dimethylbutane | 5.6 | 6.4 | 5.2 | 5.9 | 6.2 | 489 | 241.9 | 319.1 | 385.4 |
| aromatics | cyclohexane | 5.1 | 5.8 | 4.4 | 5.1 | 6.0−6.2 | 554 | 70.5 | 97.6 | 121.7 |
| | benzene | 5.1 | 5.8 | 4.4 | 5.1 | 5.3−5.9 | 562 | 68.2 | 95.1 | 119.2 |
| | toluene | 5.8 | 6.6 | 4.4 | 5.1 | 5.3 | 592 | 19.6 | 28.5 | 36.7 |
| | *p*-xylene | 6.7 | 7.4 | 4.4 | 5.1 | 5.8 | 610 | 5.8 | 8.9 | 11.7 |
| | *o*-xylene | 5.8 | 6.6 | 5.5 | 6.3 | 6.8 | 630 | 4.3 | 6.6 | 8.8 |
| | *m*-xylene | 6.6 | 7.3 | 5.2 | 5.1 | 6.8 | 617 | 5.5 | 8.3 | 11.1 |
| | styrene | 7.6 | 8.4 | 4.4 | 5.1 | N/A | 646 | 37.7 | 51.6 | 64.0 |
| | ethylbenzene | 7.1 | 7.9 | 4.4 | 5.1 | 5.8 | 617 | 6.3 | 9.5 | 12.6 |
| alcohols | methanol | 3.3 | 4.1 | 2.1 | 2.8 | 3.6 | 513 | 87.4 | 127.1 | 164.0 |
| | ethanol | 4.3 | 5.1 | 2.9 | 3.6 | 4.5 | 514 | 38.9 | 59.0 | 78.5 |
| | *n*-propanol | 5.6 | 6.3 | 2.9 | 3.6 | 4.7 | 537 | 13.3 | 21.1 | 29.0 |
| | *n*-butanol | 6.8 | 7.6 | 2.9 | 3.6 | 5.0 | 553 | 3.9 | 6.7 | 9.6 |
| | *n*-pentanol | 8.1 | 8.8 | 2.9 | 3.6 | 6.7 | 582 | 1.3 | 2.3 | 3.5 |
| | *n*-hexanol | 9.3 | 10.1 | 2.9 | 3.6 | 6.2 | 610 | 0.5 | 0.8 | 1.2 |
| others | dimethylether | 4.3 | 5.1 | 2.2 | 2.9 | 4.3 | 467 | 3534.7 | 4349.0 | 5010.5 |

[a] L1 = longest dimension of the molecule and is the distance between the centers of the two outmost atoms projected onto the *z*-axis, taken as molecular axis (Figure 3a,c), L2 = L1 + covalent radii of the two outmost atoms. D1 = distance between the centers of the two outmost atoms projected onto the *xy* plane (Figure 3b, d), D2 = D1 + covalent radii of the two outmost atoms. [b] The saturated vapor pressure of hydrocarbons [calculated from Antoine equation as described above: $\log_{10}P = A - B/(C + T)$]. [c] 291 K is the temperature typically used to activate vapor from liquid hydrocarbons in our experiments.

is incommensurate and each molecule occupies two adjacent segments (the zigzag pair). The length of *n*-C7 has a better fit to the pore size and thus, a more effective interaction (higher adsorption strength) with the MMOF pore walls. A commensurate−incommensurate transition occurs at alkanes of intermediate length, *n*-C4 and *n*-C5.

It is interesting to note that methane behaves distinctly differently from methanol. While both molecules have a length that well fits within a channel segment, the shorter methane (2.6 Å) molecules show commensurate packing based on the simulation results, whereas the packing of longer methanol (4.1 Å) molecules is incommensurate and for each segment


dx.doi.org/10.1021/cr200216x |*Chem. Rev.* 2012, 112, 836–868

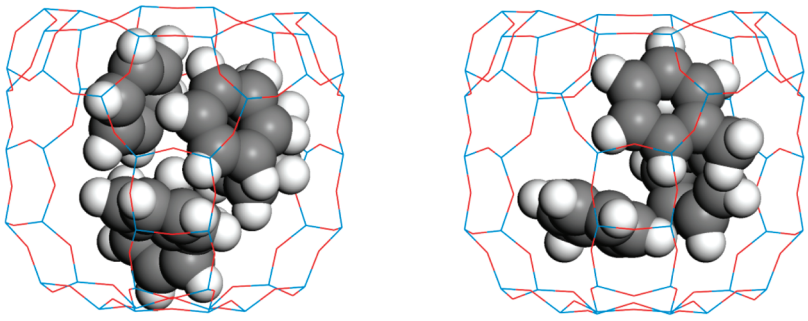

(a) (b)

**Figure 4.** Random packing of (a) benzene and (b) toluene in a single supercage of zeolite-Y. Color scheme: Si (blue), O (red), C (gray sphere), H (white sphere).

second molecule is adsorbed but straddles over to the adjacent segment. This is made possible because of strong intermolecular interactions among the $CH_3OH$ molecules (H-bonding, see Figure S1, Supporting Information), as indicated by a very high isosteric heat ($Q_{st}$ = 58 kJ/mol) which compensates for the energy loss from straddling (~1.5 molecules/segment). Such hydrogen bonding interactions are absent in the case of $CH_4$ ($Q_{st}$ = 29 kJ/mol), and thus, not a driving force for the straddling of a second molecule. The strong hydrogen bonding effect on adsorption of alcohols has also been found in several different zeolite structures.[323−325]

The adsorption of acetylene in the $[M_3(fa)_6]\cdot DMF$ (M = Mg, Mn) represents another case where the adsorbed molecules are commensurate with the pore and crystal structure. With the aid of the single-crystal X-ray diffraction technique, the structure of acetylene-adsorbed metal formate was determined at 90 K.[208] The acetylene molecules occupy one of the two independent positions (A and B) in a zig (or zag) channel at an uptake of 4 molecules per unit cell. This result is fully consistent with the data obtained from sorption experiments.[208]

In addition to linear hydrocarbons and alcohols, aromatic molecules were examined for their adsorption behavior. Interestingly, benzene also shows a strong sign of commensurate adsorption confirmed by adsorption experiment (3.94 molecules/UC), simulation, and single crystal X-ray diffraction (Figure 6d, Table 5).[130,327] Longer aromatic hydrocarbons, such as toluene, *p*-xylene, and ethylbenzene, are characterized by incommensurate adsorption because their sizes exceed the channel segment length. It is interesting to note that a significantly higher uptake amount of ethylbenzene (2.16 molecules/UC) than *p*-xylene (0.71 molecules/UC) is observed, regardless of the fact that the former is longer than the latter (7.9 and 7.4 Å, respectively).[130] This can be understood by examining the shapes and flexibility of the two molecules with respect to the zigzag pore segment. In ethylbenzene, the ethyl group is flexible and can be relatively easily extended and fit into the adjacent segment, whereas *p*-xylene is too rigid to be bent over into the neighboring segment, resulting in a very low uptake (Table 5).

**3.2.2. [Cu(hfipbb)($H_2$hfipbb)$_{0.5}$].** Cu(hfipbb)($H_2$hfipbb)$_{0.5}$ is a guest-free rigid 3D framework built on a common paddlewheel SBU (Figure 5b). Its pore structure features straight 1D channels composed of oval shaped cages (diameter ~ 5.1 Å) that are connected by small necks (diameter ~ 3.2 Å) at ~7.3 Å intervals.[239] This feature is clearly observable from the He simulation data depicted in Figure 8a. The compound displays unique adsorption properties which have been analyzed by both experimental methods and theoretical modeling.[1,107] Generally, [Cu(hfipbb)($H_2$hfipbb)$_{0.5}$] quickly adsorbs normal paraffins and olefins up to C4. Any normal paraffins and olefins longer than C4 and all branched hydrocarbons are excluded. Commensurate adsorption is observed for several gases, including propane and *n*-butane, where each cage takes one molecule (2 molecules/UC, see Table 5 and Figure 8b). Pentane has a molecular length that exceeds the cage limit, forcing it to extend into the adjacent cage through the small neck. Unlike $[Co_3(fa)_6]$, where the window opening is 4.5 Å, the very narrow neck in [Cu(hfipbb)-($H_2$hfipbb)$_{0.5}$] will lead to a very short H···H intermolecular distance (~1.86 Å) within this region, making it impossible as an equilibrium position for pentane to straddle. Gas-sorption simulations indicate that the channels are sufficiently large to allow passage of normal alkanes (diameters ~ 3.6 Å) of C5 and higher members but will exclude all branched alkanes which typically have diameters larger than those of normal alkanes.

The adsorption strength of alkanes follows the following order: propane > ethane > methane and propane > *n*-butane according to the Henry constants calculated from experimental isotherms at low loadings (Table S1, Supporting Information). Again this can be explained based on the commensurability of the adsorbates to the pore structure. Propane molecule has an optimal length and shape to best fit the cage cavity, showing the highest Henry constant among all alkanes. Butane adopts a slightly twisted configuration, similar to that observed in $[Co_3(fa)_6]$. The experimentally adsorbed 1.8 butane molecules/UC at 298 K and 1 atm is in excellent agreement with the uptake value of 2 molecules/UC modeled by molecular simulation. [Cu(hfipbb)($H_2$hfipbb)$_{0.5}$] is the first MMOF that shows capability of separating normal C4 from higher paraffins and olefins. Such behavior is unique with respect to zeolites, for which a cutoff carbon number for the adsorption of linear hydrocarbons has not been observed. Other MMOFs with a small pore opening or narrow neck sections between larger cages also demonstrate alkane separation capabilities following a similar mechanism.[172,328] In addition to paraffins and olefins, adsorption experiments and simulation are performed on methanol. The results are consistent and indicate that the adsorption of this molecule is also commensurate with the pore structure of [Cu(hfipbb)($H_2$hfipbb)$_{0.5}$] (Figure 8c).

**3.2.3. [$Cu_2$(pzdc)$_2$(pyz)]·2$H_2O$.** The framework of [$Cu_2$-(pzdc)(pyz)]·2$H_2O$ (pzdc = pyrazine-2,3-dicarboxylate, pyz = pyrazine, Figure 5c) is considered "rigid" with the understanding


dx.doi.org/10.1021/cr200216x |*Chem. Rev.* 2012, 112, 836–868

Table 4. Summary of Pore Structures of Selected MMOFs Exhibiting Commensurate Hydrocarbon Adsorption

| MMOFs[d] | pore structure | no. segment/UC | segment dimension (Å)[a] | refs |
|---|---|---|---|---|
| $[M_3(fa)_6]\cdot sol$ (M = Mg, Mn, Co, Ni, sol = solvent) | 1D zig-zag channel along the *b*-axis | 4 | Cage diameter: 5.5<br>Window size: 4.5<br>Length: 7.1[b] | 130,133,208,211 |
| $[Cu(hfipbb)(H_2hfipbb)_{0.5}]$ | 1D straight channel along the *b*-axis | 2 | Cage diameter: 5.1<br>Window size: 3.2<br>Length: 7.3 | 107 |
| $[Cu_2(pzdc)_2(pyz)]\cdot 2H_2O$ | 1D straight channel along the *a*-axis | 2 | Channel cross-section: 4.0×6.0<br>Length: ~4.7 | 318-319 |
| $[Al_{12}O(OH)_{18}(H_2O)_3(Al_2(OH)_4)(btc)_6]\cdot 24H_2O$ (MIL-96) | Two types of cages (Pore A and Pore B) | 2 for A<br>2 for B | Pore A:<br>Cage diameter: ~8.8<br>Window size: 4.5-5.5<br>Length: 8.9[b]<br>Pore B:<br>Cage diameter: ~8.8<br>Window size: 4.5-5.5<br>Length: 9.8[b] | 136,172 |
| $[Zn_2(bpdc)_2(bpee)]\cdot 2DMF$ (RPM3-Zn) | 1D straight channel along the *b*-axis | 4 | Cage size: 5.3×9.8[b,c]<br>Window size: ~5.1×8.8[b,c]<br>Length: 6.75 | 181,205 |
| $[Zn_2(bpdc)_2(bpe)]\cdot 2DMF$ (RPM4-Zn) | 1D straight channel along the *b*-axis | 4 | Cage size: 5.6×10.1[b,c]<br>Window size: ~4.5×8.0[b,c]<br>Length: 6.6 | 206 |
| $[V^{IV}O(bdc)]$ (MIL-47) | 1D straight channel along the *a*-axis | 2 | Cage dimensions: ~9.7 × 8.2<br>Window size: ~7.0 × 5.7[b]<br>Length: 6.8 | 216 |
| $[M^{III}(OH)(bdc)]$ (M = Al, Cr, Fe and Ga) (MIL-53ht) | 1D straight channel along the *a*-axis | 2 | Cr: Cage dimensions: 8.6×8.6[c]<br>Length: ~6.8<br>Al: Cage dimensions: 8.5×8.5[c]<br>Window size: ~7.2 × 5.3[b]<br>Length: ~6.6 | 176,215,320-321 |

[a] Taken from reported crystal data or based on simulated results when data are not available. [b] Distance between the centers of the two outmost He atoms calculated from the simulation data. [c] The window and cage size after removal of guest is approximated from the reported as-made structure. [d] fa = formate, $H_2$hfipbb = 4,4′-(hexafluoroisopropylidene)bis(benzoic acid), pzdc = pyrazine-2,3-dicarboxylate, pyz = pyrazine, btc = 1,3,5-benzenetricarboxylate, bpdc = 4,4′-biphenyldicarboxylate, bpee = 1,2-bis(4-pyridyl)ethene, bpe = 1,2-bis(4-pyridyl)ethane, bdc = 1,4-benzenedicarboxylate.

that while there is a gas pressure associated structure change, such a change is considerably smaller in comparison with those classified as "flexible" structures. Its pore structure consists of 1D cylindrical channels with a cross-section of 4 × 6 Å.[318,319,329] The channels are straight and run along the crystallographic *a*-axis, as easily visualized from Figure 9a. The adsorption isotherms of $C_2H_2$ measured at various temperatures (e.g., 270, 300, and 310 K) show that in all cases a maximum loading of 42 $cm^3/g$ (STP) is reached at relatively low pressure (between 5 and 60 kPa depending on the temperature), corresponding to one molecule per pore segment and 2 molecules/UC.[111] The uptake of $CO_2$, which has a similar size as $C_2H_2$ (both having a kinetic diameter of 3.3 Å), is significantly less at such pressures. The strong adsorption of acetylene was attributed to its high adsorption enthalpy as a result of strong hydrogen bonding between the uncoordinated oxygen atoms from the framework ligand and the hydrogen atoms in acetylene. The channel shape and relative positions of the O atoms, and the orientation and size of $C_2H_2$, allow the molecules to be packed in such a way to fit perfectly within the segments (Figure 9b). The periodic structure with adsorbed $C_2H_2$ at 10 kPa and 170 K was confirmed by the maximum entropy method (MEM) and Rietveld analysis using the synchrotron X-ray powder diffraction method.[111,319,326] Figure 10 shows that $C_2H_2$ molecules are located at the center of the pore segment and align along the *a*-axis with an inclination of 78.1°. The structure refinement shows that they are densely packed with an intermolecular distance of 4.7 Å, commensurate with the length of the *a*-axis and in excellent agreement with the experimental adsorption results.

**3.2.4. $Al_{12}O(OH)_{18}(H_2O)_3(Al_2(OH)_4)[btc]_6\cdot 24H_2O$ (MIL-96).** MIL-96 is a rigid 3D framework constructed from two inorganic structural motifs, a trimeric unit made of three corner sharing $AlO_5(H_2O)$ octahedra via a $\mu_3$-O, and a 2D net built on 1D interconnecting chains of corner-sharing octahedral $AlO_2(OH)_4$ and $AlO_4(OH)_2$ (Figure 5d).[136] The overall structure contains three types of cages, of which only two (A-type and B-type, two of each within a unit cell) are accessible to hydrocarbons. Both A-type and B-type cages have a very small window opening (between 2.5 and 3.5 Å) but large cage diameters (minimum ~8.8 Å). The pore volumes estimated from PLATON are ~420 and ~635 $Å^3$ for cages A and B, respectively. Upon removal of water molecules, the window aperture is enlarged to ~4.5−5.5 Å.[136] The cross sections of these cages estimated from our He simulations are 10.0 × 8.9 Å and 15.1 × 9.8 Å (center-to-center distances) for A and B, respectively. Their shape and size outlined by simulated He are shown in Figure 11. Single-component and competitive liquid-phase adsorption experiments on C5 hydrocarbons demonstrate high capability of MIL-96 for the separation of isoprene, *cis*- and *trans*-piperylene via selective adsorption.[172] The experimental single-component isotherms yielded a maximum uptake of 12 wt % for *trans*-piperylene (heptane as solvent, 298 K), which matches reasonably with the theoretical value of 13.2 wt % that corresponds to 2 molecules per cage or 8 molecules/UC. The uptakes of *cis*-piperylene and isoprene are considerably lower under the same


dx.doi.org/10.1021/cr200216x |*Chem. Rev.* 2012, 112, 836–868

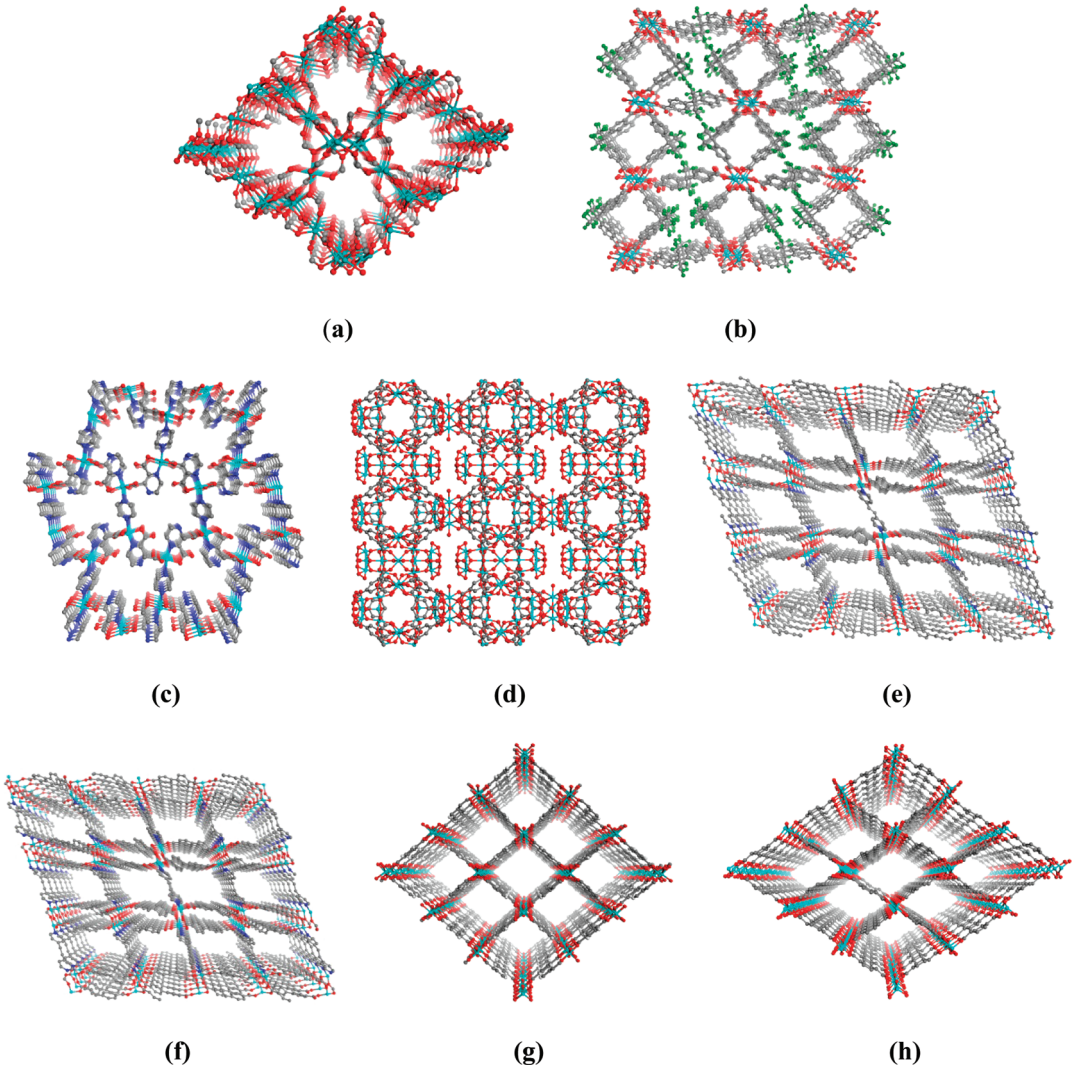


**Figure 5.** Crystal structures of guest-free MMOFs: (a) $[Co_3(fa)_6]$, (b) $[Cu(hfipbb)(H_2hfipbb)_{0.5}]$ (Cu(hfipbb)), (c) $[Cu_2(pzdc)_2(pyz)]$, (d) $[Al_{12}O(OH)_{18}(H_2O)_3(Al_2(OH)_4)(btc)_6]$ (MIL-96), (e) $[Zn_2(bpdc)_2(bpee)]$ (RPM3-Zn), (f) $[Zn_2(bpdc)_2(bpe)]$ (RPM4-Zn), (g) $[V^{IV}O(bdc)]$ (MIL-47), (h) $[Al^{III}(OH)(bdc)]$ (MIL-53ht). All structures are projected along channel direction except (e), which has two types of accessible cages. Color scheme: metal center (cyan), O (red), C (gray), N (blue), and hydrogen is omitted for clarify.

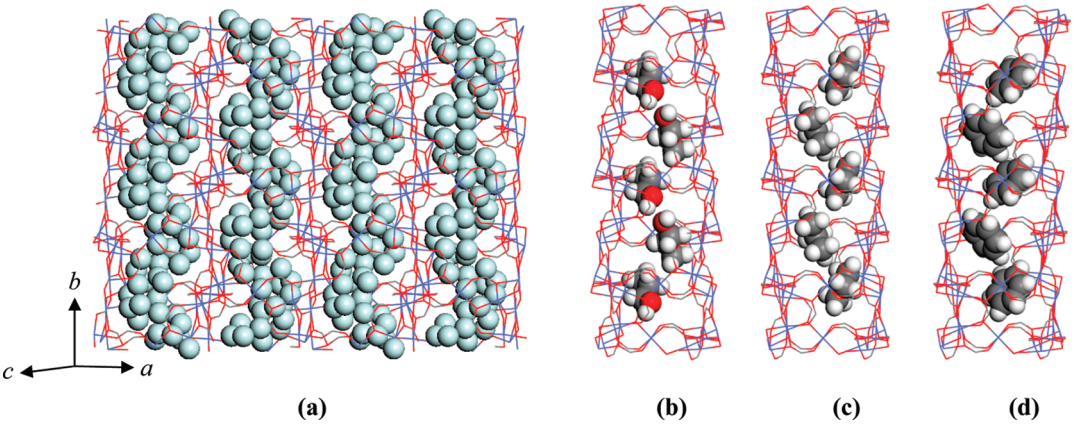


**Figure 6.** The simulated gas adsorption in the $[Co_3(fa)_6]$ structure. The 1D channels run along the crystallographic *b*-axis. (a) He at 1 K and 760 Torr; (b) *n*-propanol at 303 K and 12 Torr; (c) propane at 303 K and 684 Torr; and (d) benzene at 303 K and 61.4 Torr. Color scheme: Co (blue), O (red), C (gray), He (powder blue), H (white).


dx.doi.org/10.1021/cr200216x |*Chem. Rev.* 2012, 112, 836–868

**Table 5. Summary of Commensurate−Incommensurate Adsorption in Selected MMOFs[a]**

| MMOFs[&] | Adsorbate | Temp. (K) | Pressure (Torr) or R.C (M)[@] | Adsorbed amount (No. Molecule/UC) | | Qst (Exptl) (kJ/mol) | Refs. |
|---|---|---|---|---|---|---|---|
| | | | | Experiment[%] | Simulation/ Structure Refinement | | |
| $[M_3(fa)_6]$·sol (M = Mg, Mn, Co, Ni, sol = solvent)[$] | Methane | 303 | 684 torr | NRS* | 4 | 29 | 130,133,208,211-212 and this work |
| | Ethane | 303 | 684 torr | 3.74 | 4 | 43 | |
| | Propane | 303 | 684 torr | 3.82 | 4 | 43 | |
| | Propene | 303 | 684 torr | 3.81 | 4 | 49 | |
| | *n*-Butane | 303 | 684 torr | 3.75 | 4 | 61 | |
| | *n*-Pentane | 303 | 353 torr | 2.23 | 2 | - | |
| | *n*-Hexane | 303 | 100 torr | 2.1 | 2 | 54 | |
| | *n*-Heptane | 303 | 28 torr | 1.95 | 2 | - | |
| | *n*-Octane | 303 | - | - | 2 | - | |
| | Methanol | 303 | 85 torr | 5.47 | 6 | 58 | |
| | Ethanol | 303 | 41 torr | 4.06 | 4 | 62 | |
| | *n*-Propanol | 303 | 12 torr | 4.2 | 4 | 76 | |
| | *n*-Butanol | 303 | 3.5 torr | 4.0 | 4 | 56 | |
| | *n*-Pentanol | 303 | 1.2 torr | 2.2 | 2 | 60 | |
| | Benzene | 303 | 74 torr | 3.94 | 4 | 54 | |
| | Toluene | 303 | 18 torr | 2.84 | - | 64 | |
| | *p*-Xylene | 303 | 6.0 torr | 0.71 | - | 62 | |
| | Ethylbenzene | 303 | 5.8 torr | 2.16 | - | 56 | |
| | Acetylene | 196 | 760 torr | 4.0 | 4 | - | |
| $[Cu(hfipbb)(H_2hfipbb)_{0.5}]$ | Methane | 298 | 760 torr | 0.64 | - | - | 1,107 and this work |
| | Ethane | 298 | 760 torr | 1.06 | 2 | - | |
| | Propane | 298 | 760 torr | 1.53 | 2 | 47.8 | |
| | Propene | 298 | 760 torr | 1.23 | 2 | - | |
| | *n*-Butane | 298 | 684 torr | 1.79 | 2 | 52.3 | |
| | Methanol | 298 | 85 torr | 1.62 | 2 | 81.1 | |
| $[Cu_2(pzdc)_2(pyz)]·2H_2O$ | Acetylene | 270, 300, 310 | 760 torr | 2.0 | 2 | 42.5 | 111,318-319,326 |
| $[Al_{12}O(OH)_{18}(H_2O)_3(Al_2(OH)_4)(btc)_6]·24H_2O$ (MIL-96) | *trans*-Piperylene | 298 | 0.65M | 7.3 (L) | 8 | - | 136,172 and this work |
| | *cis*-Piperylene | 298 | 0.35M | 2.4 (L) | - | - | |
| | Isoprene | 298 | 0.35M | 2.0 (L) | - | - | |
| $[Zn_2(bpdc)_2(bpee)]$ ·2DMF (RPM3-Zn) | Methanol | 303 | 85 torr | 12.5 | - | 50.4 | 1,181,205 and this work |
| | Ethanol | 303 | 35 torr | 8.0 | 8[#] | 45.5 | |
| | *n*-Propanol | 303 | 11.8 torr | 8.0 | 8 | 57.3 | |
| | *n*-Butanol | 303 | 3.1 torr | 7.8 | 8 | 65.6 | |
| | *n*-Pentanol | 303 | 1.2 torr | 5.6 | - | - | |
| | Benzene | 303 | 61 torr | 7.8 | 8 | 44.5 | |
| | *p*-Xylene | 303 | 5.1 torr | 3.7 | 4 | 65.6 | |
| | *o*-Xylene | 303 | 3.8 torr | 3.9 | 4 | 55.6 | |
| $[Zn_2(bpdc)_2(bpe)]$ ·2DMF (RPM4-Zn) | Methanol | 303 | 85 torr | 7.9 | - | - | 206-207 and this work |
| | Ethanol | 303 | 41 torr | 5.7 | 8[#] | - | |
| | *n*-Propanol | 303 | 12 torr | 6.0 | 8 | - | |
| | *n*-Butanol | 303 | 3.5 torr | 5 | 4 | - | |
| | *n*-pentanol | 303 | 1.2 torr | 3.5 | 4 | - | |
| | Benzene | 303 | 74 torr | 4.8 | 4 | - | |
| | *p*-Xylene | 303 | 6.0 torr | 3.4 | 4 | - | |
| | *o*-Xylene | 303 | 3.9 torr | 2.2 | 4 | - | |


dx.doi.org/10.1021/cr200216x |*Chem. Rev.* 2012, 112, 836–868

**Table 5. Continued**

| MMOFs[&] | Adsorbate | Temp. (K) | Pressure (Torr) or R.C (M)[@] | Adsorbed amount (No. Molecule/UC) | | Qst (Exptl) (kJ/mol) | Refs. |
|---|---|---|---|---|---|---|---|
| | | | | Experiment[%] | Simulation/ Structure Refinement | | |
| [$V^{IV}$O(bdc)] (MIL-47) | *p*-Xylene | 298 | 0.8M | 3.1 (L) | 4 | 61.2 | 171,175,177 and this work |
| | | 343 | 30 torr | 3.4 | | | |
| | *o*-Xylene | 298 | 0.8M | 2.9 (L) | 4 | 59.6 | |
| | | 343 | 30 torr | 3.1 | | | |
| | *m*-Xylene | 298 | 0.8M | NRS* (L) | 4 | 59.7 | |
| | | 343 | 30 torr | 3.1 | | | |
| | Ethylbenzene | 298 | 0.8M | NRS (L) | 4 | 59.7 | |
| | | 343 | 30 torr | NRS | | | |
| | Styrene | 298 | 0.45M | 1.8 (L) | 8/3[#] | 57.0 | |
| | *n*-Octane | 343 | 38 torr | 1.9 | 2 | 65.7 | |
| [$Al^{III}$(OH)(bdc)] (MIL-53ht) | *p*-Xylene | 298 | 0.55M | 3.3 (L) | 4 | N/A | 171,173,176 |
| | | 343 | 27 torr | 2.8 | | | |
| | *o*-Xylene | 298 | 0.55M | 3.5 (L) | 4 | N/A | |
| | | 343 | 27 torr | 3.3 | | | |
| | *m*-Xylene | 298 | 0.55M | NRS (L) | 4 | N/A | |
| | | 343 | 27 torr | 2.9 | | | |
| | Ethylbenzene | 298 | 0.55M | NRS (L) | 4 | 48.9 | |
| | | 343 | 27 torr | NRS | | | |
| | Styrene | 298 | 0.45M | 1.9 (L) | 8/3[^] | 59.1 | |

[a] [@] R. C. = relative concentration of adsorbate in a non-interacting solvent, in unit of mol/L (M). [%] Vapor adsorption experiments. Those marked by (L) refer to liquid-phase adsorption experiments. [*] NRS = not reaching saturation. [$] All data are for [$Co_3(fa)_6$] except those of acetylene where the measurements were on [$Mg_3(fa)_6$] and [$Mn_3(fa)_6$]. [#] Crystal structure without guest removal is used in the simulations. [^] 4 pairs of styrene per triple unit cell [&] fa = formate, $H_2$hfipbb = 4,4′-(hexafluoroisopropylidene)bis(benzoic acid), tbip = 5-tert-butylisophthalicate, pzdc = pyrazine-2,3-dicarboxylate, pyz = pyrazine, btc = 1,3,5-benzenetricarboxylate, bpdc = 4,4′-biphenyldicarboxylic, bpee = 1,2-bis(4-pyridyl)ethane, bpe = 1,2-bis(4-pyridyl)ethane, bdc = 1,4-benzenedicarboxylate.

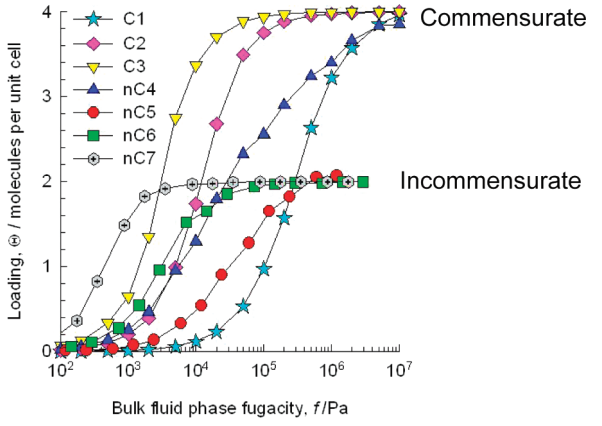


**Figure 7.** Adsorption isotherms of normal alkanes (C1−*n*-C7) in Co-FA at 300 K simulated by the CBMC method. Similar effects for both alkanes and alcohols were observed in cage type zeolite structures.[65,322] The figure was adapted with permission from Taylor & Francis Ltd: Molecular Simulation (Ref 212), copyright (2009).

experimental conditions, giving 0.6 and 0.5 molecules per cage, respectively. This difference was attributed to the steric effect as the molecular geometry of *trans*-piperylene allows a much better fit to the pore shape and more than one molecule can be packed within a single cage. Our simulated gas-phase adsorption of *trans*-piperylene gives 8 molecules per unit cell which agrees with the liquid-phase experiments, although the number of molecules in cages A and B is found to be 1 and 3, respectively (see Figure S2, Supporting Information), rather than 2 and 2 as previously assumed.[172]

**3.2.5. [$Zn_2$(bpdc)$_2$(bpee)]·2DMF (RPM3-Zn).** [$Zn_2$(bpdc)$_2$(bpee)]·2DMF (or RPM3-Zn, RPM = recyclable porous material) is a highly flexible 3D structure containing 1D straight channels running along the *b*-axis (Figure 5e). The channel is made of repeating segments (length of 6.75 Å, coincident with the unit cell length of the *b*-axis) having a parallelogram-shaped cross-section (cage and window sizes of ∼5.3 × 9.8 Å and ∼5.1 × 8.8 Å, respectively, estimated from the He simulated data using the as-synthesized [$Zn_2$(bpdc)$_2$(bpee)]·2DMF structure (Figure 12a and Table 4). Each unit cell contains four segments.[181,205] Gas adsorption experiments and simulations on selected hydrocarbons show that the uptake levels of benzene, *p*- and *o*-xylene are all indicative of adsorption commensurate with the pore and crystal structure.[1,181] For benzene, each segment takes up 2 molecules (or 8 molecules/UC), and the ring planes of the pair are not perfectly parallel but with an angle (Figure S3, Supporting Information). The molecules pack in zigzag fashion within the 1D channel[330] (Figure 12b). *p*-Xylene (length of 7.4 Å), on the other hand, is significantly longer than benzene (5.8 Å) and thus is limited to


dx.doi.org/10.1021/cr200216x |*Chem. Rev.* 2012, 112, 836–868

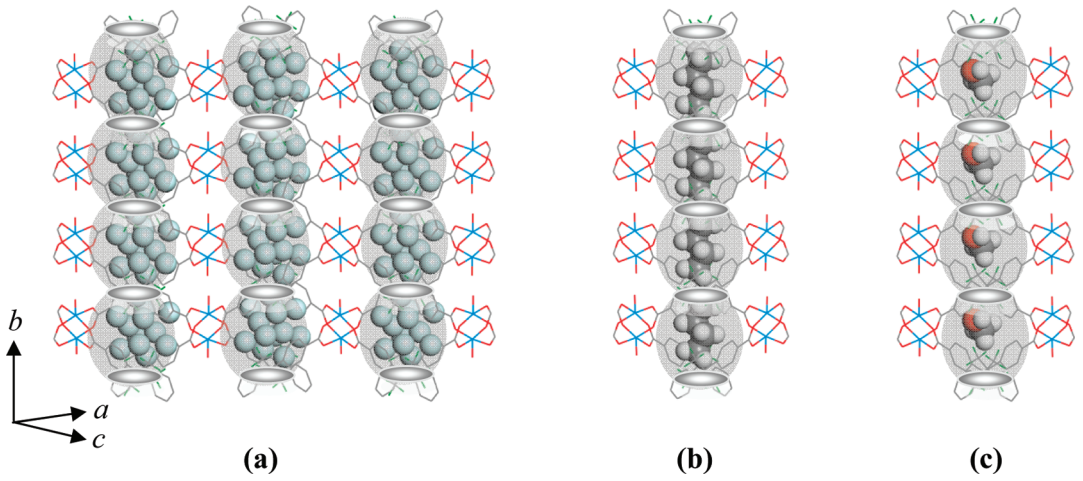


**Figure 8.** The simulated gas adsorption in the [Cu(hfipbb)($H_2$hfipbb)$_{0.5}$] structure. The 1D channels run along the crystallographic *b*-axis. (a) He at 1 K and 760 Torr; (b) *n*-butane at 303 K and 684 Torr; (c) methanol at 303 K and 78.7 Torr. Color scheme: Cu (light blue), O (red), C (gray), F (green), He (powder blue), H (white).

1 molecule per segment (4 molecules/UC). Simulations show that it packs in either a "zig" or a "zag" orientation (Figure 12c and Figure S3, Supporting Information) within a single channel of ~40 Å, which is presumably affected by how the first molecule enters the channel. Once the first molecule is adsorbed, subsequent molecules in that channel will pack along the same orientation. Simulations also show that *p*-xylenes in adjacent channels appear to pack independently with respect to the neighboring channels. *o*-Xylene, a bulkier isomer with lower symmetry, also follows an ordered adsorption pattern at a uptake of 1 molecule per channel segment (4 molecules/UC). The orientations of these molecules are slightly different in the adjacent channels, indicated as (I), (II), and (III) and shown in Figure S4, Supporting Information.

The normal C2−C4 alcohols also exhibit commensurate adsorption in RPM3-Zn near room temperature. The adsorption isotherms of both propanol and butanol display some interesting features. At 25 and 30 °C, a plateau approaching 2 molecules per pore segment (8 molecules/UC) is clearly visible (see Figure 13), which is also confirmed by simulation (Figure 12d). Having a similar length as benzene (5.8 Å), propanol (6.3 Å) also adapts the same zigzag packing configuration as benzene molecules within each channel. At higher temperatures (e.g., 50−75 °C), however, its adsorption isotherms show an inflection at a loading of ~2 molecules. Whether this behavior is due to a structure change will need to be verified by further study. For butanol, the 25 °C experimental adsorption isotherm is a classical type-I adsorption but at higher temperatures (30−40 °C), its isotherms resemble more of a type-II adsorption.[234] At and above 45 °C, the curves are essentially type-I with an adsorption limit of ~5.5 molecules/UC. Having a linear chain length of 7.6 Å, butanol seems too long to have the same adsorption capacity as propanol (8 molecules/UC), as it is more comparable with *p*-xylene (7.4 Å) of similar length (4 molecules/UC). A possible explanation is that at lower temperature (e.g., 25 °C), the butanol molecule adopts a nonlinear conformation, allowing it to pack 2 molecules per pore segment. This conformation becomes unstable at higher temperatures, therefore reducing the amount adsorbed.

**3.2.6. [$Zn_2$(bpdc)$_2$(bpe)]·2DMF (RPM4-Zn).** [$Zn_2$(bpdc)$_2$(bpe)]·2DMF (RPM4-Zn, Figure 5f) is isotypic to RPM3-Zn, with the pillar ligand bpee replaced by bpe[206] and thus has a very similar 1D channel structure as RPM3-Zn before removal of solvent (guest) molecules. The 1D open channels are made of identical segments (6.6 Å in length) with cage and window dimensions of 5.6 × 10.1 Å and 4.5 × 8.0 Å, respectively. Compared to RPM3-Zn, the carbon−carbon single bond between the two pyridine rings of the bpe ligand in RPM4-Zn leads to a higher degree of flexibility and further distortion of the pore structure upon evacuation of guest molecules. This is evident both from their PXRD patterns (before and after guest removal) and from their room temperature $CO_2$ adsorption isotherms that exhibit a hysteresis-free three- and two-step sorption for RPM4-Zn and RPM3-Zn, respectively.[206,207]

RPM4-Zn takes up a significantly less amount of benzene and *o*-xylene compared to RPM3-Zn. This is due to the more severe distortion of its framework upon guest removal, which leads to further reduction of its cage dimensions in the guest-free form. The benzene experimental adsorption isotherm at 30 °C only corresponds to a loading of ~1 molecule per channel segment, half of that of RPM3-Zn under the same conditions. For *o*-xylene, the uptake is reduced to ~0.5 molecule per channel segment, also about one-half of that for RPM3-Zn. In the case of *p*-xylene, a loading of 0.84 molecules per channel segment is achieved, comparable to 0.93 molecules per channel segment for RPM3-Zn. Simulated adsorption of *p*-xylene gives a loading limit of 1 molecule per channel segment, consistent with the experimentally observed uptake. The different adsorption levels of benzene, *o*-xylene, and *p*-xylene can be explained by molecular size. All three molecules lie approximately parallel to the longest side of the cage. As shown in Figure 14, such orientation requires the molecular width to be comparable with the length of pore segment (or the length of *b* axis, 6.6 Å). The widths of benzene and *p*-xylene are both ~6.6 Å (hydrogen VDWs radius included), and slight tilting allows each to fit fully within a segment. However, the *o*-xylene is more bulky with a width of 7.7 Å, too long to fit completely within a single segment, thereby reducing the uptake level of about one-half of benzene and *p*-xylene (one molecule per two segments).

As in the cases of aromatic hydrocarbons, all alcohols tested also show significantly lower adsorption amount in RPM4-Zn. Methanol and *n*-pentanol have an adsorption level of 2 and 1


dx.doi.org/10.1021/cr200216x |*Chem. Rev.* 2012, 112, 836–868

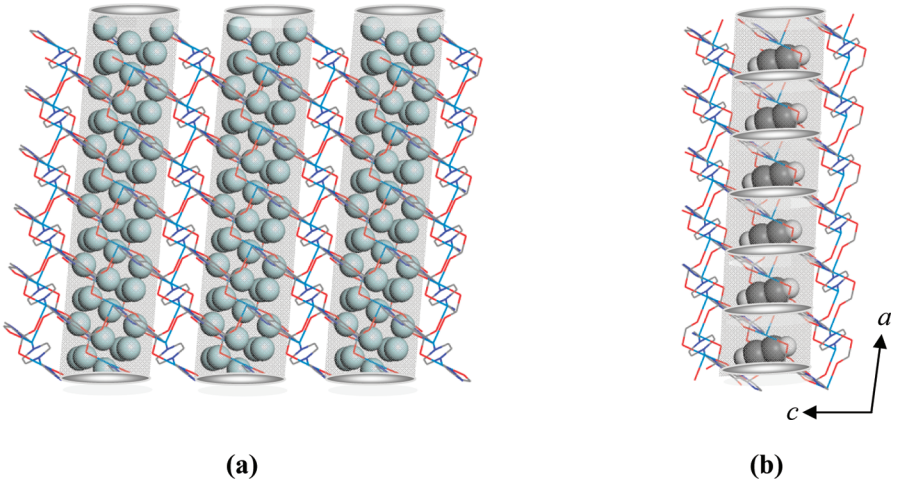


**Figure 9.** The simulated gas adsorption in the $[Cu_2(pzdc)_2(pyz)]$ structure. The 1D straight channels run along the crystallographic *a*-axis. (a) He at 1 K and 760 Torr; (b) acetylene at 303 K and 684 Torr. The channel is divided into "segments" to guide the eyes. Color scheme: Cu (light blue), O (red), C (gray), N (dark blue) He (powder blue), and H (white).

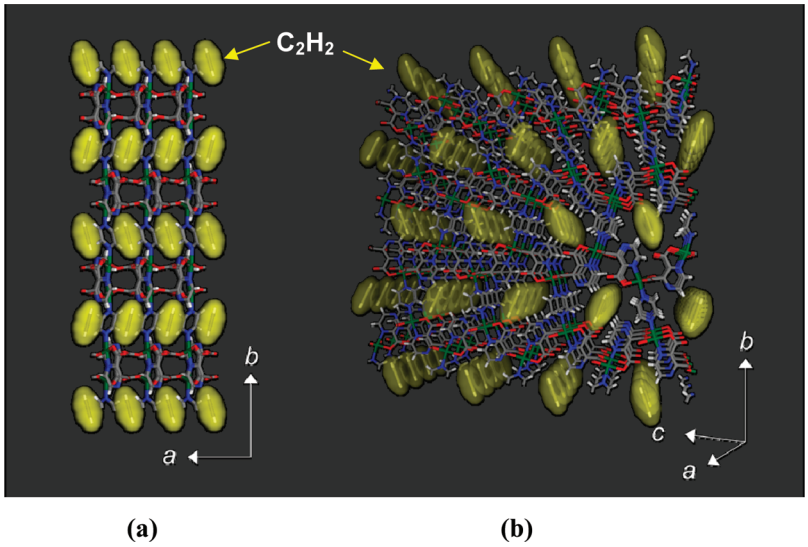


**Figure 10.** The $C_2H_2$ loaded $[Cu_2(pzdc)_2(pyz)]$ structure (170 K) from MEM/Rietveld analysis. (a) View along the *c*-axis. (b) Perspective view along the *a*-axis. Color scheme: Cu (green), O (red), C (gray), N (blue), and H (white). The figure was adapted by permission from Macmillan Publishers Ltd: Nature (Ref. 111), copyright (2005).

molecule per channel segment, respectively, indicating commensurate adsorption, while they are not commensurate in the case of the RPM3-Zn. On the other hand, ethanol, *n*-propanol, and *n*-butanol no longer show commensurate adsorption, giving less than 2 molecules per channel segment. These observations are consistent with the relative pore size and pore volume in the two structures and suggest that the cutoff limit of molecule length for commensurate adsorption shifts to a lower value in RPM4-Zn.

**3.2.7. $[V^{IV}O(bdc)]$ (MIL-47).** $[V^{IV}O(bdc)]$ (MIL-47) is the guest-free form of $[V^{III}OH(bdc)]\cdot 0.75(H_2bdc)$ (MIL-47as). The crystal structure of MIL47as is made of 1D chains of corner-sharing $VO_6$ octahedra interconnected by 1,4-benzenedicarboxylate (bdc) to give a 3D network.[216] Upon heating, the guest $H_2bdc$ molecules filling the pores can be removed, and the $\mu_2$-OH groups are converted to $\mu_2$-O, resulting in a porous framework $[V^{IV}O(bdc)]$ (Figure 5g). MIL-47 embraces large-pore 1D straight channels parallel to the crystallographic *a*-axis with a diamond-shaped cross-section. These channels contain repetitive segments having cage and window sizes of 9.7 × 8.2 Å and 7.0 × 5.7 Å, respectively (2 segments/UC). The length of the channel segment is 6.82 Å, coinciding with the length of *a*-axis. These features are apparent from the simulated He pattern shown in Figure 15. It should be pointed out that we have classified MIL-47 as a "flexible" structure based solely on the fact that its crystal structure is significantly different from that of MIL-47as, the as-synthesized parent structure before evacuation (to be consistent with our grouping for all other structures included in this review). The framework of MIL-47 itself is generally considered "rigid", as it does not undergo a substantial structure change upon adsorption and desorption of hydrocarbons (with a few exceptions).[171,177,180,331]

A number of recent experimental and simulation studies have centered on its adsorption properties with regard to C8


dx.doi.org/10.1021/cr200216x |*Chem. Rev.* 2012, 112, 836–868

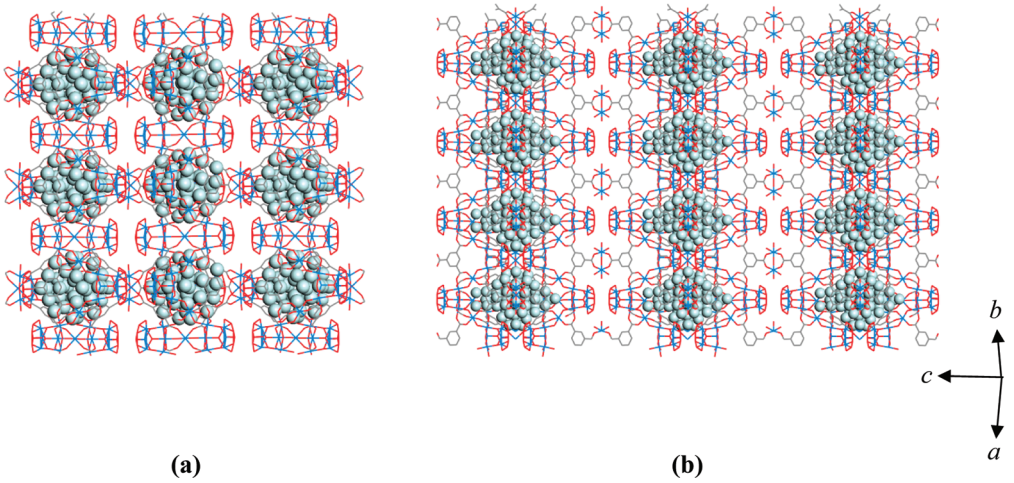


**Figure 11.** The simulated He adsorption in the MIL-96 structure at 1 K and 760 Torr. The size and shape of the two types of accessible pores are outlined by He atoms: (a) Type-A, and (b) Type-B. Color scheme: Al (light blue), O (red), C (gray), and He (powder blue).

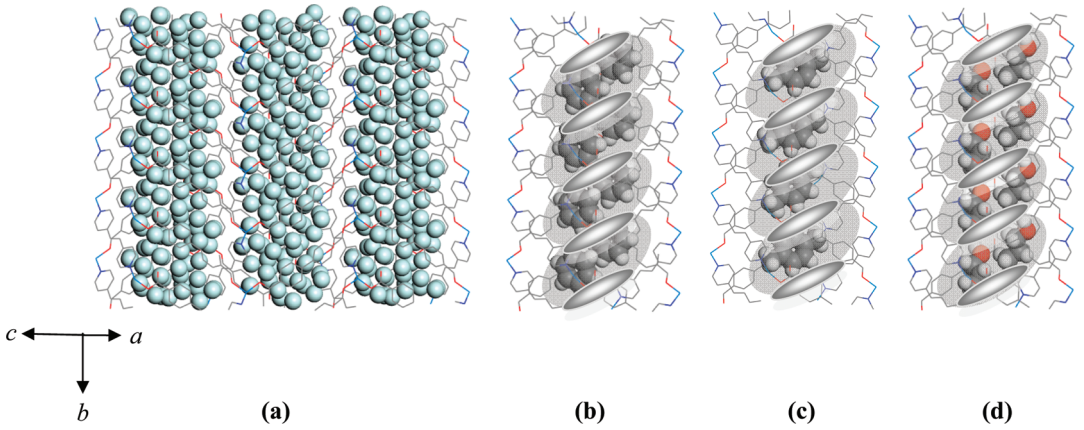


**Figure 12.** The simulated gas adsorption in the RPM3-Zn structure. The 1D channels run along the crystallographic *b*-axis. (a) He at 1 K and 760 Torr; (b) benzene at 303 K and 61.4 Torr; (c) *p*-xylene at 303 K and 5.2 Torr; (d) *n*-propanol at 303 K and 12.0 Torr. Color scheme: Zn (light blue), O (red), C (gray), N (dark blue), He (powder blue), and H (white).

hydrocarbons. Liquid-phase single-component and competitive adsorption experiments of C8 alkylaromatics on MIL-47 were performed in hexane solution at room temperature. *p*-Xylene and *o*-xylene show high uptakes and reach saturation at a loading of 37% and 35%, respectively, whereas a considerably lower adsorbed amount of *m*-xylene and ethylbenzene is noted.[177] Vapor-phase adsorption experiments carried out at various temperatures (e.g., 343, 383, and 423 K) yielded values that are consistent with liquid-phase experiments. At 343 K and up to 0.05 bar, the uptake amount approaches 4 molecules/UC for both *p*- and *o*-xylene and slightly lower for *m*-xylene and ethylbenzene.[175] The GCMC simulated adsorption isotherms at these temperatures show excellent agreement with the experimental results, giving a saturated loading of 4 *p*- and *o*-xylene molecules per unit cell.[331] As all four isomers have similar adsorption enthalpies, the higher adsorption level of *p*-xylene and *o*-xylene is attributed to their more effective packing.[175,177,331]

The location and orientation of these adsorbates were further determined by Rietveld refinements of synchrotron powder X-ray diffraction patterns of MIL-47 crystal samples saturated with individual C8 aromatics at room temperature,[175,177] and by GCMC molecular simulations at high temperature (343 K).[331] The refined structures show that all three xylene isomers form pairs within a pore segment at a loading of one pair per segment with a repeating distance of 6.8 Å along the *a*-axis, commensurate with the symmetry of crystal lattice. This accounts for 4 xylene molecules/UC. The results are in good agreement with the experimental sorption data of *p*- and *o*-xylene and are confirmed by the simulated adsorption isotherms performed at 343 K. The orientations and relative arrangement of the xylene isomers, however, are different, and such differences are attributed to the molecular geometry and pore structure. The *p*-xylene pair align their benzene rings nearly parallel to each other and to the bdc of the pore wall, with their methyl groups being staggered to each other. This packing is most effective for a strong $\pi-\pi$ interaction. The relative alignment of the *o*-xylene pair is similar to *p*-xylene, and their $CH_3$ groups are also in a staggered configuration but with a small angle between the two benzene rings the packing is less efficient. For *m*-xylene, the steric constraints between the aromatic ring of one molecule and a methyl group from a neighboring molecule force the pair to deviate from the arrangement most favorable for $\pi-\pi$ interaction.


dx.doi.org/10.1021/cr200216x |*Chem. Rev.* 2012, 112, 836–868

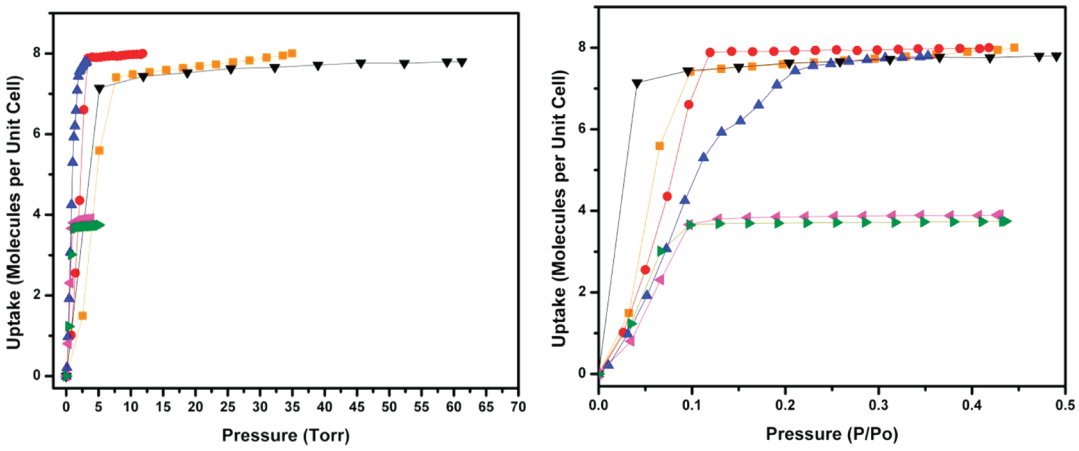


**Figure 13.** Adsorption isotherms of selected hydrocarbons and alcohols in RPM3-Zn at 30 °C plotted in (a) absolute pressure and (b) relative pressure, $P/P_o$. Color scheme: ethanol (orange), *n*-propanol (red), *n*-butanol (blue), benzene (black), *o*-xylene (pink), and *p*-xylene (green).

Different from the three xylene isomers, adsorption of C8 ethylbenzene causes significant changes in the lattice parameters of MIL-47. The relatively bulky ethyl group precludes a parallel alignment of two ethylbenzene molecules. Rather, they arrange themselves by aligning along the diagonal direction of the channel segment so that the two ethyl groups stay farthest apart from each other at the opposing corners of the rhombic-shaped pore. This arrangement favors O···H interactions between the $CH_3$ of the ethyl groups and the carboxylate of bdc ligands at the corners but greatly diminishes any $\pi-\pi$ interactions between the EB molecules and between the EB and framework. Consequently, nearly equal distanced molecules stack in a zigzag fashion within a single channel (2 EB/segment).

Separation of EB and styrene is an important part in petrochemical or petroleum refining processes.[332,333] Adsorption of styrene in MIL-47 represents another very interesting case. With a C═C double bond in place of a C−C single bond in EB, styrene is longer and more rigid than EB. Rietveld PXRD refinement reveals that while the molecules pair up as in the case of xylenes, the steric constraints make the commensurate stacking impossible to the unit cell dimensions.[171] As a result, tripling of the original length of *a*-axis is required to fit in two pairs of molecules within a single channel (four pairs per triple unit cell).

*n*-Octane, a C8 aliphatic molecule, is found to have higher adsorption enthalpy than the xylenes. This higher energy is a result of multiple O···H interactions between *n*-octane and the 1D chain of corner-sharing $VO_6$ of the MIL-47 framework. The parallel arrangement of *n*-octane molecules with respect to the $VO_6$ chain maximizes such interactions and results in 1 molecule per channel segment, as shown in Figure 15c. The simulated results are consistent with the experimental observations, which gives 23 wt % uptake at 70 °C (corresponding to 1.9 molecules/UC).[175]

CBMC simulations on lighter C1−C4 alkanes at 303 K show that these molecules do not exhibit commensurate adsorption in MIL-47.[180] The alkane molecules are randomly distributed within the pore space. The adsorption capacity increases as alkane length decreases. The simulated isotherms agree well with rescaled experimental data reported earlier.

**3.2.8. [$M^{III}$(OH)(bdc)] (M = Al, Cr, Fe and Ga) (MIL-53).** MIL-53 or [$M^{III}$(OH)(bdc)], where M denotes Al,[215] Cr,[320,321]

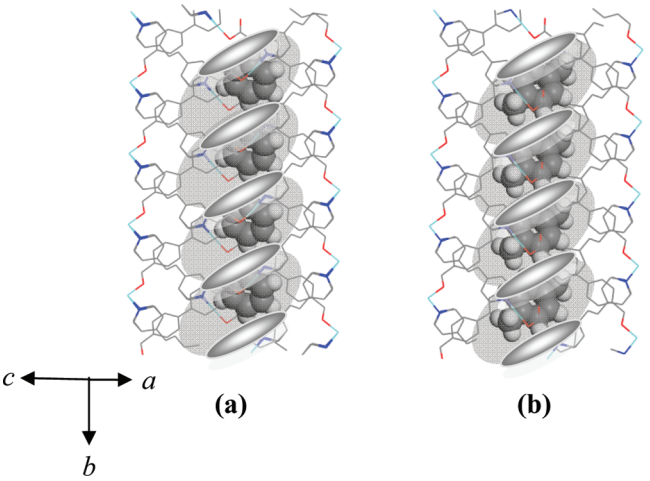


**Figure 14.** The simulated gas adsorption in the RPM4-Zn structure. The 1D channels run along the crystallographic *b*-axis. (a) Benzene at 303 K and 61.4 Torr; (b) *p*-xylene at 303 K and 5.2 Torr. Color scheme: Zn (light blue), O (red), C (gray), N (dark blue), and H (white).

Fe,[334] or Ga,[335] adopts the same structural topology as MIL-47as. In a MIL-53 crystal lattice, corner-sharing $MO_4(OH)_2$ (M = $Al^{3+}$, $Cr^{3+}$, $Fe^{3+}$ or $Ga^{3+}$) octahedra bridged by bdc ligands yield a 3D extended network containing 1D straight channels that feature a diamond-shaped cross section, as in the case of MIL-47. There are three structure forms, MIL-53as (as-synthesized form), MIL-53ht (guest-free high temperature form, Figure 5h), and MIL-53lt (hydrated low temperature form). Unlike MIL-47as, for which metal(V) undergoes an oxidation ($V^{3+}$ to $V^{4+}$) upon guest removal at elevated temperatures, the metal ion (M) in the guest-free form of MIL-53as, namely, MIL-53ht, retains its oxidation state (III). This is also the case for MIL-53-l; the hydrated structure formed spontaneously by adsorbing water in air upon cooling of the high temperature phase MIL-53ht. The three structures share the same type of 1D chains built on corner-sharing $MO_4(OH)_2$ octahedra, although their space groups and pore dimensions are all different. The cross sections of the cages are 7.5 × 9.2 Å, 8.6 × 8.6 Å, and 3.1 × 14.9 Å, for the Cr-based MIL-53as, MIL-53ht, and MIL-53lt


dx.doi.org/10.1021/cr200216x |*Chem. Rev.* 2012, 112, 836–868

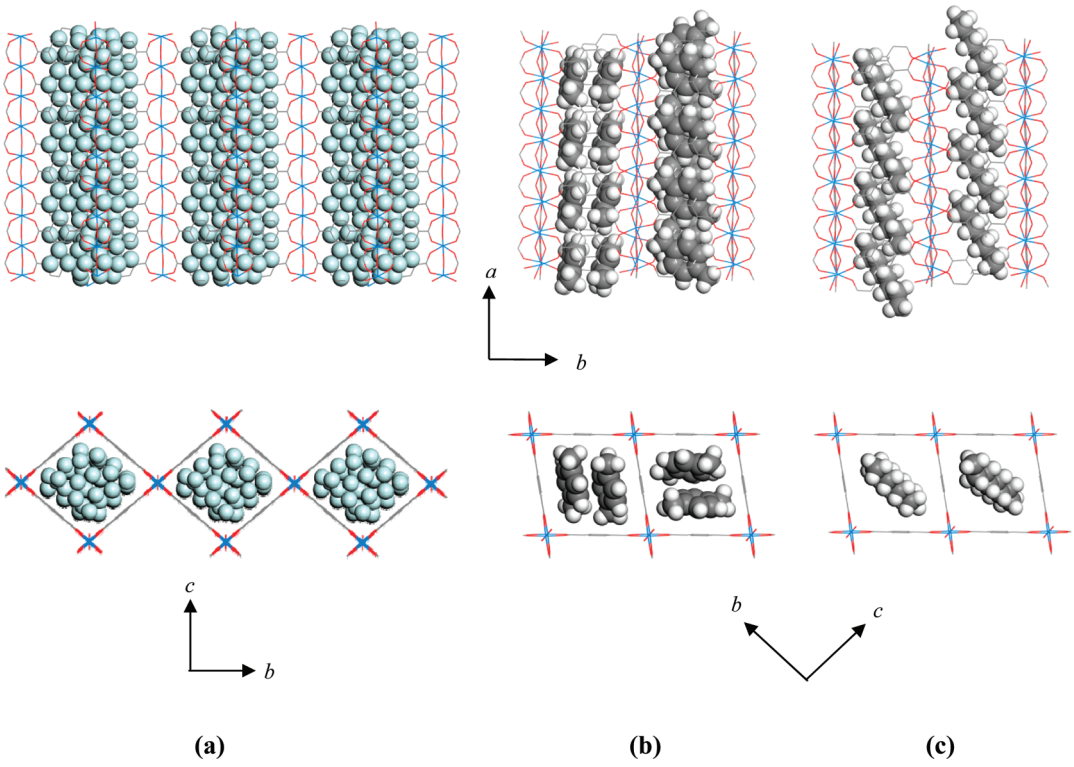


**Figure 15.** The simulated gas adsorption in the MIL-47 structure shown in two directions. (a) He at 1 K and 760 Torr; (b) *p*-xylene at 303 K and 11.7 Torr; (c) *n*-octane at 303 K and 17.2 Torr. The 1D channels run along the crystallographic *a*-axis. Color scheme: V (light blue), O (red), C (gray), He (powder blue), and H (white).

phases, respectively[320,321] and 7.3 × 7.7 Å, 8.5 × 8.5 Å and 2.6 × 13.6 Å for the Al-based MIL-53as, MIL-53ht, and MIL-53lt phases, respectively.[176,215] In addition, helium simulation was carried out to evaluate the window size of MIL-53ht(Al), which gives an estimated value of 7.2 × 5.3 Å (measured between the centers of the outmost He atoms), significantly smaller than the dimensions of the cages (11.2 × 6.9 Å), thus dividing the straight channels into segments (6.6 Å in length). Intensive and comprehensive investigations of the structure flexibility and adsorption properties of these compounds with different $M^{3+}$ metal centers have been reported.[96,121,171,176,177,182,202,215,320,336−340]

The single-component liquid-phase adsorption isotherms of C8 alkylaromatics in hexane were measured on MIL-53(Al) at room temperature (25 °C).[176] Both *o*- and *p*-xylene reached a plateau uptake of ∼45−46 wt % at a bulk concentration of ∼0.2 M and ∼0.5 M, respectively. The adsorbed amount is fairly close to 4 molecules/UC, or 2 molecules per channel segment. The uptakes of *m*-xylene and ethylbenzene were significantly lower at the maximum concentration of the experiment and far from reaching saturation. Room temperature Rietveld refinements of PXRD data were carried out on C8 alkylaromatic adsorbed MIL-53ht(Al) structures at high loading. The analysis revealed significant changes in the lattice parameters upon adsorption and different adsorption behavior of the C8 isomers. The geometric arrangement of *o*-xylene allows both of its methyl groups to interact with the bdc carboxylates and thus shows the strongest affinity to the framework. The refined structure manifests an efficient double-file packing of *o*-xylene within the channel (2 molecules/channel segment or 4 molecules/UC), commensurate with the pore structure and in excellent agreement with experimental isotherms. For *m*- and *p*-xylene, only one methyl group can be located in close proximity of carboxylate groups, and as a result, their interactions with the framework are weaker. *m*-Xylene has a higher interaction strength than *p*-xylene because its second methyl group and C2 carbon of the ring can interact with aromatic rings of the framework, while such interactions are not possible for *p*-xylene. Instead, the second methyl group of *p*-xylene interacts with the ring of an adjacent *p*-xylene molecule in a similar way as found in *p*-xylene loaded silicalite.[341,342] Ethylbenzene exhibits the weakest adsorbate−adsorbent binding among the four C8 isomers, because of the steric hindrance of its ethyl group that is absent in *m*- and *p*-xylene.

In addition to liquid-phase adsorption experiments, the vapor-phase adsorption isotherms of xylene isomers and ethylbenzene were measured at 110 °C by the same group.[173] The isotherms of all three xylene isomers feature a two-step profile with hysteresis, indicative of changes in the crystal structure during the adsorption process. For ethylbenzene, a kink rather than a step was observed in its adsorption isotherm. A similar adsorption level was achieved for all four molecules at the first inception point (∼0.003 bar), but at higher loadings (>0.03 bar) the amount of ethylbenzene adsorbed is considerably less than its xylene isomers. The uptake amount of xylene molecules corresponds to ≥3 molecules at the maximum pressure but clearly not reaching saturation. It is reasonable to envision a maximum loading of 2 molecules per channel segment, or double-file occupancy, as verified by the Rietveld structure refinements. The refinement results on *o*-xylene adsorbed structure show that structure transformation occurs between several phases as a function of hydrocarbon loadings, namely, MIL53as(Al)


dx.doi.org/10.1021/cr200216x |*Chem. Rev.* 2012, 112, 836–868

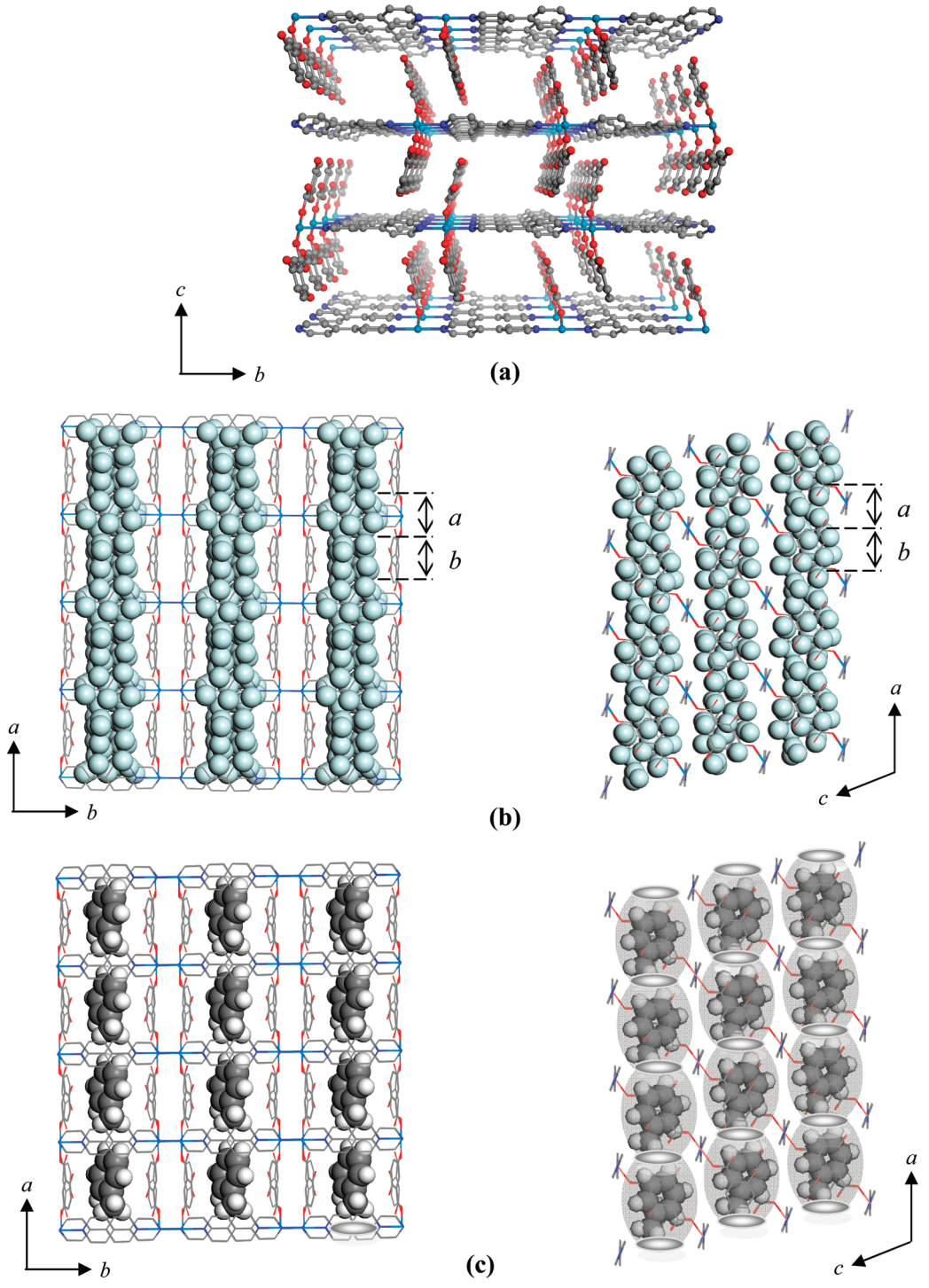


**Figure 16.** (a) Crystal structure of $[Cu(dhbc)_2(4,4'\text{-bpy})]\cdot H_2O$ viewed along the *a*-axis. (b) Simulated He gas adsorption (1 K and 760 Torr) outlining the 1D channels, viewed along the *c*- and *b*-axes. The channel segment is composed of two parts (*a* and *b*, overall length of 8.2 Å). (c) Simulated toluene adsorption at 303 K and 17.6 Torr, viewed from two directions; Color scheme: Cu (light blue), O (red), C (gray), N (dark blue), He (powder blue), H (white).

(dominating at very low loadings), MIL-53iX(Al) (dominating at intermediate loadings), and MIL-53ht(Al) (dominating at high loadings). The transition from a single-file (before infection point) to double-file (after inflection point) arrangement of adsorbed molecules depends on the molecular geometry, pore symmetry, and surface composition which governs the interaction strength of individual isomers with the host and their adsorption behavior.

Alkanes adsorption has also been reported on several MIL-53(M) compounds (M = Al,[183] Cr,[179,180,183,201] Fe[202]). For MIL-53(Al) and MIL-53(Cr), generally the adsorption capacity increases as the size of alkane decreases. Most of the


dx.doi.org/10.1021/cr200216x |*Chem. Rev.* 2012, 112, 836–868

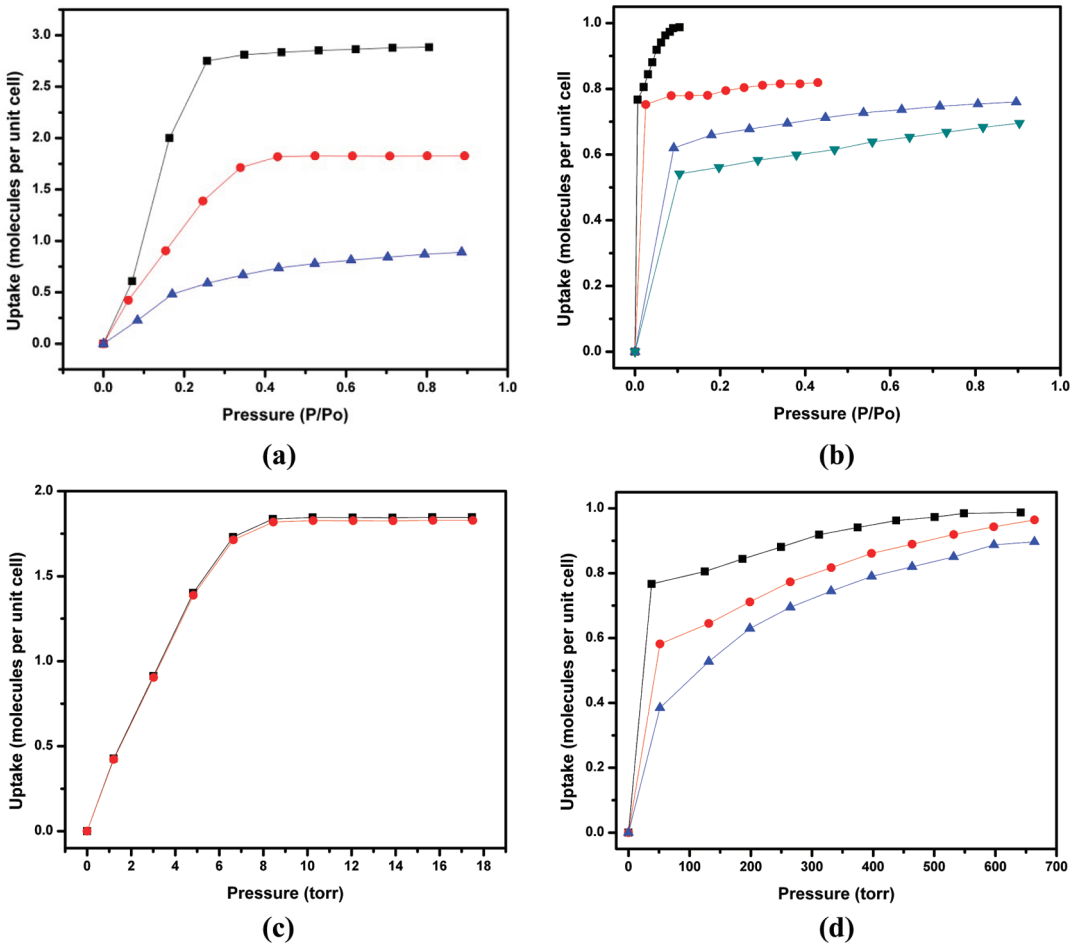


**Figure 17.** Selected experimental hydrocarbon adsorption isotherms in $[Cu(dhbc)_2(4,4'\text{-bpy})]\cdot H_2O$. (a) Adsorption isotherms of benzene (black), toluene (red), and *p*-xylene (blue) at 40 °C; (b) Adsorption isotherms of propane (black), *n*-butane (red), *n*-pentane (blue), and *n*-hexane (green) at 30 °C; (c) adsorption isotherms of toluene at 30 °C (black) and 40 °C (red); (d) Adsorption isotherms of propane at 30 °C (black), 40 °C (red), and 50 °C (blue). ($P_o$ is the saturated vapor pressure at the given experimental temperature.)

reported isotherms are classical Type-I, with a few exceptions for longer alkanes that show small kinks in their isotherms. In contrast, the gas adsorption behavior of MIL-53(Fe) is very different from its Al- or Cr-analogues. Apparent gate opening effect was observed for small alkane molecules. This could be attributed to higher flexibility of the MIL-53(Fe) structure, where very narrow pores prevent most gases from entering, and the "gate" opens only in the cases of certain small adsorbates when their pressure reaches a threshold.[334,343−345]

## 4. COMMENSURATE ADSORPTION IN OTHER POROUS STRUCTURES

All porous structures discussed in the preceding section have a common feature in that they are 3D frameworks. However, commensurate adsorption is not limited to 3D structures. The phenomenon has also been observed in other types of porous networks, such as 2D interdigitated layer structures. Here we briefly discuss two interesting examples.

### 4.1. $[Cu(dhbc)_2(4,4'\text{-bpy})]\cdot H_2O$

The structure of $[Cu(dhbc)_2(4,4'\text{-bpy})]\cdot H_2O$ ($H_2$dhbc = 2,5-dihydroxybenzoic acid) embraces 1D open channels parallel to the *a*-axis, formed by interdigitation of the adjacent 2D layers (Figure 16a).[127] Within the layer, the Cu(II) atoms form 1D linear chains through the linkage of 4,4′-bpy which are further connected via dhbc to give rise to a 2D network. The channel segment has an irregular shape and is composed of two parts (*a* and *b*, as indicated in Figure 16b). The dimensions of Part *a* and Part *b* are 2.9 × 4.8 Å and 4.7 × 2.5 Å, respectively, estimated by He simulation (see Figure 16b). There is no clear boundary between the two parts, but the sum of the two gives the overall length of the segment (8.2 Å). Each unit cell contains two segments. Experimental adsorption isotherms were measured for selected paraffins and aromatic hydrocarbons including benzene, toluene, *p*-xylene, propane, *n*-butane, *n*-pentane, and *n*-hexane at 30, 40, and 50 °C. Benzene shows an adsorption level of more than 2 molecules/UC. Toluene serves as a good case of commensurate adsorption. Its experimental uptake was 1.8 molecules/UC, very close to the simulated data of 2 molecules/UC or one molecule per segment. The fact that the adsorption amount remains the same at different temperatures (30 and 40 °C, Figure 17c) further verifies the adsorption is commensurate with the pore segment. Being longer and more rigid, *p*-xylene has the lowest uptake among the three aromatic adsorbates. The adsorbed amount was 1 molecule per two segments, and thus, a


dx.doi.org/10.1021/cr200216x |*Chem. Rev.* 2012, 112, 836–868

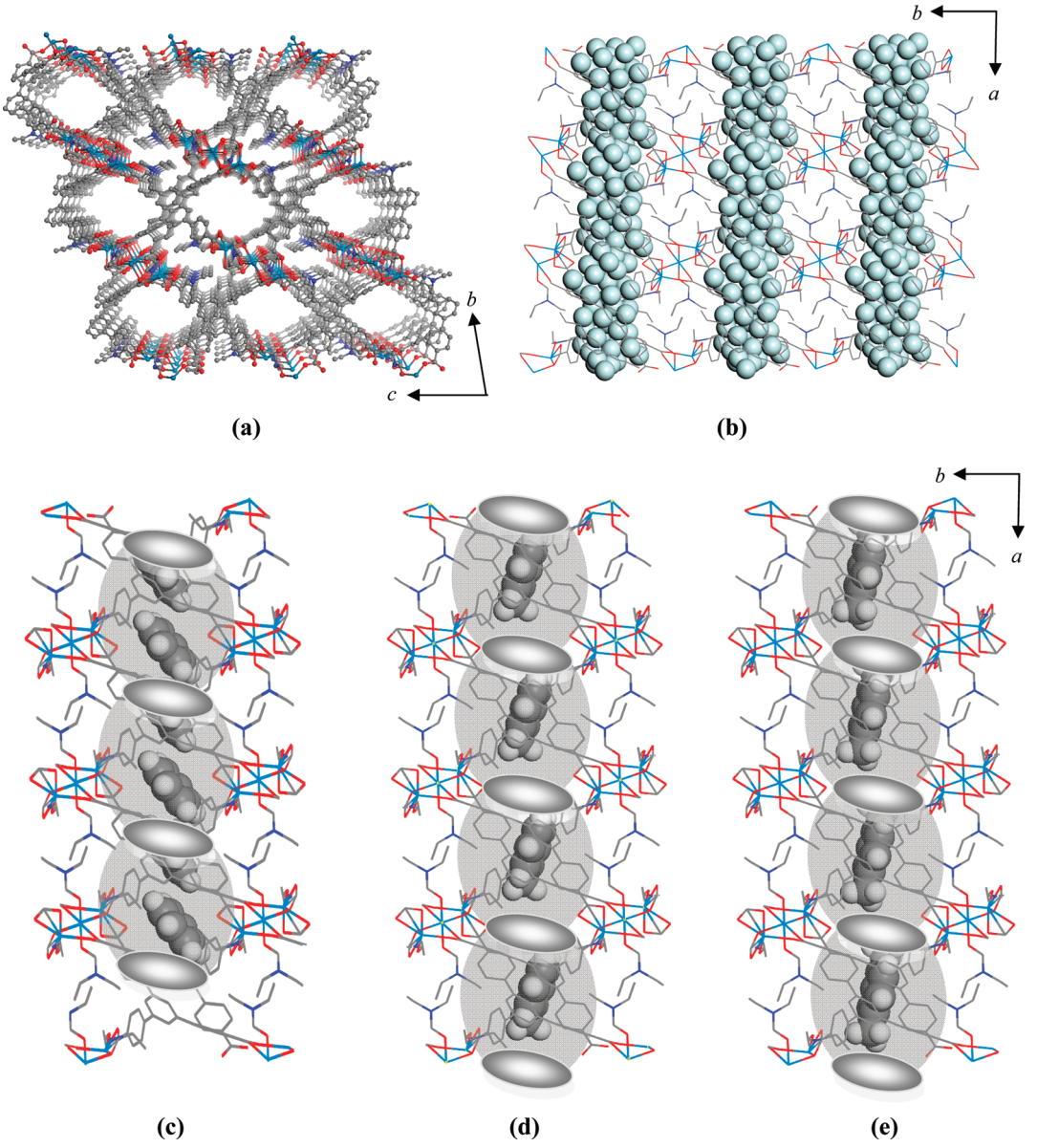


**Figure 18.** (a) Crystal structure of $[Cd_3(btb)_2(DEF)_4]\cdot 2DEF$. (b−e) The simulated gas adsorption in the $[Cd_3(btb)_2(DEF)_4]\cdot 2DEF$ structure. The 1D channels are parallel to the crystallographic *a*-axis: (b) He at 1 K and 760 Torr; (c) benzene at 303 K and 61 Torr; (d) toluene at 303 K and 17.6 Torr; (e) *p*-xylene at 303 K and 5.1 Torr. Color scheme: Cd (light blue), O (red), C (gray), N (dark blue), He (powder blue), H (white).

case of incommensurate adsorption. The same trend was found for the selected paraffins. Higher uptake was achieved for smaller members of the series. The uptakes are in the descending order of propane, *n*-butane, *n*-pentane, and *n*-hexane, corresponding to 0.99, 0.82, 0.76, and 0.70 molecules/UC or 0.50, 0.41, 0.38, and 0.35 molecules per segment (Figure 17b). Therefore, none of them represents a case of commensurate adsorption.

Simulations were performed on the same hydrocarbon adsorbates to verify their adsorption behavior. Toluene molecules preferentially take the center positions at Part *b* within each segment and are oriented to face the dhbc ring to be engaged in a $\pi-\pi$ interaction, as shown in Figure 16c. However, the width of the toluene (5.1 Å) is a bit too large for the pore. As a result, it accommodates the shape of the segment by tilting its ring slightly. Paraffin molecules, on the other hand, prefer to stay near the center of Part *a* of the segment to have a closer contact with framework. While these results may have deviations from the real situation as the simulation experiment uses the as-made crystal structure which will most likely undergoes some changes upon hydrocarbon adsorption, it is clear that experimental and simulation data agree well in the case of toluene, and it is interesting to note the incommensurate−commensurate−incommensurate (IC−C−IC) transition among benzene, toluene, and *p*-xylene (Figure 17a).

### 4.2. $[Cd_3(btb)_2(DEF)_4]\cdot 2DEF$

$[Cd_3(btb)_2(DEF)_4]\cdot 2DEF$ (btb = 1,3,5-tris(4-carboxyphenyl)benzene, DEF = *N*,*N*-diethylformamide) is another 2D structure[346] that may exhibit commensurate adsorption, as


dx.doi.org/10.1021/cr200216x |*Chem. Rev.* 2012, 112, 836–868

suggested from our simulation results. Two types of 1D channels (both of rhombus-shaped cross section) may be generated upon stacking of the 2D bilayers. A larger one (type-A) with a cage size of 8.45 × 8.45 Å becomes accessible after removal of guest (noncoordinated) DEF molecules, as indicated in Figure 18a, and a smaller one (type-B) with a cage size of 8.16 × 8.16 Å can be obtained if coordinated DEF molecules are removed.[346] The structure remains intact if only the guest DEFs are taken off, while removal of both guest and coordinated DEFs will lead to a structure change. To avoid structure alternation, simulations are performed on the structure in which only type-A channels are made accessible. The neck of the channel A is estimated to be ~4.3 × 4.5 Å (cages dimensions: ~6.7 × 5.4 Å, see Figure 18b) based on the He data using the reported crystal structure. The narrow neck cuts the 1D channel into individual segments by a repeating distance of 10.5 Å, which is coincident with the length of the *a*-axis. Simulations are performed on benzene, toluene, and *p*-xylene (Figure 18c−e). For benzene, the smallest and slimmest one among the three aromatic hydrocarbons, a pair of molecules can be fit within a single segment or a single unit cell (one segment per unit cell). For larger adsorbates such as toluene and *p*-xylene, only one molecule can be fit in a segment. Both are tilted so as to better accommodate the shape of the pores and to keep the methyl groups farther apart from the adjacent molecules. The simulated commensurate adsorption of these hydrocarbons certainly needs to be verified by future experimental isotherm measurements.

## 5. CONCLUDING REMARKS

As a new type of adsorbate materials with distinctly advantageous features, microporous metal organic frameworks demonstrate enormous potential for adsorption based applications, including storage, separation, and purification of small gases and hydrocarbons. In this review, we introduce the concept of commensurate adsorption, a fundamentally important and interesting phenomenon that plays a key role in the adsorption processes. We illustrate that commensurate adsorption of hydrocarbons occurs far more often in MMOFs than in zeolites and related materials, primarily as a result of a vastly greater variety of framework types and richer hierarchy of complexity of the pore structures for the former. Among numerous structures in which commensurate adsorption has been observed in the vicinity of room temperature, many have 1D open channels built on pore segments of distinct shape, size, and narrow pore window (aperture) that closely match with the geometries of hydrocarbon species. Clearly, the cases discussed in this review represent only a small selected group. Many existing MMOFs for which hydrocarbon adsorptions may be commensurate with their crystal symmetry and pore structures are yet to be fully recognized and investigated. It can be anticipated that further studies of this topic will reveal many more interesting features and trends, offer helpful insight, and contribute to a better understanding of the adsorbate−adsorbent interactions and the correlation between the crystal symmetry, pore structure, and adsorption behavior of hydrocarbon adsorbates, which in turn will facilitate future design and development of new MMOF systems with enhanced functions and performance in adsorption-based industrial processes.

## ASSOCIATED CONTENT

### Supporting Information

The simulated adsorption of methanol in $[Co_3(fa)_6]$ at 303 K and 78.7 Torr. The simulated adsorption of *trans*-piperylene adsorption in MIL-96 at 303 K and 164.2 Torr. The simulated adsorption of benzene in RPM3-Zn at 303 K and 61 Torr. The simulated adsorption of *o*-xylene in RPM3-Zn at 303 K and 3.8 Torr. Henry constants of selected alkanes obtained from adsorption isotherms for $[Cu(hfipbb)(H_2hfipbb)_{0.5}]$. This information is available free of charge via the Internet at http://pubs.acs.org.

## AUTHOR INFORMATION

### Corresponding Author

*E-mail: jingli@rutgers.edu.

## BIOGRAPHIES

Haohan Wu obtained his Bachelor of Science degree in Material Science and Engineering from University of Science and Technology of China in 2007. Currently he is in the fifth year of the Ph.D. program at the Department of Chemistry and Chemical Biology, Rutgers - The State University of New Jersey, under the direction of Professor Jing Li. He is a recipient of 2010 Van Dyke Award for Excellence in Research. His main research interests are on adsorption-based gas storage and separation using porous materials and investigation of gas adsorption behavior and mechanisms. He is a coauthor of more than 15 papers.

Qihan Gong received her bachelor degree in chemistry at the University of Science and Technology of China in 2009. She is going into the third year in the Ph.D. program of the

Department of Chemistry and Chemical Biology at Rutgers University under the direction of Professor Jing Li. Her current research focuses on the design and synthesis of microporous metal organic frameworks and study of their gas adsorption properties at various temperatures and pressures.

David Olson received his B.S. in chemistry from the University of Wisconsin in 1959 and his Ph.D. in physical chemistry from the Iowa State University in 1963. He was employed by Mobil Research and Development Corp. from 1963 to 1996. Since then he has been adjunct professor and visiting scientist at University of Pennsylvania and Rutgers University. Currently he is also an employee of Rive Technology Corporation. His interests have been in the areas of zeolite structure and crystal chemistry and catalysis and the adsorption properties of zeolites and MOF materials. He has 42 U.S. patents and 52 publications.

Jing Li is Distinguished Professor of Chemistry and Chemical Biology at Rutgers, the State University of New Jersey. She received her Ph.D. degree from Cornell University in 1990 under the guidance of Professor Roald Hoffmann. After postdoctoral work with Professor Francis J. DiSalvo, she joined the chemistry faculty at Rutgers University in 1991. Her research centers on the development of new and functional materials that are fundamentally important and potentially useful for clean and renewable energy applications. These include microporous metal organic framework (MMOF) structures for gas storage, carbon dioxide capture, hydrocarbon separation and purification, heterogenerous catalysis and chemical sensing; and inorganic−organic hybrid semiconductors for photovoltaics, solid-state lighting, and thermoelectrics. She has published more than 200 papers, review articles, and book chapters, and currently serves as Associate Editor of *Journal of Solid State Chemistry* and Topic Editor of *Crystal Growth & Design*.

## ACKNOWLEDGMENT

We thank Dr. Kunhao Li and Dr. Long Pan for their contributions, Dr. Thomas J. Emge for assistance in crystal structure analysis, and Dr. Matthias Thommes for valuable input on gas adsorption methodologies. We are thankful to Prof. Susumu Kitagawa and Prof. Rajamani Krishna for kindly providing us with high resolution graphs. The support from DOE (DE-FG02-08ER46491) and Rutgers University is gratefully acknowledged.

## LIST OF ABBREVIATIONS

| | |
|---|---|
| 1D | one-dimensional |
| 2-cim | 2-chloroimidazole |
| 22DMB | 2,2-dimethylbutane |
| 2-mim | 2-methylimidazole |
| 2D | two-dimensional |
| 3D | three-dimensional |
| 3MP | 3-methylpentane |
| 4,4′-bipy | 4,4′-bipyridine |
| 4-btapa | 1,3,5-benzene tricarboxylate tris[*N*-(4-pyridyl)amide] |
| bdc | 1,4-benzenedicarboxylate |
| bim | benzimidazole |
| bpdc | 4,4′-biphenyldicarboxylate |
| bpe | 1,2-bis(4-pyridyl)ethane |
| bpee | 1,2-bis(4-pyridyl)ethene |
| bptc | 4,4′-bipyridine-2,6,2′,6′-tetracarboxylate |
| btb | 1,3,5-tris(4-carboxyphenyl) benzene |
| btc | 1,3,5-benzenetricarboxylate |
| dabco | 1,4-diazabicyclo[2.2.2]-octane |
| dhbc | 2,5-dihydroxybenzoic acid |
| $C_3^{\circ}$ | propane |
| $C_3^{=}$ | propene |
| CBMC | configurational-bias Monte Carlo |
| DEF | *N*,*N*-diethylformamide |
| DFT | density functional theory |
| DME | dimethyl-ether |
| DMF | *N*,*N*-dimethylformamide |
| dpyg | 1,2-di(4-pyridyl)glycol |
| EB | ethyl benzene |
| etz | 3,5-diethyl-1,2,4-triazolate |
| fa | formate |
| GC | gas chromatography |
| GCMC | grand canonical Monte Carlo |
| gla | glutarate |
| $H_2$hfipbb | 4,4′-(hexafluoroisopropylidene)bis(benzoic acid) |
| IF | interference |
| IR | infrared |
| LEED | low energy electron diffraction |
| *m* | meta- |
| *m*X | *m*-xylene |
| MD | molecular dynamics |
| $Me_2$trzpba | 4-(3,5-dimethyl-4H-1,2,4-triazol-4-yl)benzoate |
| MIL | Materials of "Institut Lavoisier" |
| MMOF | microporous metal organic frameworks |
| molec | molecule(s) |
| MOF | metal organic frameworks |
| mol | mole(s) |
| nHEX | *n*-hexane |
| NOVA | NO void analysis |
| NRS | not reaching saturation |
| *o* | ortho- |

| | |
|---|---|
| *o*X | *o*-xylene |
| *p* | para- |
| *P* | experimental pressure |
| PBU | primary building unit |
| $P_o$ | saturation pressure |
| *p*X | *p*-xylene |
| PXRD | powder X-ray diffraction |
| pyz | pyrazine |
| pzdc | pyrazine-2,3-dicarboxylate |
| $Q_{st}$ | isosteric heat of adsorption |
| R.C. | relative concentration |
| RPM | Rutgers recyclable porous materials |
| SBU | secondary building unit |
| STP | standard temperature and pressure @ 273 K and 760 Torr |
| tbip | 5-tert butylisophthalate |
| tci | 3,3′,3″-(2,4,6-trioxo-1,3,5-triazinane-1,3,5-triyl)tri-propionate |
| TDS | thermal desorption mass spectroscopy |
| TEAS | thermal energy atom scattering |
| UC | unit cell |
| VB | vinyl benzene |
| ZIF | zeolitic imidazolate framework |

## REFERENCES


(1) Olson, D.; Lan, A.; Seidel, J.; Li, K.; Li, J. *Adsorption* **2010**, *16*, 559.
(2) Li, K.; Olson, D. H.; Li, J. *Trends Inorg. Chem.* **2010**, *12*, 13.
(3) Olson, D. H.; Kokotailo, G. T.; Lawton, S. L.; Meier, W. M. *J. Phys. Chem.* **1981**, *85*, 2238.
(4) Smit, B.; Maesen, T. L. M. *Nature* **1995**, *374*, 42.
(5) Beaume, R.; Suzanne, J.; Coulomb, J. P.; Glachant, A.; Bomchil, G. *Surf. Sci.* **1984**, *137*, L117.
(6) Phillips, J. M. *Phys. Rev. B* **1984**, *29*, 4821.
(7) Koch, S. W.; Rudge, W. E.; Abraham, F. F. *Surf. Sci.* **1984**, *145*, 329.
(8) Stephens, P. W.; Heiney, P. A.; Birgeneau, R. J.; Horn, P. M.; Moncton, D. E.; Brown, G. S. *Phys. Rev. B* **1984**, *29*, 3512.
(9) Zhang, Q. M.; Kim, H. K.; Chan, M. H. W. *Phys. Rev. B* **1985**, *32*, 1820.
(10) Gameson, I.; Rayment, T. *Chem. Phys. Lett.* **1986**, *123*, 150.
(11) Hong, H.; Peters, C. J.; Mak, A.; Birgeneau, R. J.; Horn, P. M.; Suematsu, H. *Phys. Rev. B* **1987**, *36*, 7311.
(12) Jiang, S. Y.; Gubbins, K. E.; Zollweg, J. A. *Mol. Phys.* **1993**, *80*, 103.
(13) Shrimpton, N. D.; Steele, W. A. *Phys. Rev. B* **1991**, *44*, 3297.
(14) Bruch, L. W.; Novaco, A. D. *Phys. Rev. B* **2008**, *77*, 125435.
(15) Freimuth, H.; Wiechert, H.; Lauter, H. J. *Surf. Sci.* **1987**, *189*, 548.
(16) Lauter, H. J.; Frank, V. L. P.; Leiderer, P.; Wiechert, H. *Physica B* **1989**, *156*, 280.
(17) Novaco, A. D. *Phys. Rev. B* **1992**, *46*, 8178.
(18) Frank, V. L. P.; Lauter, H. J.; Leiderer, P. *Phys. Rev. Lett.* **1988**, *61*, 436.
(19) Weimer, W.; Knorr, K.; Wiechert, H. *Phys. Rev. Lett.* **1988**, *61*, 1623.
(20) Rabedeau, T. A. *Phys. Rev. B* **1989**, *39*, 9643.
(21) Greywall, D. S. *Phys. Rev. B* **1993**, *47*, 309.
(22) Feng, Y. P.; Chan, M. H. W. *Phys. Rev. Lett.* **1990**, *64*, 2148.
(23) Kortmann, K. D.; Leinbock, B.; Wiechert, H.; Fain, S. C.; Stusser, N. *Physica B* **1997**, *234*, 167.
(24) Hansen, F. Y.; Bruch, L. W. *Phys. Rev. B* **1995**, *51*, 2515.
(25) Hansen, F. Y.; Bruch, L. W.; Taub, H. *Phys. Rev. B* **1996**, *54*, 14077.
(26) Poelsema, B.; Verheij, L. K.; Comsa, G. *Surf. Sci.* **1985**, *152*, 851.
(27) Kern, K.; David, R.; Palmer, R. L.; Comsa, G. *Phys. Rev. Lett.* **1986**, *56*, 620.
(28) Black, J. E.; Janzen, A. *Phys. Rev. B* **1989**, *39*, 6238.
(29) Kern, K.; Zeppenfeld, P.; David, R.; Comsa, G. *Phys. Rev. Lett.* **1987**, *59*, 79.
(30) Ramseyer, C.; Hoang, P. N. M.; Girardet, C. *Phys. Rev. B* **1994**, *49*, 2861.
(31) Ramseyer, C.; Pouthier, V.; Girardet, C.; Zeppenfeld, P.; Buchel, M.; Diercks, V.; Comsa, G. *Phys. Rev. B* **1997**, *55*, 13203.
(32) Berndt, W. *Surf. Sci.* **1989**, *219*, 161.
(33) Schmiedl, R.; Nichtlpecher, W.; Heinz, K.; Muller, K.; Christmann, K. *Surf. Sci.* **1990**, *235*, 186.
(34) Nichtlpecher, W.; Stammler, W.; Heinz, K.; Muller, K. *Phys. Rev. B* **1991**, *43*, 6946.
(35) Yang, S. H.; Phillips, J. M. *Phys. Rev. B* **2007**, *75*, 235408.
(36) Schuster, R.; Robinson, I. K.; Kuhnke, K.; Ferrer, S.; Alvarez, J.; Kern, K. *Phys. Rev. B* **1996**, *54*, 17097.
(37) Marinelli, F.; Grillet, Y.; Pellenq, R. J. M. *Mol. Phys.* **1999**, *97*, 1207.
(38) Reischman, P. T.; Schmitt, K. D.; Olson, D. H. *J. Phys. Chem.* **1988**, *92*, 5165.
(39) Olson, D. H.; Reischman, P. T. *Zeolites* **1996**, *17*, 434.
(40) Makowski, W.; Majda, D. *Appl. Surf. Sci.* **2005**, *252*, 707.
(41) Richards, R. E.; Rees, L. V. C. *Langmuir* **1987**, *3*, 335.
(42) Sun, X. Y.; Li, J. W.; Li, Y. X.; Yan, S. C.; Chen, B. H. *Chem. Res. Chin. Univ.* **2009**, *25*, 377.
(43) Barrett, P. A.; Boix, T.; Puche, M.; Olson, D. H.; Jordan, E.; Koller, H.; Camblor, M. A. *Chem. Commun.* **2003**, 2114.
(44) Olson, D. H.; Yang, X.; Camblor, M. A. *J. Phys. Chem. B* **2004**, *108*, 11044.
(45) Floquet, N.; Coulomb, J. P.; Bellat, J. P.; Simon, J. M.; Weber, G.; Andre, G. *J. Phys. Chem. C* **2007**, *111*, 18182.
(46) Floquet, N.; Simon, J. M.; Coulomb, J. P.; Bellat, J. P.; Weber, G.; Andre, G. *Microporous Mesoporous Mater.* **2009**, *122*, 61.
(47) Morell, H.; Angermund, K.; Lewis, A. R.; Brouwer, D. H.; Fyfe, C. A.; Gies, H. *Chem. Mater.* **2002**, *14*, 2192.
(48) Gutiérrez-Sevillano, J. J.; Dubbeldam, D.; Rey, F.; Valencia, S.; Palomino, M.; Martín-Calvo, A.; Calero, S. a. *J. Phys. Chem. C* **2010**, *114*, 14907.
(49) Zhu, W.; Kapteijn, F.; Moulijn, J. A. *Phys. Chem. Chem. Phys.* **2000**, *2*, 1989.
(50) Manos, G.; Dunne, L. J.; Chaplin, M. F.; Du, Z. M. *Chem. Phys. Lett.* **2001**, *335*, 77.
(51) van Well, W. J. M.; Wolthuizen, J. P.; Smit, B.; van Hooff, J. H. C.; van Santen, R. A. *Angew. Chem., Int. Ed.* **1995**, *34*, 2543.
(52) Vlugt, T. J. H.; Krishna, R.; Smit, B. *J. Phys. Chem. B* **1999**, *103*, 1102.
(53) Calero, S.; Smit, B.; Krishna, R. *J. Catal.* **2001**, *202*, 395.
(54) Krishna, R.; Calero, S.; Smit, B. *Chem. Eng. J.* **2002**, *88*, 81.
(55) Song, L.; Sun, Z.-L.; Ban, H.-Y.; Dai, M.; Rees, L. *Adsorption* **2005**, *11*, 325.
(56) Mentzen, B. F. *Mater. Res. Bull.* **1987**, *22*, 337.
(57) Mentzen, B. F. *Mater. Res. Bull.* **1987**, *22*, 489.
(58) Mentzen, B. F. *Mater. Res. Bull.* **1992**, *27*, 953.
(59) Mohanty, S.; Davis, H. T.; McCormick, A. V. *Chem. Eng. Sci.* **2000**, *55*, 2779.
(60) Mohanty, S.; Davis, H. T.; McCormick, A. V. *AlChE J.* **2000**, *46*, 1662.
(61) Dubbeldam, D.; Smit, B. *J. Phys. Chem. B* **2003**, *107*, 12138.
(62) Dubbeldam, D.; Calero, S.; Maesen, T. L. M.; Smit, B. *Angew. Chem., Int. Ed.* **2003**, *42*, 3624.
(63) Dubbeldam, D.; Calero, S.; Maesen, T. L. M.; Smit, B. *Phys. Rev. Lett.* **2003**, *90*, 245901.
(64) Krishna, R. *J. Phys. Chem. C* **2009**, *113*, 19756.
(65) Krishna, R.; van Baten, J. M. *Sep. Purif. Technol.* **2008**, *60*, 315.
(66) Denayer, J. F. M.; Devriese, L. I.; Couck, S.; Martens, J.; Singh, R.; Webley, P. A.; Baron, G. V. *J. Phys. Chem. C* **2008**, *112*, 16593.

(67) Santilli, D. S. *J. Catal.* **1986**, *99*, 335.
(68) Daems, I.; Singh, R.; Baron, G.; Denayer, J. *Chem. Commun.* **2007**, *13*, 1316.
(69) Hibbe, F.; Chmelik, C.; Heinke, L.; Pramanik, S.; Li, J.; Ruthven, D. M.; Tzoulaki, D.; Kärger, J. r. *J. Am. Chem. Soc.* **2011**, *133*, 2804.
(70) Krishna, R.; Smit, B.; Calero, S. *Chem. Soc. Rev.* **2002**, *31*, 185.
(71) Connolly, M. L. *J. Appl. Crystallogr.* **1983**, *16*, 548.
(72) Shah, D. B.; Guo, C.-J.; Hayhurst, D. T. *J. Chem. Soc., Faraday Trans.* **1995**, *91*, 1143.
(73) Hayhurst, D. T.; Lee, J. C. *New Developments in Zeolites Science and Technology*; Kodansha Ltd: Japan, 1986.
(74) Mueller, U.; Schubert, M.; Teich, F.; Puetter, H.; Schierle-Arndt, K.; Pastre, J. *J. Mater. Chem.* **2006**, *16*, 626.
(75) Kitagawa, S.; Kitaura, R.; Noro, S.-i. *Angew. Chem., Int. Ed.* **2004**, *43*, 2334.
(76) Rowsell, J. L. C.; Yaghi, O. M. *Microporous Mesoporous Mater.* **2004**, *73*, 3.
(77) Rosseinsky, M. J. *Microporous Mesoporous Mater.* **2004**, *73*, 15.
(78) Czaja, A. U.; Trukhan, N.; Muller, U. *Chem. Soc. Rev.* **2009**, *38*, 1284.
(79) Li, J. R.; Kuppler, R. J.; Zhou, H. C. *Chem. Soc. Rev.* **2009**, *38*, 1477.
(80) James, S. L. *Chem. Soc. Rev.* **2003**, *32*, 276.
(81) Ferey, G. *Chem. Soc. Rev.* **2008**, *37*, 191.
(82) Long, J. R.; Yaghi, O. M. *Chem. Soc. Rev.* **2009**, *38*, 1213.
(83) Li, H.; Eddaoudi, M.; O'Keeffe, M.; Yaghi, O. M. *Nature* **1999**, *402*, 276.
(84) Seki, K.; Mori, W. *J. Phys. Chem. B* **2002**, *106*, 1380.
(85) Dybtsev, D. N.; Chun, H.; Kim, K. *Angew. Chem., Int. Ed.* **2004**, *43*, 5033.
(86) Pan, L.; Adams, K. M.; Hernandez, H. E.; Wang, X.; Zheng, C.; Hattori, Y.; Kaneko, K. *J. Am. Chem. Soc.* **2003**, *125*, 3062.
(87) Rosi, N. L.; Eckert, J.; Eddaoudi, M.; Vodak, D. T.; Kim, J.; O'Keeffe, M.; Yaghi, O. M. *Science* **2003**, *300*, 1127.
(88) Rowsell, J. L. C.; Millward, A. R.; Park, K. S.; Yaghi, O. M. *J. Am. Chem. Soc.* **2004**, *126*, 5666.
(89) Kesanli, B.; Cui, Y.; Smith, M. R.; Bittner, E. W.; Bockrath, B. C.; Lin, W. *Angew. Chem., Int. Ed.* **2005**, *44*, 72.
(90) Rowsell, J. L. C.; Yaghi, O. M. *Angew. Chem., Int. Ed.* **2005**, *44*, 4670.
(91) Zhao, X.; Xiao, B.; Fletcher, A. J.; Thomas, K. M.; Bradshaw, D.; Rosseinsky, M. J. *Science* **2004**, *306*, 1012.
(92) Lee, E. Y.; Jang, S. Y.; Suh, M. P. *J. Am. Chem. Soc.* **2005**, *127*, 6374.
(93) Kubota, Y.; Takata, M.; Matsuda, R.; Kitaura, R.; Kitagawa, S.; Kato, K.; Sakata, M.; Kobayashi, T. C. *Angew. Chem., Int. Ed.* **2005**, *44*, 920.
(94) Chun, H.; Dybtsev, D. N.; Kim, H.; Kim, K. *Chem.- Eur. J.* **2005**, *11*, 3521.
(95) Kaye, S. S.; Long, J. R. *J. Am. Chem. Soc.* **2005**, *127*, 6506.
(96) Ferey, G.; Latroche, M.; Serre, C.; Millange, F.; Loiseau, T.; Percheron-Guegan, A. *Chem. Commun.* **2003**, *24*, 2976.
(97) Millward, A. R.; Yaghi, O. M. *J. Am. Chem. Soc.* **2005**, *127*, 17998.
(98) O'Keeffe, M. *Chem. Soc. Rev.* **2009**, *38*, 1215.
(99) Perry Iv, J. J.; Perman, J. A.; Zaworotko, M. J. *Chem. Soc. Rev.* **2009**, *38*, 1400.
(100) Tranchemontagne, D. J.; Mendoza-Cortes, J. L.; O'Keeffe, M.; Yaghi, O. M. *Chem. Soc. Rev.* **2009**, *38*, 1257.
(101) Murray, L. J.; Dinca, M.; Long, J. R. *Chem. Soc. Rev.* **2009**, *38*, 1294.
(102) Lee, J.; Li, J.; Jagiello, J. *J. Solid State Chem.* **2005**, *178*, 2527.
(103) Lee, J. Y.; Pan, L.; Kelly, S. P.; Jagiello, J.; Emge, T. J.; Li, J. *Adv. Mater.* **2005**, *17*, 2703.
(104) Wang, Q. M.; Shen, D.; Bülow, M.; Ling Lau, M.; Deng, S.; Fitch, F. R.; Lemcoff, N. O.; Semanscin, J. *Microporous Mesoporous Mater.* **2002**, *55*, 217.
(105) Duren, T.; Bae, Y. S.; Snurr, R. Q. *Chem. Soc. Rev.* **2009**, *38*, 1237.
(106) Pan, L.; Parker, B.; Huang, X.; Olson, D. H.; Lee, Li, J. *J. Am. Chem. Soc.* **2006**, *128*, 4180.
(107) Pan, L.; Olson, D. H.; Ciemnolonski, L. R.; Heddy, R.; Li, J. *Angew. Chem., Int. Ed.* **2006**, *45*, 616.
(108) Fletcher, A. J.; Cussen, E. J.; Bradshaw, D.; Rosseinsky, M. J.; Thomas, K. M. *J. Am. Chem. Soc.* **2004**, *126*, 9750.
(109) Eddaoudi, M.; Kim, J.; Rosi, N.; Vodak, D.; Wachter, J.; O'Keeffe, M.; Yaghi, O. M. *Science* **2002**, *295*, 469.
(110) Düren, T.; Sarkisov, L.; Yaghi, O. M.; Snurr, R. Q. *Langmuir* **2004**, *20*, 2683.
(111) Matsuda, R.; Kitaura, R.; Kitagawa, S.; Kubota, Y.; Belosludov, R. V.; Kobayashi, T. C.; Sakamoto, H.; Chiba, T.; Takata, M.; Kawazoe, Y.; Mita, Y. *Nature* **2005**, *436*, 238.
(112) Han, S. S.; Mendoza-Cortes, J. L.; Goddard, W. A. *Chem. Soc. Rev.* **2009**, *38*, 1460.
(113) Saha, D.; Bao, Z. B.; Jia, F.; Deng, S. G. *Environ. Sci. Technol.* **2010**, *44*, 1820.
(114) Mendoza-Cortés, J. L.; Han, S. S.; Furukawa, H.; Yaghi, O. M.; Goddard, W. A. *J. Phys. Chem. A* **2010**, *114*, 10824.
(115) Ma, S. Q.; Zhou, H. C. *Chem. Commun.* **2010**, *46*, 44.
(116) Kishan, M. R.; Tian, J.; Thallapally, P. K.; Fernandez, C. A.; Dalgarno, S. J.; Warren, J. E.; McGrail, B. P.; Atwood, J. L. *Chem. Commun.* **2010**, *46*, 538.
(117) Farha, O. K.; Bae, Y. S.; Hauser, B. G.; Spokoyny, A. M.; Snurr, R. Q.; Mirkin, C. A.; Hupp, J. T. *Chem. Commun.* **2010**, *46*, 1056.
(118) Furukawa, H.; Yaghi, O. M. *J. Am. Chem. Soc.* **2009**, *131*, 8875.
(119) Llewellyn, P. L.; Bourrelly, S.; Serre, C.; Vimont, A.; Daturi, M.; Hamon, L.; De Weireld, G.; Chang, J. S.; Hong, D. Y.; Hwang, Y. K.; Jhung, S. H.; Ferey, G. *Langmuir* **2008**, *24*, 7245.
(120) Bae, Y. S.; Farha, O. K.; Spokoyny, A. M.; Mirkin, C. A.; Hupp, J. T.; Snurr, R. Q. *Chem. Commun.* **2008**, *35*, 4135.
(121) Bourrelly, S.; Llewellyn, P. L.; Serre, C.; Millange, F.; Loiseau, T.; Férey, G. *J. Am. Chem. Soc.* **2005**, *127*, 13519.
(122) Sarkisov, L.; Düren, T.; Snurr, R. Q. *Mol. Phys.* **2004**, *102*, 211.
(123) Yazaydin, A. O.; Benin, A. I.; Faheem, S. A.; Jakubczak, P.; Low, J. J.; Willis, R. R.; Snurr, R. Q. *Chem. Mater.* **2009**, *21*, 1425.
(124) Demessence, A.; D'Alessandro, D. M.; Foo, M. L.; Long, J. R. *J. Am. Chem. Soc.* **2009**, *131*, 8784.
(125) Park, H. J.; Suh, M. P. *Chem.- Eur. J.* **2008**, *14*, 8812.
(126) Caskey, S. R.; Wong-Foy, A. G.; Matzger, A. J. *J. Am. Chem. Soc.* **2008**, *130*, 10870.
(127) Kitaura, R.; Seki, K.; Akiyama, G.; Kitagawa, S. *Angew. Chem., Int. Ed.* **2003**, *42*, 428.
(128) Xu, Q.; Liu, D. H.; Yang, Q. Y.; Zhong, C. L.; Mi, J. G. *J. Mater. Chem.* **2010**, *20*, 706.
(129) Britt, D.; Furukawa, H.; Wang, B.; Glover, T. G.; Yaghi, O. M. *Proc. Natl. Acad. Sci. U.S.A.* **2009**, *106*, 20637.
(130) Li, K.; Olson, D. H.; Lee, J. Y.; Bi, W.; Wu, K.; Yuen, T.; Xu, Q.; Li, J. *Adv. Funct. Mater.* **2008**, *18*, 2205.
(131) Lee, J. Y.; Olson, D. H.; Pan, L.; Emge, T. J.; Li, J. *Adv. Funct. Mater.* **2007**, *17*, 1255.
(132) Llewellyn, P. L.; Bourrelly, S.; Serre, C.; Filinchuk, Y.; Ferey, G. *Angew. Chem., Int. Ed.* **2006**, *45*, 7751.
(133) Dybtsev, D. N.; Chun, H.; Yoon, S. H.; Kim, D.; Kim, K. *J. Am. Chem. Soc.* **2004**, *126*, 32.
(134) Dincă, M.; Long, J. R. *J. Am. Chem. Soc.* **2005**, *127*, 9376.
(135) Surblé, S.; Millange, F.; Serre, C.; Düren, T.; Latroche, M.; Bourrelly, S.; Llewellyn, P. L.; Férey, G. *J. Am. Chem. Soc.* **2006**, *128*, 14889.
(136) Loiseau, T.; Lecroq, L.; Volkringer, C.; Marrot, J.; Férey, G.; Haouas, M.; Taulelle, F.; Bourrelly, S.; Llewellyn, P. L.; Latroche, M. *J. Am. Chem. Soc.* **2006**, *128*, 10223.
(137) Navarro, J. A. R.; Barea, E.; Rodríguez-Diéguez, A.; Salas, J. M.; Ania, C. O.; Parra, J. B.; Masciocchi, N.; Galli, S.; Sironi, A. *J. Am. Chem. Soc.* **2008**, *130*, 3978.
(138) Banerjee, R.; Phan, A.; Wang, B.; Knobler, C.; Furukawa, H.; O'Keeffe, M.; Yaghi, O. M. *Science* **2008**, *319*, 939.
(139) Wang, B.; Cote, A. P.; Furukawa, H.; O'Keeffe, M.; Yaghi, O. M. *Nature* **2008**, *453*, 207.

(140) Chen, B.; Ji, Y.; Xue, M.; Fronczek, F. R.; Hurtado, E. J.; Mondal, J. U.; Liang, C.; Dai, S. *Inorg. Chem.* **2008**, *47*, 5543.
(141) Xue, M.; Ma, S.; Jin, Z.; Schaffino, R. M.; Zhu, G.-S.; Lobkovsky, E. B.; Qiu, S.-L.; Chen, B. *Inorg. Chem.* **2008**, *47*, 6825.
(142) Moon, H. R.; Kobayashi, N.; Suh, M. P. *Inorg. Chem.* **2006**, *45*, 8672.
(143) Hamon, L.; Leclerc, H.; Ghoufi, A.; Oliviero, L.; Travert, A.; Lavalley, J.-C.; Devic, T.; Serre, C.; Férey, G. r.; De Weireld, G.; Vimont, A.; Maurin, G. *J. Phys. Chem. C* **2011**, *115*, 2047.
(144) Grant Glover, T.; Peterson, G. W.; Schindler, B. J.; Britt, D.; Yaghi, O. *Chem. Eng. Sci.* **2011**, *66*, 163.
(145) Ma, S.; Wang, X.-S.; Yuan, D.; Zhou, H.-C. *Angew. Chem., Int. Ed.* **2008**, *47*, 4130.
(146) Dincă, M.; Yu, A. F.; Long, J. R. *J. Am. Chem. Soc.* **2006**, *128*, 8904.
(147) Ma, S.; Wang, X.-S.; Collier, C. D.; Manis, E. S.; Zhou, H.-C. *Inorg. Chem.* **2007**, *46*, 8499.
(148) Zou, Y.; Hong, S.; Park, M.; Chun, H.; Lah, M. S. *Chem. Commun.* **2007**, *48*, 5182.
(149) Li, C.-J.; Lin, Z.-j.; Peng, M.-X.; Leng, J.-D.; Yang, M.-M.; Tong, M.-L. *Chem. Commun.* **2008**, 6348.
(150) Li, Y.; Yang, R. T. *Langmuir* **2007**, *23*, 12937.
(151) Humphrey, S. M.; Chang, J.-S.; Jhung, S. H.; Yoon, J. W.; Wood, P. T. *Angew. Chem., Int. Ed.* **2007**, *46*, 272.
(152) Yoon, J. W.; Jhung, S. H.; Hwang, Y. K.; Humphrey, S. M.; Wood, P. T.; Chang, J. S. *Adv. Mater.* **2007**, *19*, 1830.
(153) Li, J.-R.; Tao, Y.; Yu, Q.; Bu, X.-H.; Sakamoto, H.; Kitagawa, S. *Chem.- Eur. J.* **2008**, *14*, 2771.
(154) Cheon, Y. E.; Suh, M. P. *Chem.- Eur. J.* **2008**, *14*, 3961.
(155) Thallapally, P. K.; Tian, J.; Kishan, M. R.; Fernandez, C. A.; Dalgarno, S. J.; McGrail, P. B.; Warren, J. E.; Atwood, J. L. *J. Am. Chem. Soc.* **2008**, *130*, 16842.
(156) Bae, Y.-S.; Mulfort, K. L.; Frost, H.; Ryan, P.; Punnathanam, S.; Broadbelt, L. J.; Hupp, J. T.; Snurr, R. Q. *Langmuir* **2008**, *24*, 8592.
(157) Seki, K. *Phys. Chem. Chem. Phys.* **2002**, *4*, 1968.
(158) Maji, T. K.; Mostafa, G.; Matsuda, R.; Kitagawa, S. *J. Am. Chem. Soc.* **2005**, *127*, 17152.
(159) Llewellyn, P. L.; Bourrelly, S.; Serre, C.; Filinchuk, Y.; Férey, G. *Angew. Chem., Int. Ed.* **2006**, *45*, 7751.
(160) Chen, B.; Ma, S.; Hurtado, E. J.; Lobkovsky, E. B.; Zhou, H.-C. *Inorg. Chem.* **2007**, *46*, 8490.
(161) Ma, S.; Wang, X.-S.; Manis, E. S.; Collier, C. D.; Zhou, H.-C. *Inorg. Chem.* **2007**, *46*, 3432.
(162) Hayashi, H.; Cote, A. P.; Furukawa, H.; O'Keeffe, M.; Yaghi, O. M. *Nat. Mater.* **2007**, *6*, 501.
(163) Maji, T. K.; Matsuda, R.; Kitagawa, S. *Nat. Mater.* **2007**, *6*, 142.
(164) Chen, B.; Ma, S.; Hurtado, E. J.; Lobkovsky, E. B.; Liang, C.; Zhu, H.; Dai, S. *Inorg. Chem.* **2007**, *46*, 8705.
(165) Chen, B.; Ma, S.; Zapata, F.; Fronczek, F. R.; Lobkovsky, E. B.; Zhou, H.-C. *Inorg. Chem.* **2007**, *46*, 1233.
(166) Tanaka, D.; Nakagawa, K.; Higuchi, M.; Horike, S.; Kubota, Y.; Kobayashi, T. C.; Takata, M.; Kitagawa, S. *Angew. Chem., Int. Ed.* **2008**, *47*, 3914.
(167) Xiao, B.; Wheatley, P. S.; Zhao, X. B.; Fletcher, A. J.; Fox, S.; Rossi, A. G.; Megson, I. L.; Bordiga, S.; Regli, L.; Thomas, K. M.; Morris, R. E. *J. Am. Chem. Soc.* **2007**, *129*, 1203.
(168) Ingleson, M. J.; Heck, R.; Gould, J. A.; Rosseinsky, M. J. *Inorg. Chem.* **2009**, *48*, 9986.
(169) McKinlay, A. C.; Xiao, B.; Wragg, D. S.; Wheatley, P. S.; Megson, I. L.; Morris, R. E. *J. Am. Chem. Soc.* **2008**, *130*, 10440.
(170) Bárcia, P. S.; Zapata, F.; Silva, J. A. C.; Rodrigues, A. E.; Chen, B. *J. Phys. Chem. B* **2007**, *111*, 6101.
(171) Maes, M.; Vermoortele, F.; Alaerts, L.; Couck, S.; Kirschhock, C. E. A.; Denayer, J. F. M.; De Vos, D. E. *J. Am. Chem. Soc.* **2010**, *132*, 15277.
(172) Maes, M.; Alaerts, L.; Vermoortele, F.; Ameloot, R.; Couck, S.; Finsy, V.; Denayer, J. F. M.; De Vos, D. E. *J. Am. Chem. Soc.* **2010**, *132*, 2284.
(173) Finsy, V.; Kirschhock, C. E. A.; Vedts, G.; Maes, M.; Alaerts, L.; De Vos, D. E.; Baron, G. V.; Denayer, J. F. M. *Chem.- Eur. J.* **2009**, *15*, 7724.
(174) Alaerts, L.; Maes, M.; van der Veen, M. A.; Jacobs, P. A.; De Vos, D. E. *Phys. Chem. Chem. Phys.* **2009**, *11*, 2903.
(175) Finsy, V.; Verelst, H.; Alaerts, L.; De Vos, D.; Jacobs, P. A.; Baron, G. V.; Denayer, J. F. M. *J. Am. Chem. Soc.* **2008**, *130*, 7110.
(176) Alaerts, L.; Maes, M.; Giebeler, L.; Jacobs, P. A.; Martens, J. A.; Denayer, J. F. M.; Kirschhock, C. E. A.; De Vos, D. E. *J. Am. Chem. Soc.* **2008**, *130*, 14170.
(177) Alaerts, L.; Kirschhock, C. E. A.; Maes, M.; van der Veen, M. A.; Finsy, V.; Depla, A.; Martens, J. A.; Baron, G. V.; Jacobs, P. A.; Denayer, J. F. M.; De Vos, D. E. *Angew. Chem., Int. Ed.* **2007**, *46*, 4293.
(178) Ma, S.; Sun, D.; Wang, X.-S.; Zhou, H.-C. *Angew. Chem., Int. Ed.* **2007**, *46*, 2458.
(179) Trung, T. K.; Déroche, I.; Rivera, A.; Yang, Q.; Yot, P.; Ramsahye, N.; Vinot, S. D.; Devic, T.; Horcajada, P.; Serre, C.; Maurin, G.; Trens, P. *Microporous Mesoporous Mater.* **2011**, *140*, 114.
(180) Rosenbach, N., Jr.; Ghoufi, A.; Deroche, I.; Llewellyn, P. L.; Devic, T.; Bourrelly, S.; Serre, C.; Ferey, G.; Maurin, G. *Phys. Chem. Chem. Phys.* **2010**, *12*, 6428.
(181) Lan, A. J.; Li, K. H.; Wu, H. H.; Kong, L. Z.; Nijem, N.; Olson, D. H.; Emge, T. J.; Chabal, Y. J.; Langreth, D. C.; Hong, M. C.; Li, J. *Inorg. Chem.* **2009**, *48*, 7165.
(182) Coudert, F. o.-X.; Mellot-Draznieks, C.; Fuchs, A. H.; Boutin, A. *J. Am. Chem. Soc.* **2009**, *131*, 3442.
(183) Trung, T. K.; Trens, P.; Tanchoux, N.; Bourrelly, S.; Llewellyn, P. L.; Loera-Serna, S.; Serre, C.; Loiseau, T.; Fajula, F. o.; Férey, G. r. *J. Am. Chem. Soc.* **2008**, *130*, 16926.
(184) Uchida, S.; Kawamoto, R.; Tagami, H.; Nakagawa, Y.; Mizuno, N. *J. Am. Chem. Soc.* **2008**, *130*, 12370.
(185) Ghosh, S. K.; Bureekaew, S.; Kitagawa, S. *Angew. Chem., Int. Ed.* **2008**, *47*, 3403.
(186) Zhang, J.-P.; Chen, X.-M. *J. Am. Chem. Soc.* **2008**, *130*, 6010.
(187) Maji, T. K.; Uemura, K.; Chang, H.-C.; Matsuda, R.; Kitagawa, S. *Angew. Chem., Int. Ed.* **2004**, *43*, 3269.
(188) Lin, X.; Blake, A. J.; Wilson, C.; Sun, X. Z.; Champness, N. R.; George, M. W.; Hubberstey, P.; Mokaya, R.; Schröder, M. *J. Am. Chem. Soc.* **2006**, *128*, 10745.
(189) Li, K.; Olson, D. H.; Seidel, J.; Emge, T. J.; Gong, H.; Zeng, H.; Li, J. *J. Am. Chem. Soc.* **2009**, *131*, 10368.
(190) Sun, X. Q.; Wick, C. D.; Thallapally, P. K.; McGrail, B. P.; Dang, L. X. *J. Phys. Chem. B* **2011**, *115*, 2842.
(191) Lincke, J.; Lassig, D.; Moellmer, J.; Reichenbach, C.; Puls, A.; Moeller, A.; Glaser, R.; Kalies, G.; Staudt, R.; Krautscheid, H. *Microporous Mesoporous Mater.* **2011**, *142*, 62.
(192) Xu, G. H.; Zhang, X. G.; Guo, P.; Pan, C. L.; Zhang, H. J.; Wang, C. *J. Am. Chem. Soc.* **2010**, *132*, 3656.
(193) Liu, Q. K.; Ma, J. P.; Dong, Y. B. *J. Am. Chem. Soc.* **2010**, *132*, 7005.
(194) Meyers, R. A. *Handbook of Petroleum Refining processes*; McGraw-Hill, Inc.: New York, 1986.
(195) Yang, R. T. *Adsorbents: Fundamentals and Applications*; John Wiley & Sons: Hoboken, 2003.
(196) Yang, R. T. *Gas Separation by Adsorption Progress*; Butterworth: Boston, 1987.
(197) Rouquerol, F.; Rouquerol, I.; Sing, K. *Adsorption by Powders and Porous Solids-Principles Methodology and Applications*; Academic Press: London, 1999.
(198) Auerbach, S. M.; Carrado, K. A.; Dutta, P. K. *Handbook of Zeolite Science and Technology*; Marcel Dekker, Inc.: New York, 2003.
(199) Keller, J. U.; Staudt, R. *Gas Adsorption Equilibria, Experimental Methods and Adsorptive Isotherms*; Springer Science+Business Media, Inc.: Boston, 2005.
(200) Moellmer, J.; Celer, E. B.; Luebke, R.; Cairns, A. J.; Staudt, R.; Eddaoudi, M.; Thommes, M. *Microporous Mesoporous Mater.* **2010**, *129*, 345.

(201) Llewellyn, P. L.; Maurin, G.; Devic, T.; Loera-Serna, S.; Rosenbach, N.; Serre, C.; Bourrelly, S.; Horcajada, P.; Filinchuk, Y.; Férey, G. r. *J. Am. Chem. Soc.* **2008**, *130*, 12808.
(202) Llewellyn, P. L.; Horcajada, P.; Maurin, G.; Devic, T.; Rosenbach, N.; Bourrelly, S.; Serre, C.; Vincent, D.; Loera-Serna, S.; Filinchuk, Y.; Férey, G. *J. Am. Chem. Soc.* **2009**, *131*, 13002.
(203) Kitaura, R.; Fujimoto, K.; Noro, S.-i.; Kondo, M.; Kitagawa, S. *Angew. Chem., Int. Ed.* **2002**, *41*, 133.
(204) Hasegawa, S.; Horike, S.; Matsuda, R.; Furukawa, S.; Mochizuki, K.; Kinoshita, Y.; Kitagawa, S. *J. Am. Chem. Soc.* **2007**, *129*, 2607.
(205) Lan, A. J.; Li, K. H.; Wu, H. H.; Olson, D. H.; Emge, T. J.; Ki, W.; Hong, M. C.; Li, J. *Angew. Chem., Int. Ed.* **2009**, *48*, 2334.
(206) Zhang, J.; Wu, H.; Emge, T. J.; Li, J. *Chem. Commun.* **2010**, *46*, 9152.
(207) Wu, H.; Reali, R. S.; Smith, D. A.; Trachtenberg, M. C.; Li, J. *Chem.—Eur. J.* **2010**, *16*, 13951.
(208) Samsonenko, D. G.; Kim, H.; Sun, Y.; Kim, G.-H.; Lee, H.-S.; Kim, K. *Chem.—Asian J.* **2007**, *2*, 484.
(209) Uemura, K.; Yamasaki, Y.; Komagawa, Y.; Tanaka, K.; Kita, H. *Angew. Chem.* **2007**, *119*, 6782.
(210) Gucuyener, C.; van den Bergh, J.; Gascon, J.; Kapteijn, F. *J. Am. Chem. Soc.* **2010**, *132*, 17704.
(211) Wang, Z.; Zhang, B.; Kurmoo, M.; Green, M. A.; Fujiwara, H.; Otsuka, T.; Kobayashi, H. *Inorg. Chem.* **2005**, *44*, 1230.
(212) Krishna, R.; van Baten, J. M. *Mol. Simul.* **2009**, *35*, 1098.
(213) Lamia, N.; Jorge, M.; Granato, M. A.; Almeida Paz, F. A.; Chevreau, H.; Rodrigues, A. E. *Chem. Eng. Sci.* **2009**, *64*, 3246.
(214) Hartmann, M.; Kunz, S.; Himsl, D.; Tangermann, O.; Ernst, S.; Wagener, A. *Langmuir* **2008**, *24*, 8634.
(215) Loiseau, T.; Serre, C.; Huguenard, C.; Fink, G.; Taulelle, F.; Henry, M.; Bataille, T.; Férey, G. *Chem.—Eur. J.* **2004**, *10*, 1373.
(216) Barthelet, K.; Marrot, J.; Riou, D.; Férey, G. *Angew. Chem., Int. Ed.* **2002**, *41*, 281.
(217) Eldridge, R. B. *Ind. Eng. Chem. Res.* **1993**, *32*, 2208.
(218) Moulijn, J. A.; Makkee, M.; van Diepen, A. *Process Technology*; Wiley: Chichester, England, 2001.
(219) Park, K. S.; Ni, Z.; Côté, A. P.; Choi, J. Y.; Huang, R.; Uribe-Romo, F. J.; Chae, H. K.; O'Keeffe, M.; Yaghi, O. M. *Proc. Natl. Acad. Sci. U. S. A.* **2006**, *103*, 10186.
(220) Huang, X.-C.; Lin, Y.-Y.; Zhang, J.-P.; Chen, X.-M. *Angew. Chem., Int. Ed.* **2006**, *45*, 1557.
(221) Krishna, R.; van Baten, J. M. *Microporous Mesoporous Mater.* **2011**, *137*, 83.
(222) Zhu, W.; Kapteijn, F.; A. Moulijn, J. *Chem. Commun.* **1999**, *24*, 2453.
(223) Hedin, N.; DeMartin, G. J.; Roth, W. J.; Strohmaier, K. G.; Reyes, S. C. *Microporous Mesoporous Mater.* **2008**, *109*, 327.
(224) Ruthven, D. M.; Reyes, S. C. *Microporous Mesoporous Mater.* **2007**, *104*, 59.
(225) Gascon, J.; Blom, W.; van Miltenburg, A.; Ferreira, A.; Berger, R.; Kapteijn, F. *Microporous Mesoporous Mater.* **2008**, *115*, 585.
(226) ter Horst, J. H.; Bromley, S. T.; van Rosmalen, G. M.; Jansen, J. C. *Microporous Mesoporous Mater.* **2002**, *53*, 45.
(227) Olson, D. H.; Camblor, M. A.; Villaescusa, L. A.; Kuehl, G. H. *Microporous Mesoporous Mater.* **2004**, *67*, 27.
(228) Krishna, R.; van Baten, J. M. *J. Phys. Chem. C* **2010**, *114*, 18017.
(229) Krishna, R.; van Baten, J. M. *Phys. Chem. Chem. Phys.* **2011**, *13*, 10593.
(230) Pramanik, S.; Zheng, C.; Zhang, X.; Emge, T. J.; Li, J. *J. Am. Chem. Soc.* **2011**, *133*, 4153.
(231) Yoon, J. W.; Seo, Y.-K.; Hwang, Y. K.; Chang, J.-S.; Leclerc, H.; Wuttke, S.; Bazin, P.; Vimont, A.; Daturi, M.; Bloch, E.; Llewellyn, P. L.; Serre, C.; Horcajada, P.; Grenèche, J.-M.; Rodrigues, A. E.; Férey, G. *Angew. Chem., Int. Ed.* **2010**, *49*, 5949.
(232) Bux, H.; Chmelik, C.; Krishna, R.; Caro, J. *J. Membr. Sci.* **2011**, *369*, 284.
(233) Dubbeldam, D.; Galvin, C. J.; Walton, K. S.; Ellis, D. E.; Snurr, R. Q. *J. Am. Chem. Soc.* **2008**, *130*, 10884.
(234) Lowell, S.; Shields, J. E.; Thomas, M. A.; Thommes, M. *Characterization of Porous Solids and Powders: Surface Area, Porosity and Density*; Springer: New York, 2006.
(235) Keller, J. U.; Robens, E.; du Fresne von Hohenesche, C. *Stud. Surf. Sci. Catal.* **2002**, *144*, 387.
(236) Mikhail, R. S.; Robens, E. *Microstructure and Thermal Analysis of Solid Surfaces*; Wiley, Chichester, 1983.
(237) Kaneko, K.; Ohba, T.; Hattori, Y.; Sunaga, M.; Tanaka, H.; Kanoh, H. *Stud. Surf. Sci. Catal.* **2002**, *144*, 11.
(238) Sing, K. S. W.; Everett, D. H.; Haul, R. A. W.; Moscou, L.; Pierotti, R. A.; Rouquerol, J.; Siemieniewska, T. *Pure Appl. Chem.* **1985**, *57*, 603.
(239) Pan, L.; Liu, H. M.; Lei, X. G.; Huang, X. Y.; Olson, D. H.; Turro, N. J.; Li, J. *Angew. Chem., Int. Ed.* **2003**, *42*, 542.
(240) Ruthven, D. M. *Principles of Adsorption and Adsorption Processes*; John Wiley & Sons, Inc.: New York, 1984.
(241) Ocakoglu, R. A.; Denayer, J. F. M.; Marin, G. B.; Martens, J. A.; Baron, G. V. *J. Phys. Chem. B* **2002**, *107*, 398.
(242) Llewellyn, P. L.; Maurin, G. *C. R. Chim.* **2005**, *8*, 283.
(243) Salles, F.; Maurin, G.; Serre, C.; Llewellyn, P. L.; Knöfel, C.; Choi, H. J.; Filinchuk, Y.; Oliviero, L.; Vimont, A.; Long, J. R.; Férey, G. r. *J. Am. Chem. Soc.* **2010**, *132*, 13782.
(244) Salles, F.; Kolokolov, D. I.; Jobic, H.; Maurin, G.; Llewellyn, P. L.; Devic, T.; Serre, C.; Ferey, G. r. *J. Phys. Chem. C* **2009**, *113*, 7802.
(245) Chmelik, C.; Karger, J. *Chem. Soc. Rev.* **2010**, *39*, 4864.
(246) Heinke, L.; Tzoulaki, D.; Chmelik, C.; Hibbe, F.; van Baten, J. M.; Lim, H.; Li, J.; Krishna, R.; Karger, J. *Phys. Rev. Lett.* **2009**, *102*, 065901.
(247) Tzoulaki, D.; Heinke, L.; Lim, H.; Li, J.; Olson, D.; Caro, J.; Krishna, R.; Chmelik, C.; Kärger, J. *Angew. Chem., Int. Ed.* **2009**, *48*, 3525.
(248) Chmelik, C.; Heinke, L.; Kortunov, P.; Li, J.; Olson, D.; Tzoulaki, D.; Weitkamp, J.; Kärger, J. *ChemPhysChem* **2009**, *10*, 2623.
(249) Chmelik, C.; Hibbe, F.; Tzoulaki, D.; Heinke, L.; Caro, J.; Li, J.; Kärger, J. *Microporous Mesoporous Mater.* **2010**, *129*, 340.
(250) Leach, A. R. *Molecular Modelling Principles and Applications*, 2nd ed.; Prentice Hall: London, 2001.
(251) Smit, B.; Maesen, T. L. M. *Chem. Rev.* **2008**, *108*, 4125.
(252) June, R. L.; Bell, A. T.; Theodorou, D. N. *J. Phys. Chem.* **1992**, *96*, 1051.
(253) Runnebaum, R. C.; Maginn, E. J. *J. Phys. Chem. B* **1997**, *101*, 6394.
(254) Schuring, D.; Jansen, A. P. J.; van Santen, R. A. *J. Phys. Chem. B* **2000**, *104*, 941.
(255) Smit, B.; Daniel J. C. Loyens, L.; L. M. M. Verbist, G. *Faraday Discuss.* **1997**, *106*, 93.
(256) Webb, E. B.; Grest, G. S.; Mondello, M. *J. Phys. Chem. B* **1999**, *103*, 4949.
(257) Frenkel, D.; Smit, B. *Understanding Molecular Simulations: from Algorithms to Applications*, 2nd ed.; Academic Press: San Diego, 2002.
(258) Harris, J.; Rice, S. A. *J. Chem. Phys.* **1988**, *89*, 5898.
(259) Siepmann, J. I.; Frenkel, D. *Mol. Phys.* **1992**, *75*, 59.
(260) Frenkel, D.; et al. *J. Phys.: Condens. Matter* **1992**, *4*, 3053.
(261) Chmelik, C.; Heinke, L.; Karger, J.; Schmidt, W.; Shah, D. B.; van Baten, J. M.; Krishna, R. *Chem. Phys. Lett.* **2008**, *459*, 141.
(262) Granato, M. A.; Vlugt, T. J. H.; Rodrigues, A. E. *Ind. Eng. Chem. Res.* **2007**, *46*, 321.
(263) Daems, I.; Baron, G. V.; Punnathanam, S.; Snurr, R. Q.; Denayer, J. F. M. *J. Phys. Chem. C* **2007**, *111*, 2191.
(264) Krishna, R.; van Baten, J. M. *Chem. Phys. Lett.* **2006**, *420*, 545.
(265) Jobic, H.; Laloue, N.; Laroche, C.; van Baten, J. M.; Krishna, R. *J. Phys. Chem. B* **2006**, *110*, 2195.
(266) Garcia-Perez, E.; Dubbeldam, D.; Maesen, T. L. M.; Calero, S. *J. Phys. Chem. B* **2006**, *110*, 23968.
(267) van Baten, J. M.; Krishna, R. *Microporous Mesoporous Mater.* **2005**, *84*, 179.
(268) Lu, L. H.; Wang, Q.; Liu, Y. C. *J. Phys. Chem. B* **2005**, *109*, 8845.
(269) Krishna, R.; van Baten, J. M. *J. Phys. Chem. B* **2005**, *109*, 6386.

(270) Lu, L. H.; Wang, Q.; Liu, Y. C. *Langmuir* **2003**, *19*, 10617.
(271) Beerdsen, E.; Dubbeldam, D.; Smit, B.; Vlugt, T. J. H.; Calero, S. *J. Phys. Chem. B* **2003**, *107*, 12088.
(272) Beerdsen, E.; Smit, B.; Calero, S. *J. Phys. Chem. B* **2002**, *106*, 10659.
(273) Schenk, M.; Vidal, S. L.; Vlugt, T. J. H.; Smit, B.; Krishna, R. *Langmuir* **2001**, *17*, 1558.
(274) Krishna, R. *Chem. Eng. Res. Des.* **2001**, *79*, 182.
(275) Krishna, R.; Paschek, D. *Phys. Chem. Chem. Phys.* **2001**, *3*, 453.
(276) Vlugt, T. J. H.; Martin, M. G.; Smit, B.; Siepmann, J. I.; Krishna, R. *Mol. Phys.* **1998**, *94*, 727.
(277) van Well, W. J. M.; Cottin, X.; Smit, B.; van Hooff, J. H. C.; van Santen, R. A. *J. Phys. Chem. B* **1998**, *102*, 3952.
(278) Krishna, R.; Smit, B.; Vlugt, T. J. H. *J. Phys. Chem. A* **1998**, *102*, 7727.
(279) Du, Z. M.; Manos, G.; Vlugt, T. J. H.; Smit, B. *AlChE J.* **1998**, *44*, 1756.
(280) Bandyopadhyay, S. *Chem. Phys. Lett.* **1998**, *293*, 378.
(281) Granato, M. A.; Lamia, N.; Vlugt, T. J. H.; Rodrigues, A. E. *Ind. Eng. Chem. Res.* **2008**, *47*, 6166.
(282) Granato, M. A.; Vlugt, T. J. H.; Rodrigues, A. E. *Adsorption* **2008**, *14*, 763.
(283) Dijkstra, M. *J. Chem. Phys.* **1997**, *107*, 3277.
(284) Martin, M. G.; Siepmann, J. I. *J. Phys. Chem. B* **1999**, *103*, 4508.
(285) Chen, Z.; Escobedo, F. A. *J. Chem. Phys.* **2000**, *113*, 11382.
(286) Wick, C. D.; Siepmann, J. I. *Macromolecules* **2000**, *33*, 7207.
(287) Chen, B.; Siepmann, J. I. *J. Phys. Chem. B* **1999**, *103*, 5370.
(288) Maginn, E. J.; Bell, A. T.; Theodorou, D. N. *J. Phys. Chem.* **1995**, *99*, 2057.
(289) van Erp, T. S.; Dubbeldam, D.; Caremans, T. P.; Calero, S.; Martens, J. A. *J. Phys. Chem. Lett.* **2010**, *1*, 2154.
(290) Chmelik, C.; Heinke, L.; van Baten, J. M.; Krishna, R. *Microporous Mesoporous Mater.* **2009**, *125*, 11.
(291) Hansen, N.; Krishna, R.; van Baten, J. M.; Bell, A. T.; Keil, F. J. *J. Phys. Chem. C* **2009**, *113*, 235.
(292) Jiang, J.; Sandler, S. I. *Langmuir* **2006**, *22*, 5702.
(293) Zhang, L.; Wang, Q.; Wu, T.; Liu, Y.-C. *Chem.- Eur. J.* **2007**, *13*, 6387.
(294) Düren, T.; Snurr, R. Q. *J. Phys. Chem. B* **2004**, *108*, 15703.
(295) Nicholson, T. M.; Bhatia, S. K. *J. Phys. Chem. B* **2006**, *110*, 24834.
(296) Skoulidas, A. I. *J. Am. Chem. Soc.* **2004**, *126*, 1356.
(297) Babarao, R.; Jiang, J. *Langmuir* **2008**, *24*, 5474.
(298) Burchard, E. *Studies on Zeolites, Molecular Mechanics, Framework Stability, and Crystal Growth*. Ph.D. Thesis, Technische Universiteit Delft, 1992.
(299) Spicer, L. D.; Rabinovitch, B. S. *J. Phys. Chem.* **1970**, *74*, 2445.
(300) Bowen, T. C.; Li, S.; Noble, R. D.; Falconer, J. L. *J. Membr. Sci.* **2003**, *225*, 165.
(301) Poling, B. E.; Prausnitz, J. M.; O'Connell, J. P. *The Properties of Gases and Liquids*, 5th ed.; McGraw-Hill: New York, 2001.
(302) Beck, D. W. *Zeolite Molecular Sieves*; John Wiley & Sons: New York, 1974.
(303) Ohe, S. *Computer Aided Data Book of Vapor Pressure*; Data Book Publishing Company, Tokyo, Japan, 1976.
(304) Lide, D. R. *Handbook of Chemistry and Physics*, 77th ed.; CRC Press: Boca Raton, FL, 1996−1997.
(305) *NIST Chemistry Webbook*, NIST Standard Reference Database Number 69; National Institute of Standards and Technology: Gaithersburg, MD,
(306) *Selected Values of Properties of Hydrocarbons and Related Compounds*; American Petroleum Institute Research Project 44; Carnegie Institute of Technology: Pittsburgh, PA, 1952.
(307) *Selected Values of Properties of Chemical Compounds*; Manufacturing Chemists Association Research Project; Texas A&M University: College Station, TX, 1975.
(308) Rudek, M. M.; Katz, J. L.; Vidensky, I. V.; Zdimal, V.; Smolik, J. *J. Chem. Phys.* **1999**, *111*, 3623.
(309) Yaws, C. L. *Thermophysical Properties of Chemicals and Hydrocarbons*; William Andrew Publishing; Norwich, NY, 2008.
(310) Fitch, A. N.; Jobic, H.; Renouprez, A. *J. Phys. Chem.* **1986**, *90*, 1311.
(311) Hu, K.-N.; Hwang, L.-P. *Solid State Nucl. Magn. Reson.* **1998**, *12*, 211.
(312) Auerbach, S. M.; Bull, L. M.; Henson, N. J.; Metiu, H. I.; Cheetham, A. K. *J. Phys. Chem.* **1996**, *100*, 5923.
(313) Auerbach, S. M.; Henson, N. J.; Cheetham, A. K.; Metiu, H. I. *J. Phys. Chem.* **1995**, *99*, 10600.
(314) Datka, J. *J. Chem. Soc., Faraday Trans. 1 F* **1981**, *77*, 511.
(315) Angell, C. L.; Howell, M. V. *J. Colloid Interface Sci.* **1968**, *28*, 279.
(316) Simperler, A.; Bell, R. G.; Philippou, A.; Anderson, M. W. *J. Phys. Chem. B* **2002**, *106*, 10944.
(317) Zhu, J.; Trefiak, N.; Woo, T.; Huang, Y. *Microporous Mesoporous Mater.* **2008**, *114*, 474.
(318) Li, D.; Kaneko, K. *J. Phys. Chem. B* **2000**, *104*, 8940.
(319) Kitaura, R.; Kitagawa, S.; Kubota, Y.; Kobayashi, T. C.; Kindo, K.; Mita, Y.; Matsuo, A.; Kobayashi, M.; Chang, H.-C.; Ozawa, T. C.; Suzuki, M.; Sakata, M.; Takata, M. *Science* **2002**, *298*, 2358.
(320) Serre, C.; Millange, F.; Thouvenot, C.; Noguès, M.; Marsolier, G.; Louër, D.; Férey, G. *J. Am. Chem. Soc.* **2002**, *124*, 13519.
(321) Millange, F.; Serre, C.; Ferey, G. *Chem. Commun.* **2002**, *8*, 822.
(322) Krishna, R.; van Baten, J. M. *Sep. Purif. Technol.* **2011**, *76*, 325.
(323) Krishna, R.; van Baten, J. M. *J. Phys. Chem. C* **2010**, *114*, 13154.
(324) Krishna, R.; van Baten, J. M. *J. Membr. Sci.* **2010**, *360*, 476.
(325) Krishna, R.; van Baten, J. M. *Langmuir* **2010**, *26*, 10854.
(326) Kubota, Y.; Takata, M.; Matsuda, R.; Kitaura, R.; Kitagawa, S.; Kobayashi, T. C. *Angew. Chem.* **2006**, *118*, 5054.
(327) Wang, Z.; Zhang, B.; Fujiwara, H.; Kobayashi, H.; Kurmoo, M. *Chem. Commun.* **2004**, *4*, 416.
(328) Chen, B.; Liang, C.; Yang, J.; Contreras, D. S.; Clancy, Y. L.; Lobkovsky, E. B.; Yaghi, O. M.; Dai, S. *Angew. Chem., Int. Ed.* **2006**, *45*, 1390.
(329) Kondo, M.; Okubo, T.; Asami, A.; Noro, S.-i.; Yoshitomi, T.; Kitagawa, S.; Ishii, T.; Matsuzaka, H.; Seki, K. *Angew. Chem., Int. Ed.* **1999**, *38*, 140.
(330) Jorgensen, W. L.; Severance, D. L. *J. Am. Chem. Soc.* **1990**, *112*, 4768.
(331) Castillo, J. M.; Vlugt, T. J. H.; Calero, S. *J. Phys. Chem. C* **2009**, *113*, 20869.
(332) *Kirk-Othmer Encyclopedia of Chemical Technology*, John Wiley & Sons, Inc.: New York, 2008.
(333) Greim, J.; Schwetz, K. A. *Boron Carbide, Boron Nitride, and Metal Borides*; Wiley-VCH Verlag GmbH & Co. KGaA: New York, 2000.
(334) Whitfield, T. R.; Wang, X.; Liu, L.; Jacobson, A. J. *Solid State Sci.* **2005**, *7*, 1096.
(335) Vougo-Zanda, M.; Huang, J.; Anokhina, E.; Wang, X.; Jacobson, A. J. *Inorg. Chem.* **2008**, *47*, 11535.
(336) Wang, X.; Liu, L.; Jacobson, A. J. *Angew. Chem., Int. Ed.* **2006**, *45*, 6499.
(337) Boutin, A.; Springuel-Huet, M.-A.; Nossov, A.; Gédéon, A.; Loiseau, T.; Volkringer, C.; Férey, G.; Coudert, F.-X.; Fuchs, A. H. *Angew. Chem., Int. Ed.* **2009**, *48*, 8314.
(338) Neimark, A. V.; Coudert, F. o.-X.; Boutin, A.; Fuchs, A. H. *J. Phys. Chem. Lett.* **2009**, *1*, 445.
(339) Boutin, A.; Coudert, F. o.-X.; Springuel-Huet, M.-A.; Neimark, A. V.; Férey, G. r.; Fuchs, A. H. *J. Phys. Chem. C* **2010**, *114*, 22237.
(340) Ghoufi, A.; Maurin, G.; Férey, G. *J. Phys. Chem. Lett.* **2010**, *1*, 2810.
(341) van Koningsveld, H.; v. d. B., A. J.; Jansen, J. C.; de Goede, R. *J. Acta Crystallogr.* **1986**, *B42*, 491.
(342) van Koningsveld, H.; T., F.; van Bekkum, H.; Jansen, J. C. *J. Acta Crystallogr.* **1989**, *B45*, 423.

(343) Millange, F.; Guillou, N.; Walton, R. I.; Greneche, J.-M.; Margiolaki, I.; Ferey, G. *Chem. Commun.* **2008**, *39*, 4732.
(344) Devautour-Vinot, S.; Maurin, G.; Henn, F.; Serre, C.; Devic, T.; Ferey, G. *Chem. Commun.* **2009**, *19*, 2733.
(345) Millange, F.; Serre, C.; Guillou, N.; Férey, G.; Walton, R. I. *Angew. Chem., Int. Ed.* **2008**, *47*, 4100.
(346) Mu, B.; Huang, Y.; Walton, K. S. *CrystEngComm* **2010**, *12*, 2347.